A THEORETICAL INVESTIGATION OF THE EFFECTS OF SOLAR ECLIPSES ON THE IONOSPHERE.

A Thesis submitted for the
Degree of Master of Science of
Rhodes University.

by

A.D.M. WALKER.

January, 1962.

Except where it is clear from the text that I am describing the work of others, or where it is obvious that I am making a survey of existing knowledge about the ionosphere, the work described in this thesis is my own.

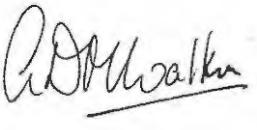

CONTENTS.

ACKNOWLEDGEMENTS.

If there had been nobody with whom I could discuss the work done in this thesis it would never have been completed. Further, if those with whom I discussed it had not been prepared to listen to my tale of woe when things were not proceeding as planned I would have plunged into the Slough of Despond much deeper than I did.

I have been more than fortunate in my Research Director, Professor J.A. Gledhill, who has been my mentor throughout the project. His encouragement has been unfailing, his fund of ideas limitless. I am very grateful.

My friends in the Rhodes University Physics Department have been most helpful. I must single out Mr. D.C. Baker and Miss L.V. Pound who, themselves working on related projects, not only helped to clarify my ideas during discussions, but also shared some of the labour of calculating the Titheridge coefficients.

I am grateful to the South African Council for Scientific and Industrial Research for two reasons. For the first part of this research I held a research grant from them. In addition I was permitted to use their ZEBRA electronic computer for some of my computations. I am grateful to the Director of the National Physical Research Laboratories for this permission. I must also thank Dr. Burger for lending me his computer manual

for some time. Dr. Neethling of the C.S.I.R. was extremely helpful while I was there. Miss Henda Scott, a student of Stellenbosch University was also working in the Mathematics Division of the C.S.I.R. at the time and helped me a great deal with my programming problems. I am very thankful.

Finally I must thank Miss K. Longfield for the skill and patience which she exercised while typing the stencils for this thesis. Portions of it are a typist's nightmare. She came up smiling.

INTRODUCTION

"Oh learn to read what silent love has writ..."

Shakespeare: Sonnets.

INTRODUCTION.

The behaviour of the ionosphere during a solar eclipse is of great interest because radiation from the sun is the cause of ionization in the upper atmosphere and it is useful to be able to conduct experiments where this radiation is cut off and restored in a known manner.

Experimental results, especially those dealing with the F2 layer, have proved puzzling. Cusps which cannot be explained appear on the records obtained from ionosphere sounders and in the F2 region the electron density at a given height shows a maximum after the eclipse where one would expect it simply to rise to a steady value.

An attempt is made in this thesis to explain some of the anomalies in terms of tilts in the ionospheric layers and minima of electron density or "valleys" between the ionospheric layers. The problem is attacked theoretically.

Part I deals with the theoretical background to ionospheric physics in general and to this problem in particular. Standard methods of dealing with radio propagation in the ionosphere as well as some methods developed by the author are discussed.

Part II deals directly with the effects of a solar eclipse on a theoretical ionosphere. Ionograms which would be obtained in the theoretical ionosphere are constructed. These are scaled by standard methods to show where errors may arise.

It appears that tilts in the layers have only a small effect. The effect of the valley is, however, extremely important, giving rise to the apparent maximum of electron density in the F2 layer at a given height after the eclipse. This maximum does not in fact exist but arises from an error in the scaling method which ignores the possibility of a valley.

Some records taken during the solar eclipse of 25 December 1954 have been scaled. They support the conclusions reached theoretically.

PART I.

THEORETICAL BACKGROUND

"'Sectaris quid?' dixit Porcellus appropinquans.

"'Interrogo ipse me. Ipse me interrogo: quid?'"

Winnie Ille Pu.

CHAPTER I.

THE IONOSPHERE.

1. A Brief History.

Before 1901 it was generally thought that radio waves were only useful for short range communication since they were known to travel in straight lines. In 1901 MARCONI found his faith justified when he succeeded in the apparently impossible task of transmitting a radio signal across the Atlantic Ocean. Attempts were made to explain the success of the experiment by investigating the effects of diffraction of the radio waves around the earth. The calculated effects were, however, much too small to explain the facts, and in 1902 KENNELLY (1) and HEAVISIDE (2) independently suggested the existence of a conducting layer in the upper atmosphere. The radio wave might then be reflected back and forth between this layer and the ocean, and so be transmitted round the curved surface of the earth. In 1881 BALFOUR-STEWART (3) had proposed a similar layer to account for magnetic disturbances.

It was in 1924 that the existence of this so-called KENNELLY-HEAVISIDE layer was proved experimentally beyond doubt. APPLETON & BARNETT (4) observed the interference between the direct signal from a BBC transmitter and the signal reflected from the KENNELLY-HEAVISIDE layer. Shortly afterwards an experiment was performed by BREIT & TUVE (5) which showed that, if a transmitter emitted a

pulse of radio waves, a receiver placed near it received two pulses or sometimes more. This indicated that the first pulse was that received by direct transmission along the ground, while the others which arrived a little later were reflections from the Kennelly-Heaviside layer. The method of Breit and Tuve is the basis of modern techniques used to investigate this region of the atmosphere which is now called the ionosphere as proposed by WATSON-WATT.

2. The Structure of the Ionosphere.

It was soon established that the Kennelly-Heaviside layer owed its properties to the ionization of the atoms of the upper atmosphere. The early experiments of Breit and Tuve showed that it was not a simple region of ionization as was first thought but that it had a complicated structure. Appleton's early experiments showed that at least two regions existed. It is now known that there are three main regions. These are shown in Fig.1 which depicts a typical distribution of electron density with height. Electrons are the only type of charged particles which affect the propagation of electro-magnetic radiation appreciably, except at very low frequencies since their mass is so much less than that of the positive ions, and we are therefore concerned only with electron density. At a height of about 60 km. is the D region which has a comparatively low electron density - less than 10^4 electrons per cubic centimetre. Next comes the E layer

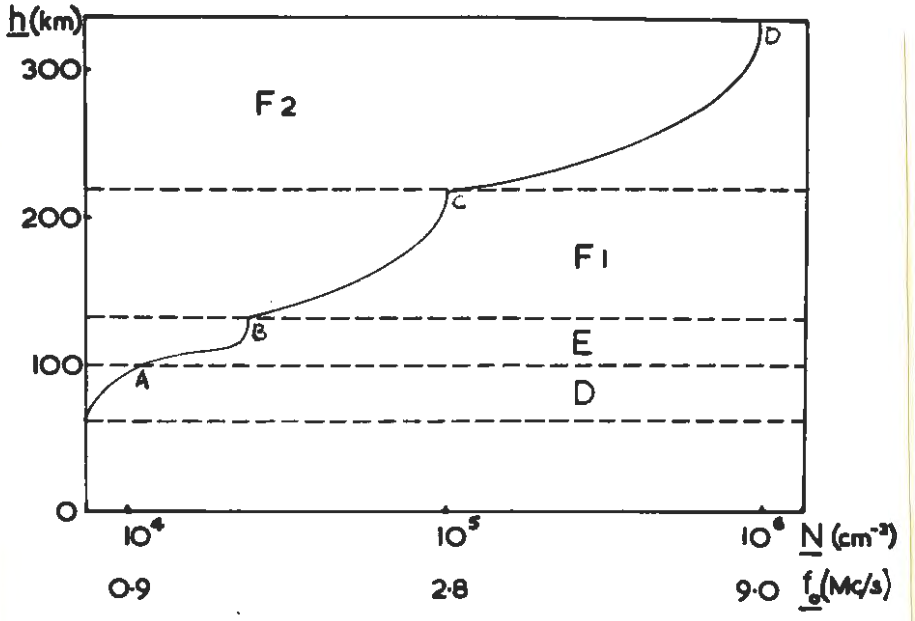

FIGURE 1: A typical distribution of electron density with height. The horizontal axis is calibrated in electron density and in plasma frequency.

at a height of about 100 km. to 120 km. It is marked by a rapid increase of electron density with a well defined maximum at the top of the layer. It is the portion of the ionosphere which corresponds to the old Kennelly-Heaviside region. Above this is the F region which is a single layer during the night, but which often splits into two strata, the F1 and F2 regions, during the day.

The distribution given in Fig.1 is typical. However, the numerical values of the electron density may vary considerably with time of day, season, year, or geographic position. The main features are nevertheless always the same.

3. The Formation of the Ionized Layers.

There is strong experimental evidence that the electron density in the E and F1 layers is controlled by the sun. The electron density at a given height undergoes diurnal, seasonal and latitude variations. There is also a correlation between the value of the maximum electron density in an ionospheric layer and sunspot number. Solar control of the F2 layer is by no means so obvious. However, RATCLIFFE (6) has evaluated the total electron content of a vertical column through the F2 region below its maximum and has hence established that the total number of electrons behaves in a regular manner with respect to the sun.

If we agree that radiation from the sun produces the ionization we must still decide whether electromagnetic radiation or

a stream of particles from the sun is the controlling factor. Observations of the ionosphere during solar eclipses could provide the answer. Very soon after the eclipse begins the electron density at a given height in the E and F1 layers begins to fall off, reaching a minimum near the maximum of the optical eclipse. It then rises as the sun's disc is again exposed. This means that the ionizing agent travels from the sun to the earth at approximately the speed of light. Particles travelling near the speed of light would, on account of their extremely high energy, penetrate deep into the atmosphere and produce ionization at a very much lower level than is observed. In fact, if particles were the controlling mechanism of ionization, their velocity would be such that their transit time would be of the order of several hours if the observed effects were to be produced. This indicates quite definitely that electromagnetic radiation is the controlling factor in producing the E and F1 layers. Of course ionization by streams of particles is not excluded as a contributory factor.

It is not so easy to be dogmatic about the mode of formation of the F2 layer. It is likely, as suggested by RATCLIFFE (7), that electron production in the whole F region is controlled by electromagnetic radiation from the sun.

The rate of production of electrons in an atmosphere consisting of a single gas at uniform temperature, under the action of gravity, over a flat earth, was investigated by CHAPMAN (8)(9).

It can be seen qualitatively that the rate of production must reach a peak at a certain height. Suppose we have radiation from the sun falling on such an atmosphere. Further, suppose that only one type of ionizing process occurs. As the radiation penetrates deeper into the atmosphere, the density of the gas increases, and thus more ions are formed for a given amount of radiation. The number of ions produced is also dependent on the amount of ionizing radiation available. Since this is absorbed as it penetrates, less is available as the depth of penetration increases. The nett result is that initially the ion density increases as the radiation penetrates, a maximum is reached when the second effect becomes dominant, and thereafter the ion density decreases. We thus get a definite maximum in the rate of ion production at a particular height. It should be noted that the rate of production is also dependent on the solar zenith angle as this decides the thickness of atmosphere through which the radiation must pass before reaching a given height.

Chapman's expression for the rate of ion production, q, is

$$q = q_m \exp(1 - z - e^{-z} \sec\chi) \qquad (1.1)$$

where $q_m = BI_\infty \cos\chi / H \exp(1)$

B = number of electrons produced when unit energy is absorbed.

I_∞ = power flux per unit area, incident from above at an angle χ to the zenith.

z = normalized height

= $(h - h_m)/H$

h = height

h_m = height of the layer maximum

H = RT/Mg

R = the gas constant

T = the absolute temperature

M = the weight of 1 gm molecule of the gas ~~the molecular weight of the gas~~

g = the acceleration due to gravity.

Two different combinations of radiation and ionizable gas are thought to give rise to the E and F1 layers.

While electrons are being produced by the above mechanism they are also being lost. The chief loss mechanisms can be pictured as the recombination of electrons and positive ions, and the attachment of electrons to neutral molecules.

Consider recombination first. If we have an electron density of N electrons/cm^3 then there are also N positive ions per cm^3. The rate of recombination is proportional to the electron density and to the positive ion density. If the constant of proportionality is α then the rate of recombination is given by

$$\frac{dN}{dt}\,(\text{recombination}) = -\alpha N^2 \qquad (1.2)$$

α is known as the recombination coefficient.

The rate of attachment is proportional only to the electron density if we can suppose that the number of neutral molecules is sufficiently large to be unaffected by the number of atoms which are ionized. If the constant of proportionality is β then

$$\frac{dN}{dt} \text{ (attachment)} = -\beta N \qquad (1.3)$$

We can now write down an expression for the time rate of change of the electron density at a given height:

$$\frac{dN}{dt} = q - \alpha N^2 - \beta N \qquad (1.4)$$

If recombination is the dominant mechanism of electron loss this reduces to

$$\frac{dN}{dt} = q - \alpha N^2 \qquad (1.5)$$

and if attachment is the dominant mechanism to

$$\frac{dN}{dt} = q - \beta N \qquad (1.6)$$

Eclipse measurements, where the rate of production varies in a known manner, have indicated that in the E and F1 layers recombination is predominant. Various workers have found values for α of the order of 10^{-8} cm^3 sec^{-1}. Attempts to decide which mechanism was dominant in the F2 region have yielded results which are inconclusive but which favour attachment as the chief mechanism.

There are two major difficulties in the above simple picture.

Firstly, no simple recombination process corresponds to a value of α as high as 10^{-8} cm^3 sec^{-1} in the E and F1 layers. Secondly, no known atmospheric gas absorbs any known solar radiation so strongly that a peak could be formed as high as the F2 peak.

BATES & MASSEY (10)(11) have proposed an electron loss mechanism which resolves the first of these difficulties. Instead of the relatively simple processes of recombination and attachment they suggest that the positive oxygen ion exchanges charge with a neutral oxygen molecule, leaving a positively charged ion and a neutral atom. A free electron then combines with the charged molecule and dissociates it into two neutral atoms.

The equations of the reactions are

$$O + h\nu \rightarrow O^+ + e \qquad \text{(ionization)}$$

$$O^+ + O_2 \rightarrow O_2^+ + O$$

$$O_2^+ + e \rightarrow O' + O'' \qquad \text{(electron loss)}$$

If the electrons are produced at a constant rate, q, it can be shown that when equilibrium has been set up

$$q = \frac{\alpha\gamma n N^2}{\alpha N + \gamma n} \qquad (1.6)$$

where α and γ are constants, n is the density of O_2 molecules, and the other symbols have the meanings given previously.

At low levels n is large and at high levels it is small. Thus at the levels of the E and F1 layers, where $\gamma n >> \alpha N$,

the equation ~~(1.6)~~ reduces to

$$q = \alpha N^2 \qquad (1.7)$$

and the electron density behaves as if it were determined by a recombination coefficient, α. Bates and Massey estimated α from theory and found that it could well be of the order of 10^{-8} cm^3 sec^{-1}. This approach also suggested a way out of the second difficulty, the mode of formation of the F2 layer. In the case where $N\alpha >> n\gamma$ - at high altitudes where most of the atoms are ionized - equation (1.6) reduces to

$$q = \gamma nN = \beta N, \quad \text{say} \qquad (1.8)$$

Here the loss coefficient is γ n, and since n decreases upwards so does β. In other words we have an attachment-like process where the attachment coefficient, β, decreases with height. BRADBURY (12) considered the distribution of electrons with altitude when the loss coefficient is a function of height. RATCLIFFE (7) describes what happens when the F2 layer is assumed to be a so-called Bradbury layer. He shows that under the practical conditions the electron concentration in the F2 layer should increase upwards without limit. The F2 maximum is thought to be the result of a so-called "ambipolar" diffusion process, due to the concentration gradient of the positive ions. Positive and negative ions diffuse together at the same rate due to electro-static interaction.

It thus seems that we can work on the assumption that elec-

tron loss in the E and F1 layers is due to a recombination-like process and in the F2 region to an attachment-like process.

4. Magneto-Ionic Theory.

Since the ionosphere plays a vital part in the propagation of radio waves, and since our knowledge of it is obtained almost entirely from radio measurements, it is important to understand how propagation is affected by the ionization.

Magneto-ionic theory deals with the propagation of electromagnetic waves through a gas consisting of neutral molecules, throughout which an equal number of positive ions and of electrons are uniformly distributed, in the presence of a uniform magnetic field.

None of these conditions obtains in the ionosphere. The electron density is not uniform and the magnetic field varies with height.

A complete discussion of the propagation of electromagnetic radiation in the ionosphere requires a complicated full-wave treatment. However, it is possible, without any significant inaccuracy, to assume that at each level the wave behaves as if it were in a homogeneous medium, since generally neither the electron density nor the magnetic field changes appreciably within a distance of several wavelengths.

The velocity of the wave at any point can be described by

means of a refractive index, n. APPLETON (13)(14) and HARTREE (15) independently derived an expression for the refractive index. The equation is now known as the Appleton-Hartree equation. It gives an expression for the complex refractive index, n, in terms of the wave frequency, the electron density, the magnetic field, and the frequency of collision of electrons with heavy particles. The full expression is

$$n^2 = 1 - \frac{X}{1 - iZ - \frac{1}{2}Y_T^2/(1-X-iZ) \pm \left\{ Y_T^4/4(1-X-iZ)^2 + Y_L^2 \right\}^{\frac{1}{2}}} \qquad (1.9)$$

where $n = \mu - i\chi$, the complex refractive index

μ = phase refractive index = c/v

χ = attenuation factor

c = velocity of electromagnetic radiation in vacuo

v = velocity of electromagnetic radiation in the medium

$X = f_o^2/f^2$

$Y_T = Y \sin\theta$, $Y_L = Y \cos\theta$, $Y = f_H/f$

$Z = \nu/2\pi f$

f = wave frequency

f_o = plasma frequency $= (1/2\pi)\,(Ne^2/\epsilon_o m)^{\frac{1}{2}}$

f_H = gyro frequency $= Be/2\pi m$

ν = frequency of collisions of electrons with heavy particles.

N = electron density

e = charge on the electron

m = mass of the electron

ϵ_o = electric permittivity of free space

μ_o = magnetic permittivity of free space

B = magnitude of the magnetic induction in the medium = $\mu_o H$ if the relative magnetic permeability of the medium is unity.

θ = angle made by the magnetic field with the direction of the radiation.

Rationalized units are used in the above.

Derivations of the equation using modern nomenclature are given by RATCLIFFE (16) (unrationalized units) and BUDDEN (17) (rationalized units).

In most cases with which we shall deal collisions may be neglected and the Appleton-Hartree equation takes the form:

$$n^2 = 1 - \frac{X}{1 - \frac{Y_T^2}{2(1-x)} \pm \left\{ \frac{Y_T^4}{4(1-x)^2} + Y_L^2 \right\}^{\frac{1}{2}}} \qquad (1.10)$$

The equation is extremely complicated and we shall discuss a simple case and some approximations before investigating it fully. We note, however, that it is double valued giving rise to two waves known, by analogy with doubly refracting media in

optics, as the ordinary and extraordinary waves. The plus sign in the denominator corresponds to the ordinary wave and the minus to the extraordinary except in the special case where the wave normal coincides with the direction of the imposed field.

5. Propagation when the Earth's Magnetic Field is Neglected.

If we ignore the earth's magnetic field then $Y = 0$ and equation (1.10) takes the much simpler form,

$$n^2 = 1 - X \qquad (1.11)$$

In this case we see that if $X < 1$ (or if $f_o^2 < f^2$) then n^2 is positive and n is real, that is $n = \mu$ and $\chi = 0$. If $X > 1$ (or $f_o^2 > f^2$) then n^2 is negative and n purely imaginary, that is $n = \chi$ and $\mu = 0$. The physical interpretation of this is that when n is real the wave is propagated with its phase velocity given by a phase refractive index μ, while when n is imaginary so-called "evanescent" waves occur and there is no transport of energy. Of course if collisions are considered n may be complex. If we then consider some field quantity $F = F_o e^{-iknz}$ then, since $n = \mu - i\chi$,

$$F = F_o e^{-ik\mu z} \; e^{-k\chi z}$$

and this represents a wave travelling with velocity c/μ and attenuated as it travels at a rate which is determined by χ. When n is purely imaginary and evanescent waves occur the phase velocity is infinite and the field components vary har-

monically with time, but there is no variation in space and hence no transport of energy.

If we consider a wave entering a stratified dispersive medium such as we have been considering at an angle of incidence, i, we see that if Snell's Law is obeyed then

$$\mu \sin\theta = \sin i \qquad (1.12)$$

where θ is the angle which the wave normal makes with the normal to the stratifications of the medium. Reflection will occur when $\theta = 0$ or when

$$\mu = \sin i \qquad (1.13)$$

In the limiting case of normal incidence when $i = 0$ the wave is reflected when $\mu = 0$. To prove this rigorously it is necessary to use full wave theory as given by BUDDEN (18). Even when the magnetic field is not neglected, and the refractive index is given by equation (1.10), reflection can be shown to take place where $\mu = 0$.

In our simple model, neglecting the earth's field, the only zero in n occurs when $f = f_o$, the plasma frequency. This happens when

$$f = \frac{Ne^2}{4\pi^2 \epsilon_o m}$$

If we substitute numerical values for the constants in this equation we obtain the useful relation:

$$N = 1.24 \times 10^4 f^2 \qquad (1.14)$$

at the reflection point, where N is in electrons per cubic

centimetre and f in megacycles per second.

6. The Quasi-Transverse (QT) and Quasi-Longitudinal (QL) Approximations.

In practical cases the Appleton-Hartree equation is cumbersome and calculation of values of n laborious and time-consuming. Two approximations, first suggested by BOOKER (19), are often used.

The quasi-longitudinal approximation holds when

$$Y_T^4/4Y_L^2 \ll (1 - X)^2 + Z^2 \qquad (1.15)$$

It is generally quoted as

$$n^2 = 1 - \frac{X}{1 - iZ \pm |Y_L|} \qquad (1.16)$$

However, as has been pointed out by the author, (20), equation (1.16) is incorrect as can easily be seen by considering the denominator of the second term of equation (1.9):

$$1 - iZ - Y_T^2/2(1 - X - iZ) \pm (Y_T^4/(1 - X - iZ)^2 + Y_L^2)^{\frac{1}{2}}$$

When the inequality (1.15) holds this becomes

$$1 - iZ - Y_T^2/2(1 - X - iZ) \pm |Y_L|$$

and $Y_T^2/2(1 - X - iZ)$ is not necessarily negligible compared with Y_L. In fact if we assume the numerical condition suggested by RATCLIFFE (21) that the inequality is satisfied if the larger quantity is nine times the smaller, then $Y_T^2/2(1-X-iZ)$ may be as large as $Y_L/3$. The correct approximation if we

assume (1.15) is thus:

$$n^2 = 1 - \frac{X}{1 - iZ - Y_T^2/2(1 - X - iZ) \pm Y_L} \qquad (1.18)$$

and the wave does not behave as if it were propagated along that direction. It will only behave as if it were when

$$Y_T^2/2Y_L \ll \left|(1 - X) - iZ\right| \qquad (1.19)$$

It is in this form that BUDDEN (22) quotes the condition for the QL approximation.

The QT approximation is valid when

$$Y_T^4/4Y_L^2 \gg \left|1 - X - iZ\right|^2 \qquad (1.20)$$

and not only - as BUDDEN (22) suggests - when

$$Y_T^2/2Y_L \gg \left|1 - X - iZ\right| \qquad (1.21)$$

It takes the form

$$n^2 = 1 - X/\left\{1 - iZ + (1 - X - iZ)\cot^2\theta\right\} \qquad (1.22)$$

for the ordinary wave and

$$n^2 = 1 - \frac{X}{1 - iZ - Y_T^2/(1 - X - iZ)} \qquad (1.23)$$

for the extraordinary wave. These expressions can be compared with those for truly transverse propagation when the direction of the wave normal is perpendicular to the direction of the magnetic field. These expressions are

$$n^2 = 1 - \frac{X}{1 - iZ} \qquad (1.24)$$

for the ordinary wave, and

$$n^2 = 1 - \frac{X}{1 - iZ - Y^2/(1 - X - iZ)} \qquad (1.25)$$

for the extraordinary wave.

We see that for the extraordinary wave the QT expression is analogous to the expression for the transverse case while for the ordinary wave an extra term, $(1 - X - iZ)\cot^2\theta$ is added to the denominator of the second term in the QL expression. The necessity for including this term was pointed out by WHITEHEAD (23). It only becomes negligible when θ is near to 90°, that is when propagation is nearly transverse.

It should be noted that the QT and QL approximations, equations 1.16, 1.22, and 1.23, do not only hold when propagation is nearly transverse or nearly longitudinal but over a much wider range of conditions, although not so wide a range as suggested by RATCLIFFE (24) in Fig.3.1 of his book because of the reason pointed out above.

7. The Complete Expression for the Complex Refractive Index.

RATCLIFFE (25) gives a very full discussion of the behaviour of the refractive index, n, in terms of a graphical representation. We shall concern ouselves only with the zeros of n and with the question of whether there exists a definite value of n for a given electron density, i.e. for a given value of X. We shall henceforth ignore collisions.

Let us consider the expression (1.10) as related to an ionosphere where the electron density is a function of height only. If a wave is incident vertically on this ionosphere it will be split into two waves, the ordinary and the extra-ordinary, which will travel vertically with a phase velocity at any point given by the value of n obtained from equation (1.10) at that point. Since the angle of incidence is zero the direction of the wave normal will, by Snell's law, remain vertical. The wave will then be reflected where $\mu = 0$.

For the ordinary wave this zero in μ (and hence in n) occurs when $X = 1$. This means that reflection takes place where the probing frequency is equal to the plasma frequency as is the case when there is no magnetic field.

For the extraordinary wave we have two possibilities. When $Y < 1$, or the wave frequency is greater than the gyro-frequency, $n = 0$ when $X = 1 \pm Y$. The case when $X = 1 + Y$ is not of much interest since in the ionosphere the extra-ordinary wave is reflected at $X = 1 - Y$ before it reaches this level. This case does, however, form the basis of one explanation of the so-called Z-trace given by ECKERSLEY (26) and RYDBECK (27)(28). When $Y > 1$, or the wave frequency is less than the gyro-frequency, $n = 0$ when $X \mp 1 + Y$. In many ionosphere sounders the lower frequency limit is greater than the gyrofrequency and thus this case does not occur as often as the first.

There is an infinity in n for the extraordinary wave when $Y < 1$ at $X = (1 - Y^2)/(1 - Y_L^2)$, and for the ordinary wave when $Y > 1$ at the same value of X. These would correspond to an infinite velocity of energy propagation. These cases cannot occur in practice as the wave must always be reflected before such a value of X is reached.

Suppose now the wave is incident obliquely on the ionosphere. By Snell's Law it will be deviated. The value of the refractive index depends on the angle which the wave normal makes with the magnetic field and this complicates the problem considerably. BOOKER (29) has shown that oblique incidence can be studied in terms of a quantity, q, defined by

$$q = n \cos\theta \tag{1.26}$$

By Snell's law

$$n \sin\theta = \sin i \tag{1.27}$$

for both ordinary and extraordinary waves. Then, if n is considered as a vector inclined at an angle θ to the vertical, q is its vertical component and sin i its horizontal component. Thus, if q can be found at some point, n and θ may be derived from

$$n^2 = q^2 + \sin^2 i \tag{1.28}$$

and

$$\tan\theta = \frac{\sin i}{q} \tag{1.29}$$

Booker showed that q is one root of a quartic equation, known as the Booker quartic.

8. Group and Phase Velocity.

As we shall see in Chapter 2, the most valuable way of investigating the ionosphere is based on the timing of radio frequency pulses as they travel through the medium. Such pulses can be represented by a Fourier integral. The Fourier function has a maximum at the wave frequency and only frequencies near this play a significant part in propagation of the pulse. As is shown in standard textbooks on wave motion, the energy in such a pulse will not in general be propagated with the phase velocity, u, but with a group velocity, U. For a wave of frequency f and phase velocity u the velocity of propagation of the group is given by

$$\frac{1}{U} = \frac{d}{df}\left(\frac{f}{u}\right) \qquad (1.30)$$

By analogy with the phase refractive index we define the group refractive index, μ', by

$$\mu' = c/U \qquad (1.31)$$

Equations (1.30) and (1.31) lead to

$$\mu' = \mu + f\frac{d\mu}{df} \qquad (1.32)$$

It is interesting to note that in the case of no magnetic field where $\mu^2 = 1 - X = 1 - f_o^2/f^2$

$$\mu\mu' = 1 \qquad (1.33)$$

SHINN and WHALE (30) have calculated μ' for South East England for a number of values of X and Y. The basis of the method is differentiation of equation (1.10) with respect to f and substitution in equation (1.32) getting

$$\mu' = \frac{1}{\mu[1-X][1-Y_T^2/(1-X)^2\{Y_T^4/4(1-X)^2 + Y_L^2\}^{\frac{1}{2}}} \times$$

$$\left\{1-\mu^2-X^2+\frac{(1-\mu^2)(1+X)\,Y_L^2}{2\{Y_T^4/4(1-X)^2+Y_L^2\}^{\frac{1}{2}}}\right\}+\mu \qquad (1.34)$$

The author, using the method of Shinn and Whale, had calculated values of μ' over Grahamstown. Values of Y from Y = 0.100 to Y = 0.500 at intervals of 0.025 have been used. For each value of Y a number of values of μ' were calculated corresponding to values of X ranging from X = 0.01 to X = 0.98 at intervals of 0.01. To calculate only one value of μ' takes about one hour so an electronic computer was of course essential. The ZEBRA computer of the South African Council for Scientific and Industrial Research was used for the computation. Details of the program used and the computation are given in Appendix A. The results were in tabular form as supplied by the computer but are shown graphically for convenience in figures 2 and 3. Not all the values of Y are shown

in the figure to avoid crowding it. Figure 2 shows μ' plotted against X for the ordinary ray and Figure 3 μ' against X/(1-Y) for the extraordinary ray. It will be noted that μ' is plotted on a scale which is proportional to $1/\mu'$ so that large values of μ' can be included.

Since μ' is infinite when μ is zero it is often useful to use the quantity $\mu't$, as suggested by MILLINGTON (31), where

$$t^2 = 1 - X \tag{1.35}$$

for the ordinary ray, and

$$t^2 = 1 - \frac{X}{1 - Y} \tag{1.36}$$

for the extraordinary ray. This quantity tends to a finite limit as μ' tends to infinity. This limit is

$$\mu't = \operatorname{cosec}\theta \tag{1.37}$$

for the ordinary ray, and

$$\mu't = \frac{2 - Y}{1 - Y} \frac{1}{\sqrt{2 + 2\cos^2\theta}} \tag{1.38}$$

for the extraordinary ray, as is proved in Appendix B.

The author has calculated values for $\mu't$ for both ordinary and extraordinary rays, using the ZEBRA computer for values of μ' which were not calculated in the normal course of events. The results are shown in figures 4 and 5 for the ordinary and extraordinary rays respectively.

9. Oblique Incidence and Lateral Deviation.

BOOKER (32)(33) has discussed this problem. The root

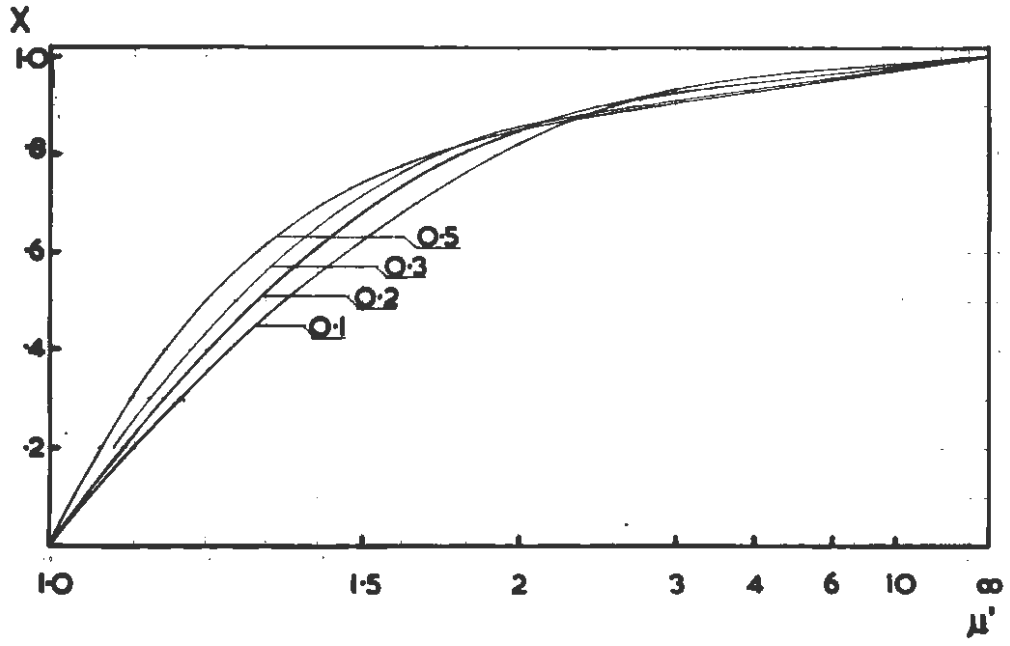

FIGURE 2: μ' versus X for the ordinary ray. The parameters shown are values of Y.

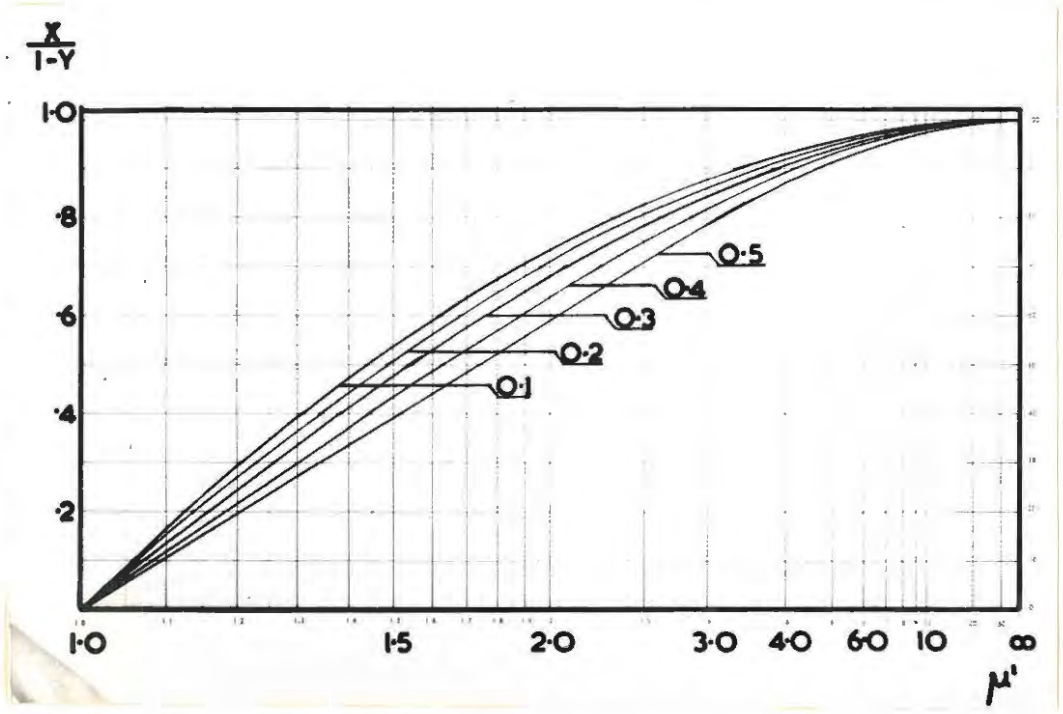

FIGURE 3: μ' versus $\frac{X}{1-Y}$ for the extraordinary ray. The parameters shown are values of Y.

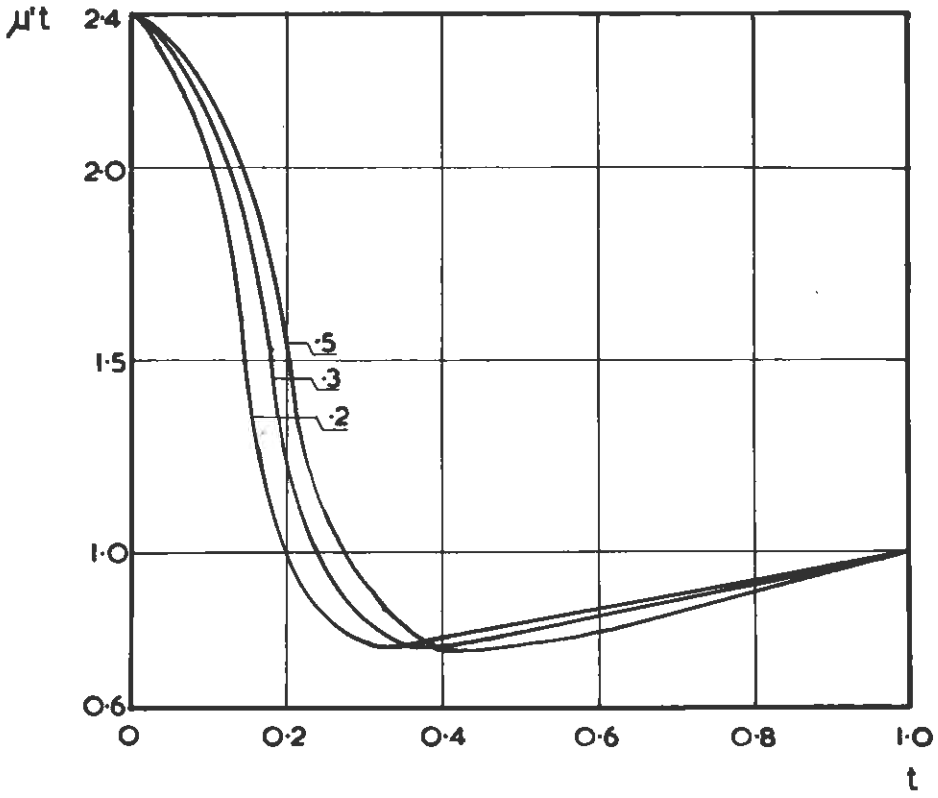

FIGURE 4: μ't versus t for the ordinary ray. The parameters shown are values of Y.

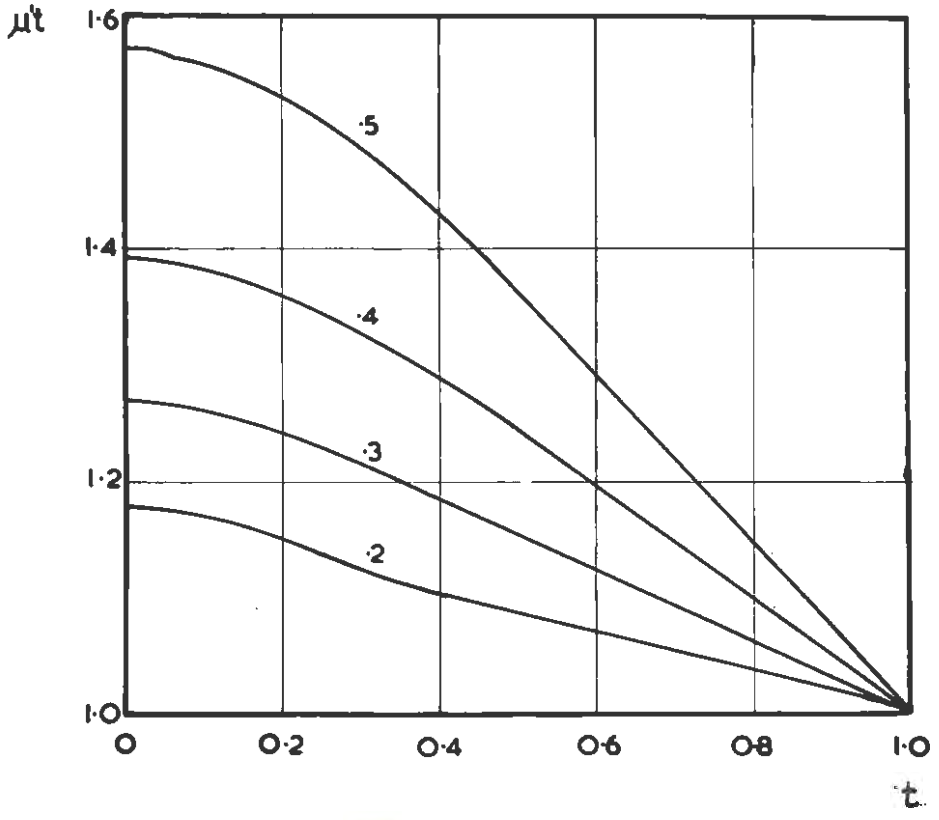

FIGURE 5: μ't versus t for the extraordinary ray. The parameters shown are values of Y.

of the Booker quartic equation, q, describes phase propagation. A peculiar result is that reflection does not in general take place where q = 0, that is to say when the wave normal is horizontal, but at a different level. This is because the ray direction (which defines the group path) and the direction of the wave normal do not in general coincide. Reflection takes place when the ray becomes horizontal. In the special case of vertical propagation $q \equiv \mu$ and the ray direction and wave normal coincide. Booker shows that both ordinary and extraordinary rays are deviated from the vertical plane. In the limiting case of vertical incidence the rays are also deviated laterally, the ordinary ray towards the nearer magnetic pole and the extraordinary ray towards the equator. In some cases this lateral deviation may be as large as 50 km.

CHAPTER II.

RADIO EXPLORATION OF THE IONOSPHERE.

1. Experimental Methods.

Modern methods of investigating the ionosphere are almost exclusively based on the method of BREIT & TUVE (5). A train of pulses is transmitted. This travels directly to an adjacent receiver and also by way of reflection from the ionosphere. The time delay between the two trains of pulses so received is measured and an estimate of the height of reflection can be made from the relationship

$$2h' = ct \qquad (2.1)$$

where h' is the apparent or virtual height, c the velocity of light, and t the time taken for a pulse to travel to the reflection point and return, a distance of 2h'. The height of reflection, h', obtained in this way is not the true height of the ionosphere layer because as soon as the wave reaches the ionosphere its group velocity decreases and is no longer equal to c so that it suffers retardation. The virtual height is thus always greater than the true height of the layer. The calculation of the true height from the virtual height is a complicated process which will be discussed in Chapter III.

2. The Virtual Height.

Consider a slab, thickness dh, height h, in a horizontally stratified ionosphere. A ray passing through it will travel

with a group velocity U where

$$U = c/\mu' \qquad (1.31)$$

The time, dt, taken for it to pass through the slab will be given by

$$dt = dh/U \qquad (2.2)$$

The total time taken for the group to travel from the ground, through the ionosphere, to be reflected, and to return to the ground will then be

$$t = 2\int_o^h dh/U \quad \text{or} \quad ct = 2\int_o^h \mu' \, dh$$

But by (2.1) $ct = 2h'$ and thus

$$h' = \int_o^h \mu' \, dh \qquad (2.3)$$

This relationship is the basis of all methods of determining the true height from the experimentally determined virtual height.

In the case of no magnetic field equation (2.3), in combination with equation (1.33), becomes

$$h' = \int_o^h dh/\mu \qquad (2.4)$$

3. The Pulse Equipment.

A typical ionosonde consists of four main components:-

(a) A transmitter which is able to transmit a train of pulses, the carrier frequency of which may be varied continuously and automatically.

(b) A receiver which is capable of receiving these pulses, and which automatically remains tuned to the transmitter as it

sweeps through its frequency range.

(c) An antenna system, preferably directional, but not necessarily so.

(d) Some method of displaying the results in permanent form. This usually takes the form of an oscilloscope display which may be photographed, giving a graph of virtual height vs frequency.

We shall describe briefly the ionosonde operated at Rhodes University to obtain records during the solar eclipse of 25 December 1954. This instrument is typical of its kind. It has since been modified to improve its frequency range, power output, and - to some extent - its reliability. We shall give specifications as they were on 25 December 1954. A full description of the equipment is given by McELHINNY (34).

4. The Transmitter.

This transmitted pulses of length 100 microseconds and spacing 20 milliseconds. These were obtained by squaring and differentiating the wave from the 50 c/s A.C. mains. The power input to the aerial was nominally about 2 kilowatts. The frequency range was from 1.5 Mc/s to 15.0 Mc/s, covered in a single band by the method due to WADLEY (35). Essentially, a fixed oscillator of frequency 30 Mc/s beating against a variable oscillator with frequency range 31.5 Mc/s to 45.0 Mc/s was used to vary the frequency.

5. The Receiver.

This was designed to receive the pulses without being saturated by the strong ground pulse. The same variable oscillator as was used in the transmitter was the local oscillator of a superheterodyne receiver giving an intermediate frequency of 30 Mc/s with the incoming signals of 1.5 Mc/s to 15.0 Mc/s. In this way transmitter and receiver remained tuned to one another and the frequency could be swept over the whole range by the rotation of a single condenser.

6. The Display System.

The method used in the Rhodes University ionosonde for displaying the records is a standard one which is almost universally in use. As an understanding of its operation is essential to a proper insight into records, or ionograms, obtained from it, we shall describe it in some detail.

The received pulses are displayed on a cathode ray oscilloscope. This could have a sweep equal to the interval between pulses. Since this interval is 20 milliseconds a maximum virtual height of 3,000 km. could be recorded. This is unnecessary as the maximum virtual height recorded under normal conditions is very much less than this. It is therefore desirable to have the whole width of the oscilloscope trace corresponding to something like 1,500 km. If the time base were merely amplified so that only the first half was displayed

on the screen distortion might arise. A delay type time base of the form shown in Figure 6a is therefore used in the Rhodes University ionosonde. We now get a display on the screen as shown in Fig.6b. The large pulse on the left is the ground pulse, while the other pulses are, from left to right, the pulse received after one reflection from the ionosphere, the pulse received after it has been reflected from the ionosphere, the earth, and the ionosphere again, and so on. Usually absorption prevents more than the first two or three from being seen but this is not important as the only pulses which are normally of interest are the ground pulse and the first reflection. All the screen except the portion between the dotted lines is masked. A camera, which has a device for moving the film continuously in the direction of the arrow, is placed in front of the screen and operated while the transmitter and receiver sweep through their frequency range. The time base is of course recorded over the whole width of the film except at those points where there are discontinuities on account of the pulses. These discontinuities leave their trace on the film, a record of the variation of h' with f thus being obtained. In addition frequency and height marks are recorded on the film at intervals. The frequency marks are supplied by a 500 kc/s oscillator which provides a wave rich in harmonics. This produces audio beats with the main variable oscillator, the 60th harmonic beating with 30 Mc/s, the 61st with 30.5 Mc/s and so on.

FIGURE 6a: Delay type time base.

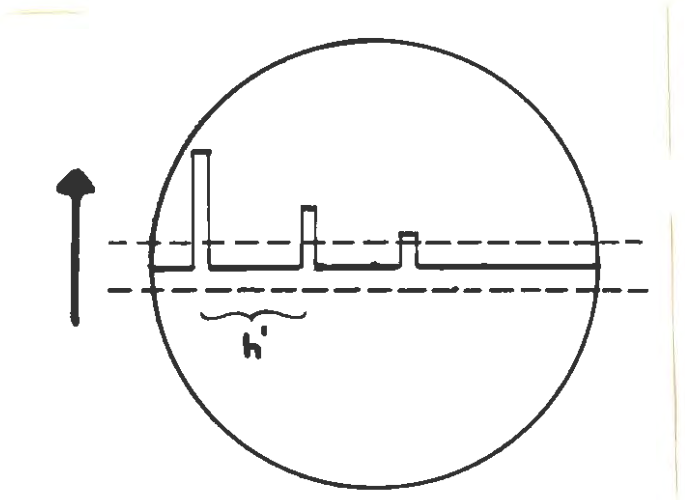

FIGURE 6b: The display on the oscilloscope screen.

Beats also occur with the second harmonic of the variable oscillator so that a frequency mark is, in fact, produced every 0.25 Mc/s. The height marks are produced by a 3 kc/s oscillator which is made to produce a series of pulses on the time base of the oscilloscope. The time delay between these pulses is $\frac{1}{3,000}$ sec., corresponding to a distance of 100 km. for a wave travelling with the velocity of light and thus to a virtual height of 50 km. These marks are only applied to the oscilloscope when the frequency mark is applied. Fig. 7 shows how the calibration marks on a normal record appear.

We are now in a position to discuss the form of the ionograms or h'-f records.

7. The form of the h'-f Curves.

Suppose we have an electron distribution such as that shown in Figure 1. Suppose an ionosonde with its frequency sweeping from about 1 Mc/s to about 12 Mc/s is used to probe this distribution. The lower horizontal scale in Figure 1 shows the plasma frequencies corresponding to the electron densities in the upper horizontal scale.

Consider the ordinary ray. It is reflected when its frequency becomes equal to the plasma frequency. Normally very little reflection is observed from the D region but when the frequency reaches a value corresponding to point A in the

FIGURE 7: The frequency calibrations.

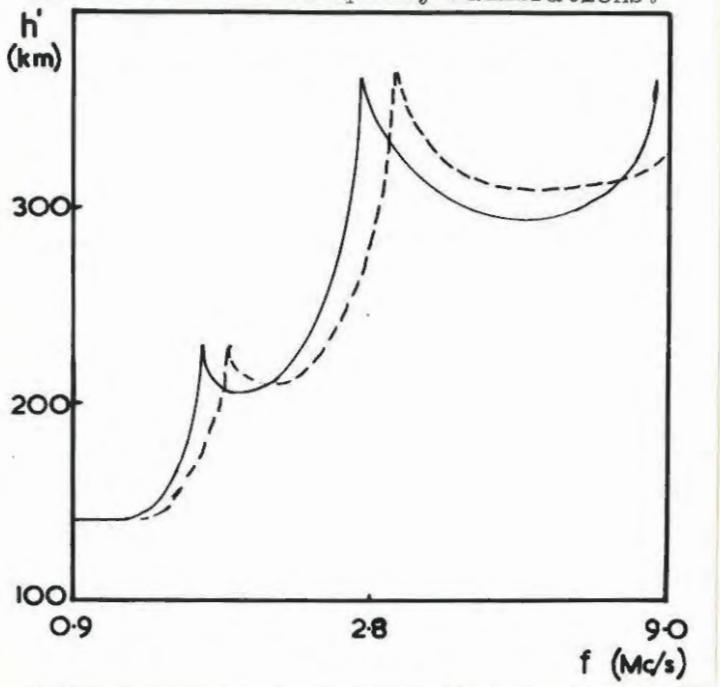

FIGURE 8: Typical h'-f distribution.

FIGURE 9: Typical daytime record.

figure reflection is first observed. Most of the retardation takes place when the wave frequency is close to the plasma frequency. This means that when the slope, dh/df_o, is small there will not be a great deal of retardation since for most of its path the plasma frequency is well removed from the wave frequency. Near point B, however, the slope, dh/df_o, is large and for a considerable portion of its path the ray is in a region where the plasma frequency is near to the wave frequency. There is a great deal of retardation and h' will be considerably greater than h, rising to an extremely large value when the point B is reached and the ray penetrates the E layer. Now as the frequency increases the retardation decreases so that the virtual height once more decreases. The curve shows similar characteristics at point C, the maximum of the F1 layer. At D it finally penetrates the ionosphere and no further reflections are observed.

The extraordinary ray behaves in much the same manner. The frequency which is reflected at a given height is, however, different since reflection takes place where $X = 1 - Y$

or $$f_o^2/f^2 = 1 - f_H/f$$

or $$f_o^2 = f^2 - ff_H \qquad (2.5)$$

so that for a given frequency, f, the extraordinary wave is reflected at a lower electron density. The result is that the extraordinary h'-f curve is shifted to the right. In figure 8 the h'-f curve which would be obtained from a distribution

such as that in figure 1 is shown. Figure 9 shows a typical daytime record obtained by the Rhodes Ionosonde.

CHAPTER III.

THE REDUCTION OF IONOGRAMS.

1. The Problem.

The only experimental data obtainable in normal circumstances are the h'-f curves supplied by an ionosonde. From these we must obtain some idea of the distribution of electrons with height. We know that

$$h' = \int_0^h \mu' dh \qquad (2.3)$$

μ' is a complicated function of f, N, and H while N is a function of h. It is thus possible in principle to solve the equation for h. Because of the complicated nature of the expression for μ' an analytic solution of equation (2.3) is impossible. Numerical methods of one kind or another must be used.

2. An Outline of the Types of Method Used.

A complete survey of methods of finding N-h profiles from h'-f curves is given by THOMAS (36). A very complete list of references is included in the survey.

Methods of attacking the problem can be divided into three types:

(a) Model methods: A layer of the ionosphere is assumed to have a shape such that substitution into (2.3) gives an

integral which can be evaluated analytically. An h'-f curve is calculated for the assumed distribution and compared with the observed curve. It is made to fit the observed curve as well as possible by choosing the parameters appropriately. It has the great disadvantage that an ionospheric layer is not always willing to be thrust into a mould which suits the mathematician. These methods are now chiefly of historical interest having largely been superseded by methods in the other two groups.

(b) Direct inversion of equation (2.3): The equation is inverted to give an analytic solution for h. The expression for h then takes the form of an integral which must be evaluated. This is done by a numerical method. KELSO's method (37) is typical of these and in its simple form (ignoring the earth's magnetic field) has been used in some of the work described in this thesis. It is described below in more detail.

(c) Lamination methods: The N-h profile is divided into a number of horizontal laminations and some assumption is made about the shape of the curve within the lamination. Usually this is that N or f_o is linear with h although TITHERIDGE (38) for convenience in calculation uses a linear variation of $N^{\frac{1}{2}}$ with h. The shape assumed is immaterial provided that the laminations are sufficiently thin. Any degree of accuracy may be attained by taking a sufficient number of laminations.

If the thickness of a lamination is Δh the integral (2.3) can be replaced by a sum

$$h' = \Sigma \mu' \Delta h \qquad (3.1)$$

The principle was first used by MURRAY & HOLG (39)(40) in 1937. It was neglected for some time but has now become very important. BUDDEN's (41) matrix method was the start of the revival. JACKSON's (42) and TITHERIDGE's (38) methods are now typical of the class. Titheridge's method is discussed in some detail below as it is used extensively in the present work.

3. Kelso's Method.

KELSO first suggested a method of reduction ignoring the earth's magnetic field (37) and later one which was based on the same ideas and which included the earth's field (43). We shall consider only the simple method which is the one used in this thesis.

Equation (2.4) is inverted getting an expression for h

$$h = \frac{1}{\pi} \int_0^1 \frac{h' dX}{\sqrt{X(1 - X)}}$$

$$= \frac{1}{2\pi} \int_{-1}^{1} \frac{h' dX}{\sqrt{X(1 - X)}} \qquad (3.2)$$

where h' is defined to be an even function of $X^{\frac{1}{2}}$, this being

possible since it is normally defined only for positive values of the frequency, f, i.e. for positive values of $X^{\frac{1}{2}}$ so that we are free to define it for negative values of $X^{\frac{1}{2}}$ so that the desired condition is fulfilled.

The substitution

$$\cos^2\theta = X \tag{3.3}$$

is then made, getting

$$h = \frac{1}{\pi} \int_0^{\pi} h' d\theta \tag{3.4}$$

where h' is now a function of $\cos\theta$. By dividing the h' curve into n equal steps in θ the function to be integrated is replaced by a polynomial. On this basis Kelso, using the Gauss-Christoffel quadrature formula, shows that

$$h = \frac{1}{n} \sum_{k=1}^{n} h'_k \tag{3.5}$$

where h is the real height corresponding to a frequency f_k at which the virtual height is h'_k; the set of frequencies f_k are given by

$$f_k = f \cos \frac{2k - 1}{2n} \tag{3.6}$$

k being an integer between 1 and n.

The number of terms in the polynomial is n and the larger we make n the more accurate the fit. In practice it is found that if the h'-f curve is reasonably smooth n = 5 is sufficiently accurate. If the curve contains any cusps

then it is better to take n = 10.

In practice all that is needed to determine the true height at a frequency, f, is the average of the virtual heights at a number of frequencies, f_k, each of which is a fixed fraction of f. If we plot f_k vs. f we get a set of straight lines from which the f_ks corresponding to any f can be read. Figure 10 which is based on Kelso's figure 1 shows these lines for n = 5 and n = 10.

4. Titheridge's Method.

The N-h curve is divided into a series of heights, h_r, corresponding to a set of virtual heights h_r' at a given series of frequencies f_r. If $\overline{\mu'_{r,n}}$ is the mean value of μ' over the lamination h_{r-1} to h_r for a probing frequency f_n then from equation (2.3)

$$\overline{\mu'_{r,n}} = \frac{1}{h_r - h_{r-1}} \int_{h_{r-1}}^{h_r} \mu' dh \qquad (3.7)$$

Now at any frequency the virtual height is given by the height of the bottom of the ionosphere, h_o, plus the sum of the virtual path lengths in each lamination up to the nth. If we let $\Delta h_r = h_r - h_{r-1}$ then we get the following set of equations for the virtual heights corresponding to r = 1, r = 2,...

...r.

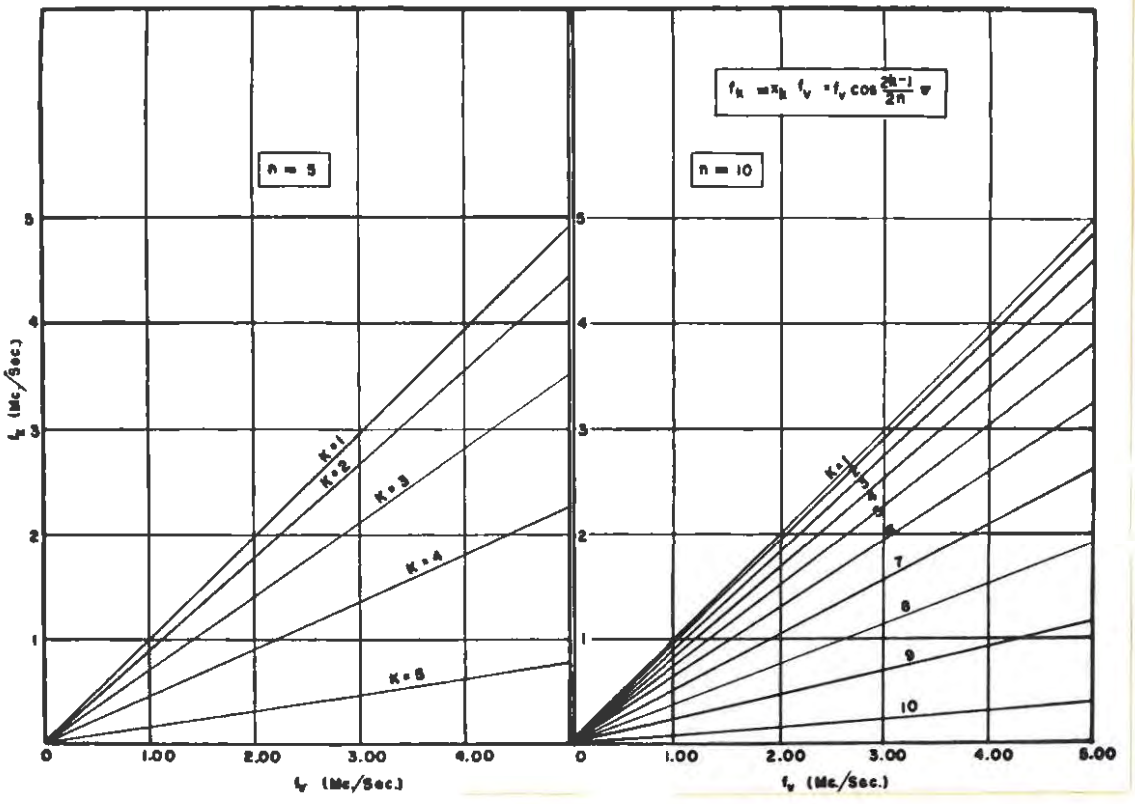

FIGURE 10: Kelso's diagrams giving frequencies, f_k, at which heights must be read for obtaining the true height at a frequency f_v.

$$h'_o = h_o$$

$$h'_1 = h_o + \overline{\mu'_{1,2}}\,\Delta h_1$$

$$h'_2 = h_o + \overline{\mu'_{1,2}}\,\Delta h_1 + \overline{\mu'_{2,2}}\,\Delta h_2$$

$$\cdots\cdots\cdots\cdots\cdots\cdots\cdots\cdots\cdots\cdots$$

$$h'_r = h_o + \overline{\mu'_{1,r}}\,\Delta h_1 + \overline{\mu'_{2,r}}\,\Delta h_2 + \cdots\cdots$$

$$\overline{\mu'_{r,r}}\,\Delta h_r \qquad (3.8)$$

By subtraction

$$h'_o = h_o$$

$$\Delta h'_1 = \overline{\mu'_{1,1}}\,\Delta h_1$$

$$\Delta h'_2 = \overline{\mu'_{2,2}}\,\Delta h_2 - (\overline{\mu'_{1,1}} - \overline{\mu'_{1,2}})\,\Delta h_1$$

$$\cdots\cdots\cdots\cdots\cdots\cdots\cdots\cdots\cdots\cdots$$

$$\Delta h'_n = \overline{\mu'_{n,n}}\,\Delta h_n - (\overline{\mu'_{n-1,n-1}} - \overline{\mu'_{n-1,n}})\,\Delta h_{n-1} - \cdots$$

$$\cdots - (\overline{\mu'_{r,n-1}} - \overline{\mu'_{r,n}})\,\Delta h_r - \cdots\cdots$$

$$\cdots - (\overline{\mu'_{1,n-1}} - \overline{\mu'_{1,n}})\,\Delta h_1 \qquad (3.9)$$

Now write $\beta_{r,n} = \overline{\mu'_{r,n-1}} - \overline{\mu'_{r,n}} \qquad r < n$

and $\beta_{n,n} = \overline{\mu'_{n,n}} \qquad r = n \qquad (3.10)$

and the equations (6.7)becomes

$$h'_o = h_o$$

$$\Delta h'_1 = \beta_{11}\Delta h$$

$$\Delta h'_2 = \beta_{22}\Delta h_2 - \beta_{12}\Delta h_1$$

.....

$$\Delta h'_n = \beta_{nn}\Delta h_n - \beta_{n-1,n}\Delta h_{n-1} - .....$$

$$- \beta_{r,n}\Delta h_r - .... - \beta_{1,n}\Delta h_1 \qquad (3.11)$$

Solving these successively

$$h_o = h'_o$$

$$\Delta h_1 = \frac{1}{\beta_{1,1}} \Delta h'_1$$

$$\Delta h_2 = \frac{1}{\beta_{2,2}} \left\{ \Delta h'_2 + \beta_{1,2} \Delta h_1 \right\}$$

.....

$$\Delta h_n = \frac{1}{\beta_{n,n}} \left\{ \Delta h'_n + \sum_{r=1}^{n-1} \beta_{r,n} \Delta h_r \right\} \qquad (3.12)$$

If the coefficients, β, are known it is easy to obtain $\Delta h_1, \Delta h_2, \Delta h_3$, etc. successively from the above equations. In practice it is found that only when r is not much smaller than n, is β of any importance so that summation of only a few terms is necessary.

5. The Calculation of Titheridge's Coefficients, β.

The method suggested by Titheridge for calculating the coefficients, β, for a given locality involves making an approximation for the quantity μ'. Since exact values of μ' were available for Grahamstown, having been calculated by the author as described in section 8 of Chapter I, this was unnecessary. $\beta_{r,n}$ in the lamination h_{r-1} to h_r was found by getting $\mu'_{r,n-1}$ and $\mu'_{r,n}$ from Figure 2 or Figure 3 for the ordinary or extraordinary ray respectively, and calculating the difference. The method adopted by the author for the calculation of the coefficients is described below.

First a set of frequencies must be chosen to define the boundaries of the laminations. It was decided for comparison purposes to take the same number of laminations as did Titheridge. The frequencies chosen were given by

$$f_n = A \log (1 + \frac{n}{2}) \qquad (3.13)$$

where n goes from 1 to 25 and A is a constant chosen so that $f_{25} = 6$ Mc/s. After the calculation of the coefficients it was found that owing to an error in Titheridge's paper this was not the form of the expression giving the frequencies which Titheridge himself had used. However, this was not important as any frequency interval which gives values of Δh which are not too wildly unequal is sufficiently good.

For the ordinary ray the values of Y corresponding to the various frequencies were first calculated. Values of X_r, the value of X corresponding to the mean value of N in the rth lamination when the probing frequency is f_n, were calculated for each f_n, and are shown tabulated in Table 1. Next the values of $\mu'_{r,n}$ corresponding to each value of X were found. It was assumed in doing this that the variation of N with h in each lamination was linear. $\mu'_{n,n}$ was found by a rather more complicated calculation since we cannot assume that near the reflection point the mean value of μ' corresponds to the mean value of X in the lamination. The method of calculating $\mu'_{n,n}$ is described below. The values of $\mu'_{r,n}$ are shown in Table 2. Finally the coefficients, β, are found from Table 2 by cross subtraction between the columns according to equation (3.10). β is tabulated in Table 3.

For the extraordinary ray the procedure appears to be slightly more complicated. The frequencies defining the boundaries of the layers are plasma frequencies. The extraordinary ray frequencies which correspond to them (i.e. the frequency of the extraordinary wave which is reflected at the level which has that plasma frequency) must now be calculated from equation (2.5). Values of Y and 1-Y are now found for these frequencies. The quantity X/(1-Y) is now calculated and the values of $\overline{\mu'_{r,n}}$ corresponding to this value of

X/(1-Y) found from Figure 3. However, it can easily be shown from equation (2.5) that the quantity X/(1-Y) for the extraordinary ray at a given plasma frequency is equal to the quantity X for the ordinary ray at the same plasma frequency so that the values of X in Table 1 can be used as values of X/(1-Y) and the values of μ' and hence β found. $\overline{\mu'}_{r,n}$ for the extraordinary ray is shown in Table 4 and β in Table 5. The values of $\beta_{n,n}$ must be found as described below.

μ' varies extremely rapidly with N in the last lamination before it is reflected. Its value at the bottom of the lamination is likely to be about 3 or 4, while at the reflection point it is of course infinite. It only attains extremely large values over a very small part of the lamination near the top. For this reason the mean value of μ' in the lamination is considerably higher than the value of μ' which corresponds to the mean value of N in the lamination. The following approach is therefore adopted.

Ordinary Ray:

By equation (2.3)

$$\Delta h'_n = \int_{h_{n-1}}^{h_n} \mu' \, dh \qquad (3.14)$$

$$= \int_{X_n}^{1} \mu' \frac{dh}{dX} \, dX$$

where X_n is the value of X corresponding to the value of N at the bottom of the lamination. The value of X_n given in Table 1 is this value and not the value corresponding to the mean value of N in the lamination. Now if we once more assume that N - and therefore X - varies linearly with h within the lamination then dh/dX is constant so that we get

$$\Delta h'_n = \frac{dh}{dX} \int_{X_n}^{1} \mu' \, dX \qquad (3.15)$$

Equation (1.35) is

$$t^2 = 1 - X$$

Differentiating

$$2t \, dt = - dX$$

Substituting in (3.15)

$$\Delta h'_n = -2\frac{dh}{dX} \int_{t_n}^{o} \mu' t \, dt$$

$$= +2\frac{dh}{dX} \int_{o}^{t_n} \mu' t \, dt \qquad (3.16)$$

But if dh/dX is constant

$$dh/dX = \Delta h/\Delta X$$

$$= \Delta h/(1-X_n)$$

$$= \Delta h/t^2{}_n$$

Thus (3.16) becomes

$$\frac{\Delta h'_n}{\Delta h_n} = \frac{2}{t_n^2} \int_0^{t_n} \mu' t \, dt \qquad (3.17)$$

But $\Delta h'_n / \Delta h_n$ is by definition equal to $\overline{\mu'_{n,n}}$, the mean value of the refractive index in the lamination so that equation (3.17) is an equation giving $\overline{\mu'_{n,n}}$. The integral can easily be found by using Figure 4. The method adopted by the author was to evaluate the integral by means of a planimeter and hence calculate $\overline{\mu'_{n,n}} = \beta_{n,n}$. The values obtained are shown in Tables 2 and 3.

Extraordinary Ray:

An exactly analogous procedure is adopted. Equation (3.15) applies to the extraordinary as well as to the ordinary ray except that the upper limit is 1-Y instead of unity. Equation (1.36) is

$$t^2 = 1 - \frac{X}{1-Y}$$

Differentiating

$$2t \, dt = - \frac{dX}{1-Y}$$

for a given value of Y. Substituting in (3.15)

$$\Delta h'_n = +2\frac{dh}{dX}(1-Y) \int_0^{t_n} \mu' t \, dt$$

Thus $\overline{\mu'_{n,n}} = \frac{\Delta h'_n}{\Delta h_n} = \frac{2(1-Y)}{\Delta X} \int_0^{t_n} \mu' t \, dt$

But $\Delta X = 1-Y-X_n$ so that this becomes

$$\overline{\mu' n,n} = \frac{2}{t^2_n} \int_o^{t_n} \mu' t \, dt \qquad (3.18)$$

as before.

6. Approximate Titheridge Coefficients.

Titheridge in his paper shows how the coefficients $\beta_{r,n}$ rapidly become negligible in comparison with $\beta_{n,n}$ as r decreases. Only the few largest coefficients near the bottom of Tables 3 and 5 need be considered. To improve accuracy the lower coefficients in the table may be increased to compensate for the neglected upper coefficients so that the value of $\sum_{r=1}^{n} \beta_{r,n}$ remains unchanged. The coefficients for the ordinary ray, modified in this manner, are shown in Table 6 and those for the extraordinary ray in Table 7.

TABLE 1: Tables of X and Y corresponding to the frequencies chosen for the evaluation of the Titheridge coefficients.

$f_H = 0.82$ Mc/s.

n	1	2	3	4	5	6	7	8
f_1 Mc/s	0.95	1.62	2.14	2.56	2.93	3.24	3.51	3.76
Y	0.862	0.506	0.383	0.348	0.280	0.253	0.234	0.218
X_1	0	0.069	0.039	0.027	0.021	0.017	0.015	0.013
X_2		0.343	0.360	0.252	0.192	0.157	0.134	0.117
X_3			0.572	0.539	0.411	0.336	0.287	0.250
X_4				0.695	0.644	0.526	0.448	0.391
X_5					0.769	0.718	0.612	0.533
X_6						0.817	0.772	0.673
X_7							0.850	0.806
X_8								0.873

n	9	10	11	12	13	14	15	16
f_1 Mc/s	3.98	4.19	4.38	4.54	4.70	4.85	5.00	5.13
Y	0.206	0.196	0.187	0.181	0.174	0.169	0.164	0.160
X_1	0.011	0.010	0.009	0.009	0.008	0.008	0.007	0.006
X_2	0.104	0.094	0.086	0.080	0.075	0.070	0.066	0.063
X_3	0.223	0.201	0.184	0.171	0.160	0.150	0.141	0.134
X_4	0.349	0.314	0.288	0.268	0.250	0.235	0.220	0.210
X_5	0.476	0.429	0.393	0.366	0.341	0.320	0.301	0.286
X_6	0.601	0.542	0.496	0.462	0.431	0.404	0.381	0.361
X_7	0.719	0.649	0.594	0.553	0.516	0.484	0.455	0.432
X_8	0.834	0.752	0.689	0.641	0.598	0.562	0.528	0.502
X_9	0.891	0.853	0.781	0.727	0.678	0.637	0.599	0.569
X_{10}		0.905	0.870	0.810	0.756	0.710	0.667	0.634
X_{11}			0.916	0.891	0.831	0.781	0.734	0.698
X_{12}				0.925	0.900	0.845	0.795	0.756
X_{13}					0.932	0.907	0.853	0.811
X_{14}						0.939	0.912	0.866
X_{15}							0.944	0.972
X_{16}								0.948

Table 1 continued:

n	17	18	19	20	21	22	23	24
f_1 Mc/s	5.26	5.39	5.49	5.59	5.71	5.81	5.91	6.00
Y	0.153	0.152	0.149	0.147	0.144	0.141	0.139	0.137
X_1	0.006	0.006	0.006	0.006	0.005	0.005	0.005	0.006
X_2	0.060	0.057	0.055	0.053	0.051	0.049	0.047	0.046
X_3	0.128	0.122	0.117	0.113	0.108	0.105	0.101	0.098
X_4	0.200	0.190	0.183	0.177	0.169	0.164	0.158	0.155
X_5	0.272	0.259	0.250	0.241	0.231	0.223	0.216	0.209
X_6	0.344	0.328	0.316	0.305	0.292	0.282	0.273	0.264
X_7	0.412	0.392	0.378	0.364	0.349	0.337	0.326	0.315
X_8	0.478	0.455	0.438	0.423	0.405	0.391	0.378	0.397
X_9	0.542	0.516	0.497	0.479	0.460	0.444	0.479	0.416
X_{10}	0.603	0.514	0.554	0.534	0.512	0.494	0.478	0.463
X_{11}	0.664	0.632	0.509	0.588	0.563	0.544	0.526	0.571
X_{12}	0.719	0.685	0.660	0.637	0.610	0.589	0.570	0.552
X_{13}	0.772	0.734	0.708	0.683	0.655	0.632	0.611	0.591
X_{14}	0.824	0.785	0.756	0.730	0.699	0.675	0.653	0.633
X_{15}	0.877	0.835	0.805	0.776	0.744	0.719	0.695	0.674
X_{16}	0.927	0.883	0.851	0.821	0.787	0.760	0.735	0.712
X_{17}	0.952	0.929	0.895	0.864	0.828	0.799	0.773	0.750
X_{18}		0.956	0.941	0.908	0.870	0.840	0.812	0.787
X_{19}			0.959	0.947	0.908	0.876	0.847	0.820
X_{20}				0.962	0.949	0.909	0.879	0.852
X_{21}					0.964	0.950	0.914	0.888
X_{22}						0.966	0.950	0.921
X_{23}							0.968	0.952
X_{24}								0.970

TABLE 2: μ' at Titheridge frequencies for ordinary ray.

$f_H = 0.82$ Mc/s.

f	0.948	1.621	2.143	2.570	2.931	3.243	3.578	3.765
n	1	2	3	4	5	6	7	8
r=1	2.347	1.02	1.01	1.01	1.01	1.01	1.01	1.01
2		3.177	1.15	1.11	1.09	1.08	1.07	1.06
3			4.007	1.28	1.19	1.15	1.12	1.11
4				4.837	1.41	1.28	1.22	1.19
5					5.667	1.54	1.33	1.31
6						6.497	1.67	1.47
7							7.327	1.80
8								8.157

f	3.988	4.191	4.378	4.552	4.713	4.864	5.006	5.139
n	9	10	11	12	13	14	15	16
r=1	1.01	1.01	1.01	1.01	1.01	1.01	1.01	1.01
2	1.05	1.05	1.05	1.05	1.05	1.05	1.05	1.05
3	1.10	1.09	1.08	1.07	1.07	1.07	1.07	1.07
4	1.17	1.15	1.14	1.13	1.12	1.11	1.10	1.09
5	1.26	1.22	1.20	1.18	1.17	1.16	1.15	1.14
6	1.39	1.33	1.29	1.26	1.23	1.21	1.19	1.17
7	1.56	1.45	1.39	1.34	1.31	1.28	1.25	1.23
8	1.93	1.64	1.53	1.46	1.42	1.38	1.34	1.32
9	8.987	2.06	1.75	1.60	1.51	1.46	1.40	1.36
10		9.807	2.19	1.85	1.67	1.58	1.50	1.46
11			10.627	2.32	1.94	1.75	1.64	1.55
12				11.447	2.45	2.01	1.80	1.69
13					12.267	2.58	2.08	1.86
14						13.087	2.71	2.14
15							13.907	2.84
16								14.727

f	5.266	5.386	5.500	5.609	5.713	5.813	5.908	6.000
n	17	18	19	20	21	22	23	24
r=1	1.01	1.01	1.01	1.01	1.01	1.01	1.01	1.01
2	1.05	1.05	1.05	1.05	1.05	1.05	1.05	1.05
3	1.07	1.07	1.07	1.07	1.07	1.07	1.07	1.07
4	1.09	1.08	1.08	1.08	1.08	1.08	1.08	1.08
5	1.13	1.12	1.12	1.11	1.11	1.11	1.11	1.11
6	1.16	1.15	1.14	1.13	1.12	1.12	1.11	1.11
7	1.21	1.20	1.19	1.18	1.17	1.16	1.15	1.15
8	1.30	1.28	1.27	1.25	1.24	1.23	1.22	1.21
9	1.34	1.32	1.30	1.28	1.27	1.26	1.25	1.24
10	1.42	1.38	1.36	1.34	1.32	1.30	1.29	1.28
11	1.50	1.46	1.43	1.40	1.37	1.36	1.35	1.33
12	1.61	1.54	1.30	1.47	1.44	1.41	1.39	1.37
13	1.75	1.65	1.59	1.55	1.51	1.47	1.44	1.42
14	1.92	1.80	1.71	1.65	1.59	1.55	1.52	1.49
15	2.21	1.98	1.85	1.76	1.68	1.62	1.58	1.54
16	2.97	2.26	2.06	1.93	1.80	1.73	1.66	1.62
17	15.537	3.10	2.38	2.14	1.96	1.85	1.74	1.68
18		16.347	3.23	2.54	2.18	2.00	1.90	1.81
19			17.157	3.36	2.54	2.23	2.04	1.93
20				17.967	3.49	2.59	2.25	2.08
21					18.767	3.62	2.60	2.31
22						19.567	3.75	2.75
23							20.367	3.88
24								21.167

TABLE 3: Titheridge's coefficients β, ordinary ray.

f_H = 0.82 Mc/s.

f	0.948	1.621	2.143	2.570	2.931	3.243	3.518	3.765
n	1	2	3	4	5	6	7	8
r=1	2.347	1.33	0.01	0.00	0.00	0.00	0.00	0.00
2		3.177	2.03	0.04	0.02	0.01	0.01	0.01
3			4.007	2.73	0.09	0.04	0.03	0.01
4				4.837	3.43	0.13	0.06	0.03
5					5.667	4.13	0.16	0.07
6						6.497	4.83	0.20
7							7.327	5.53
8								8.157

f	3.983	4.191	4.378	4.552	4.713	4.864	5.006	5.139
n	9	10	11	12	13	14	15	16
r=1	0.00	0.00	0.00	0.00	0.00	0.00	0.00	0.00
2	0.01	0.00	0.00	0.00	0.00	0.00	0.00	0.00
3	0.01	0.01	0.01	0.01	0.00	0.00	0.00	0.00
4	0.02	0.02	0.02	0.01	0.01	0.01	0.01	0.01
5	0.05	0.04	0.02	0.02	0.01	0.01	0.01	0.01
6	0.03	0.06	0.04	0.03	0.03	0.02	0.02	0.02
7	0.24	0.11	0.06	0.05	0.03	0.03	0.03	0.02
8	6.23	0.29	0.11	0.07	0.04	0.04	0.04	0.02
9	8.987	6.93	0.31	0.15	0.09	0.05	0.06	0.04
10		9.807	7.62	0.34	0.18	0.09	0.08	0.04
11			10.627	8.31	0.38	0.19	0.11	0.09
12				11.447	9.00	0.44	0.21	0.11
13					12.267	9.69	0.50	0.22
14						13.087	10.38	0.57
15							13.907	11.07
16								14.727

f	5.266	5.386	5.500	5.609	5.713	5.813	5.908	6.000
n	17	18	19	20	21	22	23	24
r=1	0.00	0.00	0.00	0.00	0.00	0.00	0.00	0.00
2	0.00	0.00	0.00	0.00	0.00	0.00	0.00	0.00
3	0.00	0.00	0.00	0.00	0.00	0.00	0.00	0.00
4	0.00	0.01	0.00	0.00	0.00	0.00	0.00	0.00
5	0.01	0.01	0.00	0.01	0.00	0.00	0.00	0.00
6	0.01	0.01	0.01	0.01	0.01	0.00	0.01	0.00
7	0.02	0.01	0.01	0.01	0.01	0.01	0.01	0.00
8	0.02	0.02	0.01	0.02	0.01	0.01	0.01	0.01

f	5.266	5.376	5.500	5.609	5.713	5.813	5.908	6.000
n	17	18	19	20	21	22	23	24
r=9	0.02	0.02	0.02	0.02	0.01	0.01	0.01	0.01
10	0.04	0.04	0.02	0.02	0.02	0.02	0.01	0.01
11	0.05	0.04	0.03	0.03	0.03	0.01	0.01	0.02
12	0.08	0.07	0.04	0.03	0.03	0.03	0.02	0.02
13	0.11	0.11	0.05	0.04	0.04	0.04	0.03	0.02
14	0.22	0.12	0.09	0.06	0.07	0.04	0.03	0.03
15	0.63	0.23	0.13	0.09	0.08	0.06	0.04	0.04
16	11.76	0.71	0.20	0.13	0.13	0.07	0.07	0.04
17	15.537	12.44	0.72	0.24	0.18	0.11	0.11	0.06
18		16.347	12.12	0.69	0.36	0.18	0.10	0.09
19			17.157	13.80	0.82	0.31	0.19	0.11
20				17.967	14.48	0.90	0.34	0.17
21					18.767	15.15	1.02	0.29
22						19.567	15.82	1.00
23							20.367	16.19
24								21.167

TABLE 4: μ' for the extraordinary ray at the Titheridge frequencies. $f_H = 0.82$ Mc/s.

f_o max	0.948	1.621	2.143	2.570	2.931	3.243	3.518	3.765
f	1.443	2.082	2.592	3.013	3.369	3.679	3.952	4.193
Y	5.683	3.929	3.164	2.722	2.434	2.229	2.075	1.953
n	1	2	3	4	5	6	7	8
μ'_1	2.480	1.920	1.04	1.03	1.02	1.015	1.01	1.01
μ'_2		2.998	2.155	1.203	1.15	1.11	1.09	1.076
μ'_3			3.509	2.387	1.395	1.275	1.22	1.18
μ'_4				4.013	2.616	1.55	1.41	1.325
μ'_5					4.510	2.842	1.71	1.53
μ'_6						5.000	3.065	1.86
μ'_7							5.483	3.285
μ'_8								5.959

Table 4 continued:

f_o max.	3.988	4.191	4.378	4.552	4.713	4.864	5.006	5.139
f_x	4.419	4.621	4.807	4.981	5.141	5.291	5.430	5.565
Y	1.856	1.775	1.706	1.646	1.595	1.550	1.510	1.473
n	9	10	11	12	13	14	15	16
μ'_1	1.01	1.01	1.008	1.008	1.008	1.007	1.007	1.007
μ'_2	1.07	1.06	1.055	1.051	1.045	1.04	1.04	1.04
μ'_3	1.155	1.141	1.125	1.115	1.108	1.10	1.09	1.09
μ'_4	1.275	1.24	1.215	1.191	1.172	1.165	1.151	1.145
μ'_5	1.435	1.37	1.325	1.290	1.26	1.24	1.22	1.206
μ'_6	1.66	1.545	1.465	1.407	1.365	1.33	1.305	1.280
μ'_7	2.02	1.78	1.65	1.55	1.49	1.44	1.398	1.365
μ'_8	3.502	2.16	1.92	1.77	1.64	1.565	1.51	1.470
μ'_9	6.428	3.716	2.33	2.03	.1847	1.73	1.65	1.585
μ'_{10}		6.890	3.927	2.43	2.15	1.95	1.82	1.725
μ'_{11}			7.345	4.135	2.58	2.25	2.05	1.905
μ'_{12}				7.793	4.340	2.72	2.35	2.145
μ'_{13}					8.234	4.542	2.85	2.48
μ'_{14}						8.668	4.741	3.00
μ'_{15}							9.095	4.937
μ'_{16}								9.515

f_o max.	5.266	5.386	5.500	5.609	5.713	5.813	5.908	6.000
f_x	5.695	5.810	5.925	6.030	6.140	6.235	6.330	6.425
Y	1.440	1.411	1.384	1.360	1.336	1.315	1.295	1.276
n	17	18	19	20	21	22	23	24
μ'_1	1.007	1.007	1.006	1.006	1.006	1.005	1.005	1.005
μ'_2	1.038	1.035	1.035	1.03	1.03	1.03	1.03	1.03
μ'_3	1.08	1.078	1.075	1.07	1.065	1.065	1.06	1.06
μ'_4	1.135	1.128	1.125	1.115	1.11	1.108	1.105	1.10
μ'_5	1.195	1.18	1.175	1.165	1.155	1.152	1.145	1.143
μ'_6	1.26	1.248	1.235	1.220	1.205	1.200	1.190	1.180
μ'_7	1.34	1.315	1.298	1.280	1.265	1.25	1.24	1.23
μ'_8	1.43	1.395	1.365	1.350	1.325	1.31	1.298	1.277
μ'_9	1.525	1.490	1.455	1.420	1.398	1.375	1.355	1.34
μ'_{10}	1.645	1.590	1.548	1.505	1.475	1.45	1.425	1.405
μ'_{11}	1.800	1.72	1.66	1.605	1.560	1.525	1.498	1.465
μ'_{12}	1.99	1.875	1.79	1.72	1.66	1.615	1.575	1.542
μ'_{13}	2.22	2.08	1.948	1.85	1.775	1.72	1.67	1.62
μ'_{14}	2.55	2.32	2.13	2.02	1.920	1.84	1.77	1.71
μ'_{15}	3.05	2.67	2.40	2.22	2.085	1.975	1.900	1.825
μ'_{16}	5.130	3.20	2.75	2.51	2.28	2.16	2.05	1.955

Table 4 continued:

f_o max.	5.266	5.386	5.500	5.609	5.713	5.813	5.908	6.000
f_x	5.695	5.310	5.925	6.030	6.140	6.235	6.330	6.425
Y	1.440	1.411	1.384	1.360	1.336	1.315	1.295	1.276
n	17	18	19	20	21	22	23	24
μ'_{17}	9.928	5.320	3.30	2.85	2.56	2.385	2.22	2.11
μ'_{18}		10.334	5.507	3.43	2.92	2.65	2.45	2.29
μ'_{19}			10.733	5.691	3.53	3.05	2.75	2.52
μ'_{20}				11.126	5.872	3.68	3.13	2.80
μ'_{21}					11.513	6.050	3.81	3.22
μ'_{22}						11.894	6.225	3.90
μ'_{23}							12.269	6.398
μ'_{24}								12.639

TABLE 5: Titheridge's Coefficients, β, for the extraordinary ray. f_H = 0.82 Mc/s.

f_o	0.948	1.621	2.143	2.570	2.931	3.243	3.518	3.765
f_x	1.443	2.082	2.592	3.013	3.369	3.679	3.952	4.198
Y	0.568	0.394	0.316	0.272	0.243	0.223	0.208	0.195
n	1	2	3	4	5	6	7	8
r=1	2.480	0.560	0.880	0.010	0.010	0.005	0.005	0.000
2		2.998	0.843	0.952	0.053	0.040	0.020	0.014
3			3.509	1.122	0.992	0.120	0.055	0.040
4				4.013	1.397	1.066	0.140	0.085
5					4.510	1.668	1.132	0.180
6						5.000	1.935	1.205
7							5.483	2.198
8								5.959

f_o	3.988	4.191	4.378	4.552	4.713	4.864	5.006	5.139
f_x	4.419	4.621	4.807	4.981	5.141	5.291	5.430	5.565
Y	0.186	0.178	0.171	0.165	0.160	0.155	0.151	0.147
n	9	10	11	12	13	14	15	16
r=1	0.000	0.000	0.000	0.000	0.000	0.000	0.000	0.000
2	0.006	0.010	0.005	0.004	0.006	0.005	0.000	0.000
3	0.025	0.014	0.016	0.010	0.007	0.008	0.010	0.000
4	0.050	0.035	0.025	0.024	0.014	0.012	0.014	0.006
5	0.095	0.065	0.045	0.035	0.030	0.020	0.020	0.014

Table 5 continued:

f_o	3.988	4.191	4.378	4.552	4.713	4.864	5.006	5.139
f_x	4.419	4.621	4.807	4.981	5.141	5.291	5.430	5.565
Y^x	0.186	0.178	0.171	0.165	0.160	0.155	0.151	0.147
n	9	10	11	12	13	14	15	16
r=6	0.200	0.115	0.080	0.053	0.042	0.035	0.025	0.025
7	1.265	0.240	0.130	0.100	0.060	0.050	0.042	0.033
8	2.457	1.342	0.240	0.150	0.130	0.075	0.055	0.040
9	6.248	2.712	1.386	0.280	0.183	0.117	0.080	0.065
10		6.890	2.963	1.497	0.300	0.200	0.130	0.095
11			7.345	3.210	1.555	0.330	0.200	0.145
12				7.793	3.543	1.620	0.370	0.205
13					8.234	3.692	1.692	0.370
14						8.668	3.927	1.741
15							9.095	4.158
16								9.515

f_o	5.266	5.386	5.500	5.609	5.713	5.813	5.908	6.000
f_x	5.695	5.810	5.925	6.030	6.140	6.235	6.330	6.425
Y^x	0.144	0.141	0.138	0.136	0.134	0.132	0.130	0.128
n	17	18	19	20	21	22	23	24
r=1	0.000	0.000	0.000	0.000	0.000	0.000	0.000	0.000
2	0.002	0.003	0.000	0.005	0.000	0.000	0.000	0.000
3	0.010	0.002	0.003	0.005	0.005	0.000	0.005	0.000
4	0.010	0.007	0.003	0.010	0.005	0.002	0.003	0.005
5	0.011	0.015	0.005	0.010	0.010	0.003	0.007	0.002
6	0.020	0.012	0.013	0.015	0.015	0.005	0.010	0.010
7	0.025	0.025	0.017	0.018	0.015	0.015	0.010	0.010
8	0.040	0.035	0.030	0.015	0.025	0.015	0.012	0.021
9	0.060	0.035	0.035	0.035	0.022	0.023	0.023	0.015
10	0.080	0.055	0.042	0.043	0.030	0.025	0.025	0.020
11	0.105	0.080	0.060	0.055	0.045	0.035	0.027	0.033
12	0.155	0.115	0.085	0.070	0.060	0.045	0.040	0.033
13	0.260	0.140	0.132	0.098	0.075	0.055	0.050	0.050
14	0.380	0.230	0.190	0.110	0.100	0.080	0.070	0.060
15	1.887	0.450	0.270	0.180	0.135	0.110	0.075	0.075
16	4.385	1.930	0.450	0.240	0.230	0.120	0.110	0.095
17	9.928	4.608	2.020	0.450	0.290	0.175	0.165	0.110
18		10.334	4.827	2.077	0.480	0.270	0.200	0.160
19			10.733	5.042	2.161	0.510	0.300	0.230
20				11.126	5.254	2.192	0.550	0.330
21					11.513	5.463	2.240	0.590
22						11.894	5.669	2.325
23							12.269	5.871
24								12.639

TABLE 6: Simplified Titheridge Coefficients. Ordinary Ray.

f_H = 0.82 Mc/s.

n	1	2	3	4	5	6	7	8
f	0.948	1.621	2.143	2.570	2.930	3.243	3.518	3.765
			0.01	0.04	0.11	0.18	0.26	0.32
		1.33	2.03	2.73	3.43	4.13	4.83	5.53
	2.35	3.13	4.01	4.84	5.67	6.50	7.33	8.16

n	9	10	11	12	13	14	15	16
f	3.988	4.191	4.378	4.562	4.713	4.864	5.006	5.139
								0.36
	0.41	0.53	0.58	0.64	0.70	0.84	1.00	0.66
	6.23	6.93	7.62	8.31	9.00	9.69	10.38	11.07
	8.99	9.81	10.63	11.45	12.27	13.09	13.91	14.73

n	17	18	19	20	21	22	23	24
f	5.266	5.386	5.500	5.609	5.713	5.813	5.908	6.000
	11.76	12.44	13.12	13.80	14.48	15.15	15.82	16.49
	15.54	16.35	17.16	17.97	18.77	19.57	20.37	21.17

TABLE 7: Simplified Titheridge Coefficients. Extraordinary Ray. f_H = 0.82 Mc/s.

n	1	2	3	4	5	6	7	8
f	0.948	1.621	2.143	2.570	3 931	3.243	3.518	3.765
								0.20
			0.88	0.96	1.05	1.23	1.35	1.32
		0.56	0.84	1.12	1.40	1.67	1.94	2.20
	2.48	3.00	3.15	4.01	4.51	5.00	5.48	5.96

n	9	10	11	12	13	14	15	16
f	3.983	4.191	4.378	4.552	4.713	4.864	5.006	5.139
	0.23	0.29	0.30	0.36	0.40	0.43	0.48	0.51
	1.41	1.53	1.62	1.80	1.93	2.05	2.15	2.21
	2.46	2.71	2.96	3.21	3.45	3.69	3.93	4.16
	6.43	6.89	7.35	7.79	8.23	8.67	9.10	9.52

CHAPTER IV.

THE VALLEY AMBIGUITY.

1. Limitations of Scaling Methods.

Two unjustified assumptions are made when applying the scaling methods described in Chapter III. First it is assumed that below the lower frequency limit of the ionosonde there is no ionization. Second it is assumed that the N-h curve increases monotonically. JACKSON (44) and TITHERIDGE (45) give methods whereby these assumptions are made unnecessary. Both involve the use of the extraordinary ray. The principle in the case of the low level ionization and in the case of the so-called valley effect is much the same. We shall discuss only Titheridge's method of dealing with the valley since the valley effect is the only one of the two with which this thesis deals and Titheridge's method is basically the method used to attack the problem.

2. Titheridge's Method for Dealing with a Valley.

The basis of the method is as follows. First the h'-f record for the ordinary ray is scaled to obtain an N-h curve. This curve shows no valley. It is used to compute an h'-f curve for the extraordinary ray. Because of the extra retardation produced by the valley the computed h'-f curve is lower than the real one. The difference in height between the two curves is found at a number of frequencies. It is

convenient to use the same frequencies as were used to perform the Titheridge scaling. From this difference, Δ, the amount which must be added to the true height at each frequency can be found. As a first approximation it can be assumed that Δ is directly proportional to the thickness of the valley and independent of the valley shape. Titheridge shows that this is true provided that the valley is not too deep, i.e. provided that the minimum of electron density in the valley is not much less than the layer maximum. The value of Δ is found for a standard valley of 10 km thickness and constant electron density. The value of δ, the difference in height between the computed and true height profiles is also found. This gives a set of coefficients as are shown in Table 8. The calculation of these coefficients is shown in appendix C. Since Δ and δ in any record are both approximately proportional to the valley thickness we can find the constant of proportionality, k, by evaluating

$$k = \Delta / \Delta_o \qquad (4.1)$$

The amount which must be added to the height at each frequency is then $k\delta_o$ at that frequency.

The method which Titheridge suggests for computing the h'-f curve for the extraordinary ray from the N-h curve obtained in the scaling is to use the coefficients in Table 5 in conjunction with equations (3.11). The coefficients are simpli-

fied as described in section 6 of Chapter III. The author has tried this method and finds it subject to considerable inaccuracy for the following reasons.

In reducing an h'-f record each height difference can be calculated to an accuracy of about 0.1 km. This is not a serious error and is not cumulative. In the reverse process, where we scale an N-h curve to give an h'-f curve, a different set of circumstances obtains. We have from the equations (3.11) that

$$\Delta h'_n = \beta_{nn} \Delta h_n - \sum_{r=1}^{n} \beta_{r,n} \Delta h_r$$

Δh_n is typically about 5 km. and $\beta_{n,n}$ something of the order of 10. Thus $\beta_{n,n} \Delta h_n$ is of the order of 50 km. and known to an accuracy of about 2 or 3% since this is the accuracy of Δh. The sum $\Sigma \beta \Delta h$ is of the same order of magnitude and is known to the same degree of accuracy (about 1 or 2 km.). $\Delta h'_n$ is given by the difference of these two quantities and is about 5 or 6 km. in magnitude with a possible error of 4 km. Since the value of h' depends on all the values of $\Delta h'$ at lower frequencies, the error in h' so calculated may be very large. Now Δ is the difference between the true h'-f curve and the derived one which may, as we have seen, be many kilometers in error. Δ is typically only a few kilometers in magnitude so that it is obvious that the method lends itself to gross inaccuracy. It is necessary to use a more accurate

method to obtain the extraordinary h'-f curve.

3. Method of Obtaining the Extraordinary h'-f Curve from an N-h Curve.

It is possible to write down equation (2.3) in the form

$$h'_n = \sum_{r=0}^{n} \mu' \Delta h \qquad (4.2)$$

when the ionosphere is stratified with stratifications of thickness Δh. In this expression each term is known to an accuracy of about 0.1 km. and errors are not cumulative. Using the values of μ' given in Table 4 for the laminations corresponding to the Titheridge frequencies, it is easy, by means of a desk calculator, to evaluate the sum to a far greater accuracy than by the method of section 2, from the values of Δh found in the scaling of the h'-f profile for the ordinary ray. Further, the accuracy of any one value of h' is independent of the accuracy of the others so that errors may be removed by smoothing.

TABLE 8: The values of Δ and δ at various frequencies for a square valley of 10 km. thickness at a plasma frequency of 4 Mc/s.

f_o	4.191	4.378	4.552	4.713	4.864	5.006	5.139	
Δ_o	12.8	7.4	5.8	5.1	4.1	5.2	5.5	
δ_o	8.6	7.6	7.0	6.5	6.1	5.9	5.8	
f_o	5.266	5.386	5.500	5.609	5.713	5.813	5.908	6.000
Δ_o	6.4	-	-	-	-	-	-	
δ_o	5.8	5.9	6.0	6.1	6.2	6.3	6.3	6.4

PART II.

THE EFFECTS OF SOLAR ECLIPSES.

"Over that valley hang the discouraging clouds of confusion...."

"Pilgrim's Progress."

CHAPTER V.

SOME EXPERIMENTAL RESULTS.

1. Early observations.

Until rapid methods of scaling h'-f records became available most workers dealt only with the behaviour of the critical frequency and virtual height during eclipses. Any attempt to scale the records obtained in order to deduce the electron density profile would not have been of very great value because, in the first place, the early model methods were not sufficiently accurate, being based for the most part on the assumption of a parabolic layer and, in the second place, the amount of computation required to provide an adequate amount of control data would have been prohibitive. The development of methods such as Kelso's (37) method encouraged rather more extensive investigation of the variation of electron density with height. We shall concern ourselves largely with the observations of SZENDREI & McELHINNY (46), (47), (48) and McELHINNY (49), (50). These were taken on 25 December 1954 at Rhodes University using the ionosonde described in Chapter II. We shall also discuss the results of MINNIS (51) and SAVITT (52).

2. The Results of Savitt.

SAVITT (52) analysed ionosphere soundings taken during the solar eclipse of 20 May 1947 at Bocayuva in Brazil using

MANNING's method (53). He plotted graphs of electron density versus time at various real heights in the F region of the ionosphere. His results are shown in Figure 11. It will be noted that after the eclipse the electron density is higher than that on the control days. Savitt explained this by suggesting that the F layer descended during the eclipse bringing greater electron densities to lower levels.

3. The Results of Minnis.

MINNIS (51) analysed ionosphere soundings taken during the solar eclipse of 25 February 1952 at Khartoum using Kelso's method. He plotted the same quantities as Savitt. His graphs of electron density versus time are shown in Figure 12a. Control data taken a few days before are shown in Figure 12b.

4. The Solar Eclipse of 25 December 1954.

The eclipse was annular. Grahamstown lay within the belt of annularity. At the eclipse maximum 85.8% of the solar disc was covered. The times of various phases of the eclipse are shown in Table 9.

TABLE 9: Times of contact at various heights. South African standard time is used. (SAST = UT + 2 hours).

Height (km.)	1st contact	2nd contact	3rd contact	4th contact
100	0646	0800	0807	0935
200	0645	0758	0805	0934
300	0643	0757	0803	0932

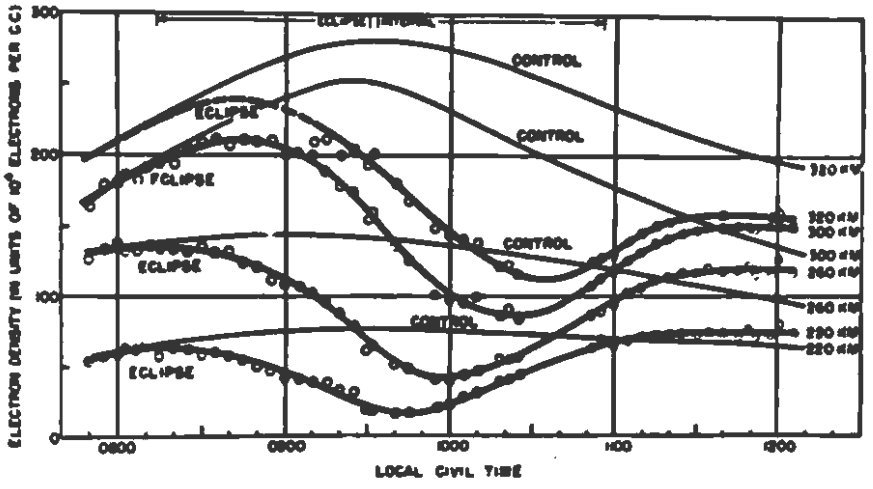

FIGURE 11: Savitt's curves of the variation of electron density with time at various fixed heights, during the eclipse of 20 May 1947, compared with control data.

(a)

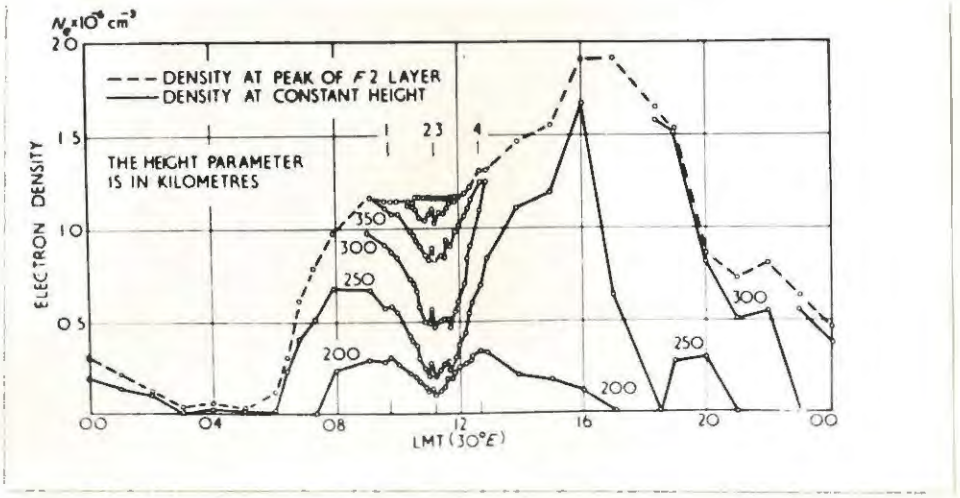

(b)

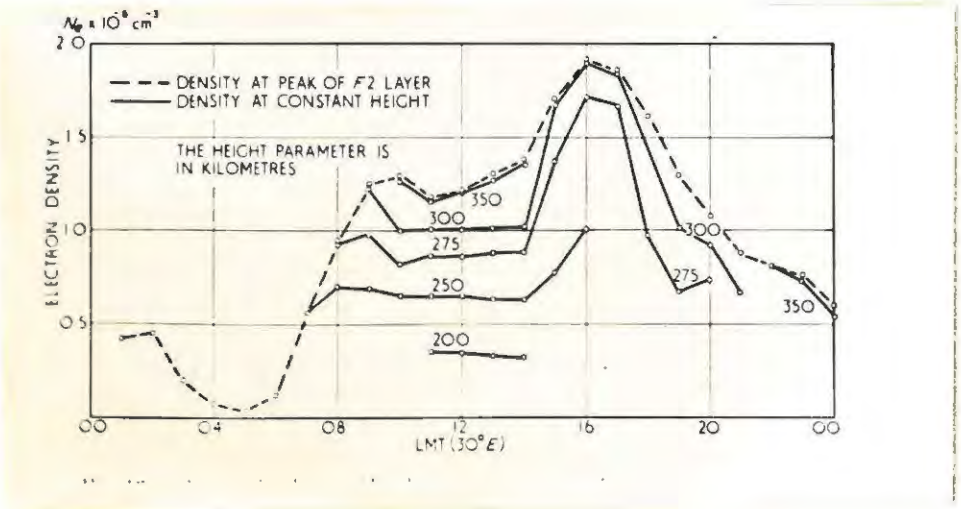

FIGURE 12: (a) Minnis's curves of electron density vs time at various fixed heights during the eclipse of 25 February 1952 (b) The same quantities on control days.

5. The results of Szendrei and McElhinny.

Szendrei and McElhinny took readings on thirty control days centred on the eclipse days. The readings were taken every 15 minutes from 0500 to 1000 SAST and at hourly intervals for the rest of the day. During the eclipse itself readings were taken at $2\frac{1}{2}$-minute intervals.

Kelso's method of scaling the records was adopted, ignoring the earth's magnetic field. Every record was scaled unless it was impossible to do so. The variation of the electron density at a fixed height with time was plotted. Owing to absorption at the lower frequencies no significant change in the true height of the E layer could be detected so that the E layer measurements are based on measurements of the maximum value of the electron density in the E layer. Curves showing the variation of electron density with time at various fixed heights in the F2 layer are shown in Figure 13. They are compared with the curves which show the mean behaviour of the electron density on the control days.

In the E layer Szendrei and McElhinny investigated the effects of non-uniform radiation from the sun's disc and temperature variations during the eclipse. The analysis in terms of temperature variation was unsuccessful but that in terms of non-uniform radiation from the sun's disc was rather more successful. Later McELHINNY (49), (50) performed more detailed work on the basis of this model and obtained theoretical curves

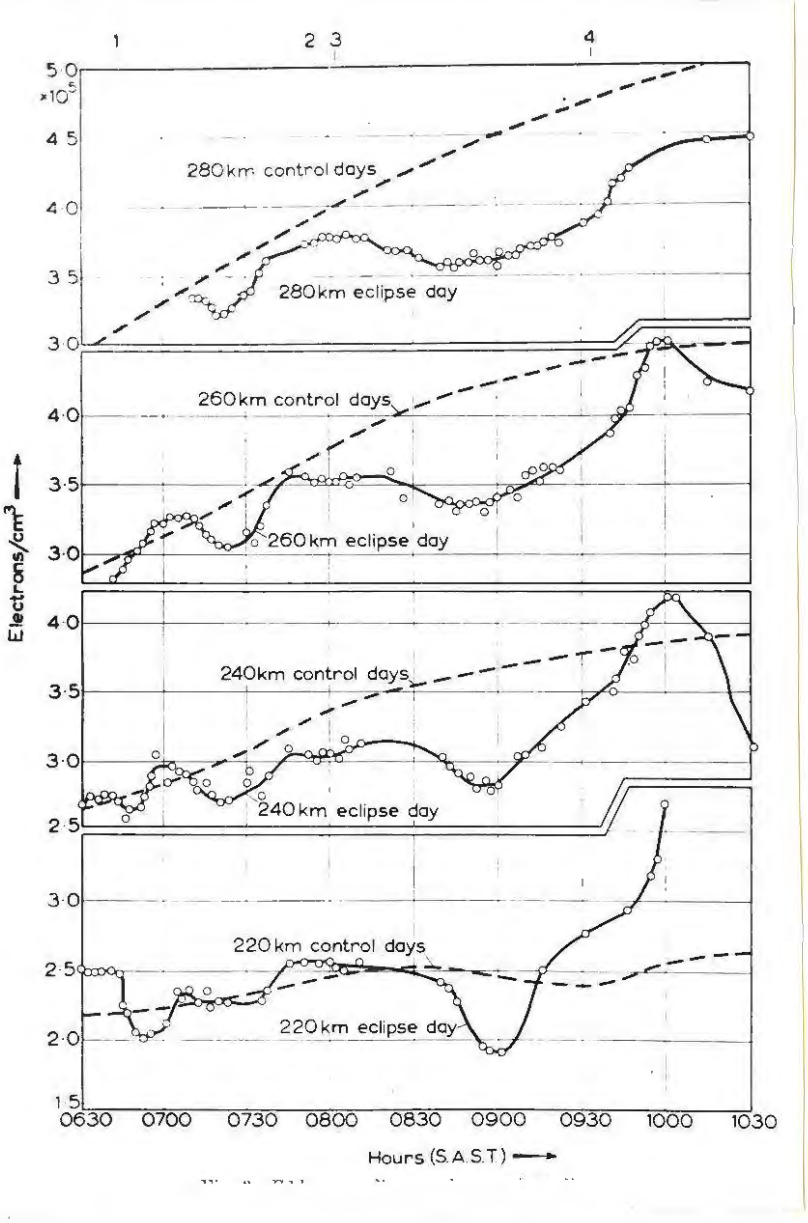

FIGURE 13: Szendrei & McElhinny's curves of the variation of electron density with time at various fixed heights during the eclipse of 25 December 1954 compared with control data.

showing the variation of the maximum electron density with time at Grahamstown, Cape Town and Johannesburg. The agreement with the practical results is good. The value of the recombination coefficient was chosen so that the minimum value of the electron density was the same for both theoretical and practical curves. The curve calculated on the basis of uniform radiation from the sun's disc is displaced to the right of the experimental curve while that calculated on the basis of non-uniform radiation agrees with the experimental curve rather well. An estimate of α, the recombination coefficient was made for the E layer by choosing that value of α which gave the best fit to the experimental results. If uniform radiation from the sun's disc was assumed, a value of 7×10^{-9} cm^3 sec^{-1} was obtained for Grahamstown and if the non-uniform solar model was assumed a value of 1.5×10^{-8} cm^3 sec^{-1} was obtained. Another model where some of the radiation came from outside the sun's disc was also discussed by McElhinny and gave results very similar to those given by the first model, the recombination coefficient being 4×10^{-8} cm^3 sec^{-1} if this model was assumed.

In the F1 layer calculations were made on the assumption that the radiation from the sun's disc was uniform. Curves were calculated from equations 1.5 and 1.6. It was found that the best fit to the experimental curves was obtained when recombination rather than attachment was effective. The re-

combination coefficient which gave the best results was 5×10^{-9} cm^3 sec^{-1} throughout the F1 layer. Not very much work was done on the assumption that the source of radiation was not distributed uniformly over the sun's disc. The F1 layer was obscured for the middle part of the eclipse and its behaviour for that time was uncertain.

Figure 14 shows the best fit of the theoretical curves to the experimental curves for the F2 layer, assuming that attachment was effective. A similar fit was obtained assuming recombination. It will be noticed that the attachment coefficient decreases with height as is suggested in section 3 of Chapter I. The fit is poor. It will be noticed that there is a maximum of electron density when the eclipse is nearly over.

6. Discussion.

In all cases the results predicted from theory for the E and F1 layers agree reasonably well with the experimental results. The position in the F2 layer is not so happy. The electron density fluctuates considerably and in some cases there is doubt whether there is any eclipse effect in the F2 region at all since many of the effects observed could just as well be due to random fluctuation in the electron density. Further, the h'-f records obtained by many workers show puzzling cusps and extra traces.

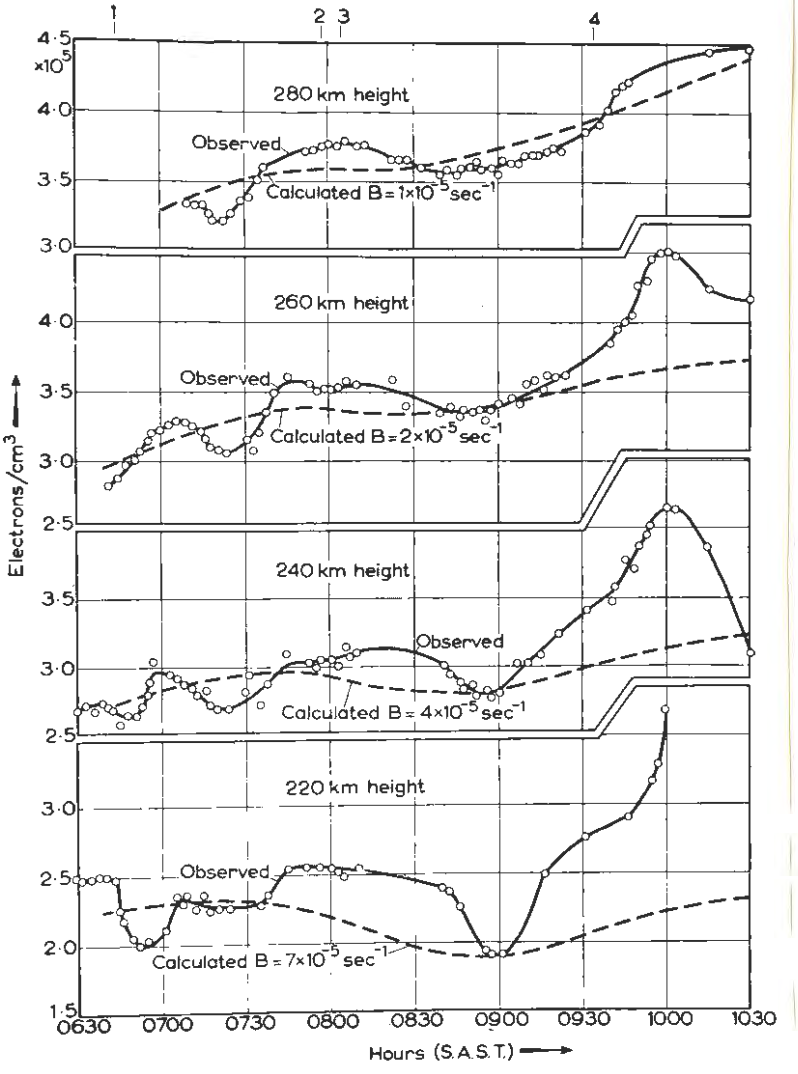

FIGURE 14: Szendrei & McElhinny's curves of the variation of electron density with time at various fixed heights compared with the curves obtained assuming attachment was effective.

It should be noted that both Savitt's N-t curves and those of Szendrei and McElhinny show that the value of the electron density in the F2 layer after the eclipse is higher than it should be. The curves of Szendrei and McElhinny show a definite maximum. Those of Savitt may well do the same but no scaling of the records was performed after the ionosphere had apparently returned to more or less normal conditions. The maximum in Minnis's curves after the eclipse is the normal one occurring some time after midday when the sun is past its zenith. If there were any maximum after the eclipse it would be masked by this.

The puzzling features discussed above stimulated the work performed in this thesis. We shall continue in the following chapters by describing the methods adopted to try to explain some of them and the results achieved.

CHAPTER VI.

THE BEHAVIOUR OF A THEORETICAL IONOSPHERE DURING AN ECLIPSE.

1. Introduction.

MUNRO & HEISLER (53) first suggested that some of the unusual features shown by eclipse records might be on account of tilts developing in the ionospheric layers during the eclipse. Since the electron density in general increases with height in the ionosphere it is obvious that any localised reduction in electron density as would be caused by an eclipse must produce tilts in the surfaces of constant electron density. These tilts would cause the rays to be deviated from the vertical so that the virtual heights would be incorrectly measured.

MINNIS (54) criticised the above on the grounds that any errors so produced would be negligible but his view was itself questioned by GLEDHILL (55). As is shown in this thesis Minnis's contention may well be correct, though his arguments supporting this view are not necessarily so.

GLEDHILL (56) therefore computed the effects of an eclipse on a typical electron distribution and so constructed a map showing isoelectronic contours in the ionosphere. The remainder of this chapter is concerned with the details of Gledhill's computation and the results obtained by him.

2. The Ionosphere Model.

The electron distribution was based on one of the records taken by Szendrei and McElhinny at Grahamstown on one of the control days. The record chosen was taken at about the same time of day as the commencement of the eclipse. It was simplified to some extent. The E layer was assumed to be a Chapman layer with a scale height of 10 km. and a maximum at 120 km. The maximum electron density in this layer was supposed to be exactly 10^5 cm^{-3}. This E layer was joined smoothly onto the bottom of the F layer with no valley between them. It was assumed that recombination was effective at all heights and not attachment. The recombination coefficients were based on those obtained by Szendrei and McElhinny but were modified to lie on a smooth curve between the layers. The figures used in the model are shown in Table 10. The electron density at any fixed height was then assumed to follow the equation

$$\frac{dN}{dt} = fq - \alpha N^2 \qquad (6.1)$$

which follows directly from equation (1.5) if q, the rate of production of ions, is replaced by fq, where f is the unobscured fraction of the sun's disc. The initial conditions assumed by Gledhill were that a steady state had been reached before the eclipse started, i.e. $dN/dt = 0$ and thus $q = \alpha N^2$ initially. Further q was assumed to remain constant throughout the eclipse,

TABLE 10: Data for the ionosphere model.

Height (km)	Electron density (cm^{-3})	α (cm^3/sec)
300	49.0×10^4	2.5×10^{-11}
280	48.0	3
260	44.0	5
240	38.0	15
220	24.0	40
200	23.0	150
180	22.5	500
160	19.5	500
140	14.0	700
130	10.3	1000
120	10.0	1000
110	7.0	1000
100	1.1	1000

equivalent to neglecting the rotation of the earth. The values used for f were those for the solar eclipse at Grahamstown on 25 December 1954, calculated by Szendrei and McElhinny and shown in Figure 31 of McElhinny's thesis (50).

3. Results.

Gledhill solved equation (6.1) numerically, step by step, throughout the eclipse at selected heights. Figure 15 shows the resulting curves at given heights throughout the eclipse. From these he found N-h curves at a number of times during the eclipse. These are shown in Figures 16 and 17. It will be noted that, as a result of the crossing over of the curves for 180, 200 and 220 km., a valley forms between the F1 and F2 layers after the maximum of the eclipse.

4. The Ionosphere Map.

From these curves Gledhill constructed a map showing the ionosphere at points along the central line of the eclipse. The earth's curvature was neglected and it was assumed that the undisturbed ionosphere had the same value at all points before the onset of the eclipse. Thus before the eclipse the isoelectronic surfaces would be horizontal planes. It was assumed that the shadow of the eclipse moved from west to east at a velocity of 40 km./min. Now consider a given point A on the central line of the eclipse. At a point B, 40 km. east

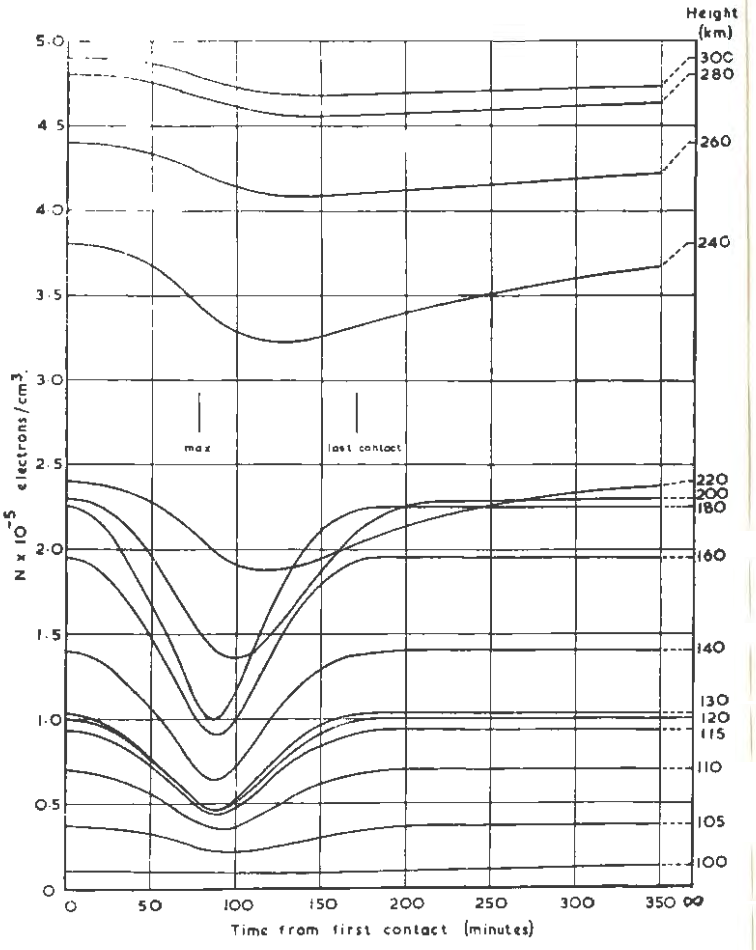

FIGURE 15: Gledhill's curves of electron density versus time at various fixed heights during an eclipse in a model ionosphere.

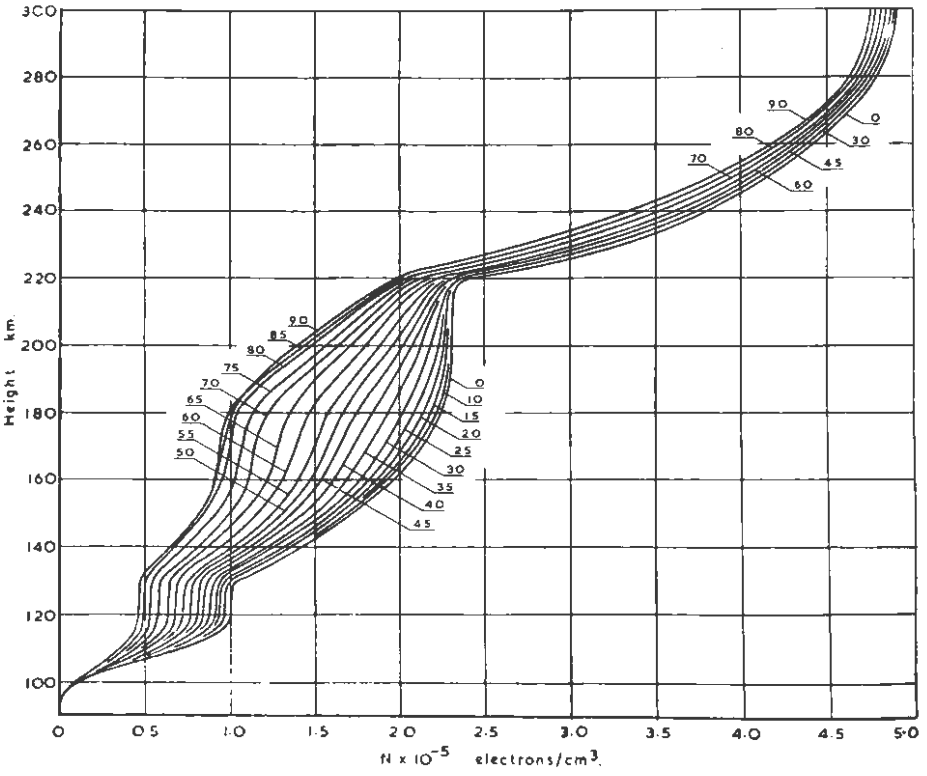

FIGURE 16: Gledhill's N-h curves obtained from Figure 15.

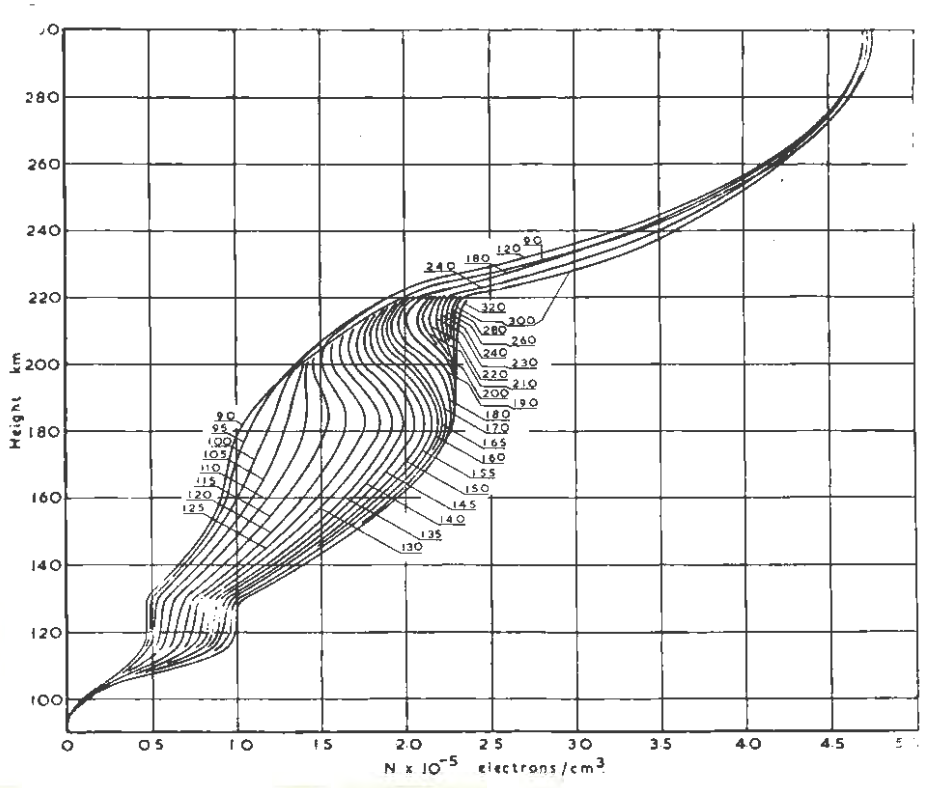

FIGURE 17: Gledhill's N-h curves obtained from Figure 15.

of A, the state of the ionosphere is that which will exist at A a minute later while at a point C, 40 km. west of A, its state is that which existed at A one minute earlier. Thus if we plot curves of height on a vertical scale versus time on a horizontal scale for various electron densities and if we make a unit of 40 km. on the vertical scale equal in length to 1 minute on the horizontal scale, then it is obvious that the h-t curves represent isoelectronic contours during the eclipse. Portions of the map so deduced by Gledhill are shown in Figure 18. It will be noted that there are sharp tilts in the contours especially after the eclipse maximum.

5. Discussion.

In view of the behaviour shown by the theoretical ionosphere described above it is desirable to investigate the effects which the tilts in the layers have on supposedly vertical incidence soundings and also the effect of the valley between the F1 and F2 layers on the scaling of the records. The investigation of these problems carried out by the author is the subject of the remainder of this thesis. Chapter VII deals with ray tracing in the ionosphere when the earth's magnetic field is neglected, Chapter VIII with the effect of the valley, ignoring the earth's field, Chapter IX with the extension of the work to include the effects of the earth's field, and Chapter X with the scaling of some practical records.

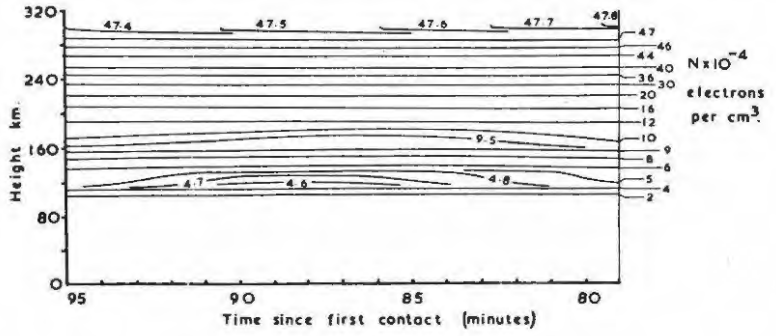

Fig. 3a.

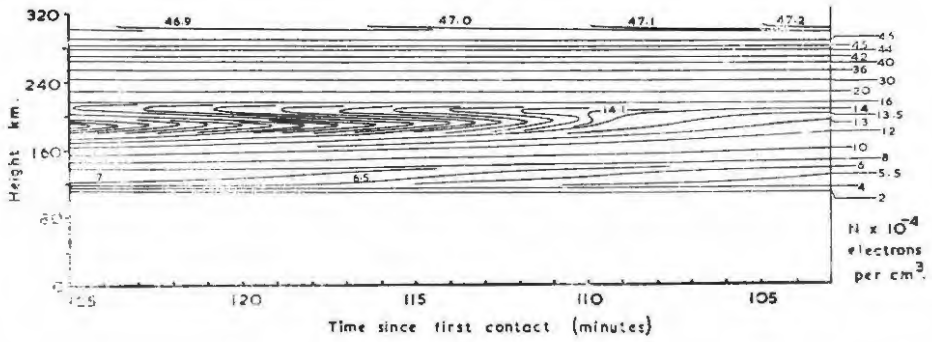

FIGURE 18: Portions of the ionosphere map constructed by Gledhill.

CHAPTER VII.

RAY TRACING IN AN IONOSPHERE WITHOUT MAGNETIC FIELD.

1. Introduction.

In an ionosphere where the layers are tilted as in Figure 19 the rays which return to the starting point are not in general vertical. Types of path which may occur are shown in Figure 19. Type (a), although not vertical, reaches the reflecting layer at normal incidence and thus retraces its path. Type (b) travels along a curved path and although it does not retrace its path it returns to the starting point. In each case if we use Snell's Law to trace the path of the ray through the ionosphere we can find the virtual height by evaluating the integral in equation (2.4) (with different limits) along the path of the ray. This is best done by dividing the path into small segments and evaluating the sum, $\sum_{r=1}^{n} \Delta s/\mu_r$, along the path where μ_r is the mean value of μ in the rth segment. μ_r can be found by assuming a linear variation of N in each segment and finding the value of μ corresponding to the mean value of N in the segment. Since μ is given by equation (1.11) which can, if collisions are neglected, be written in the form

$$\mu^2 = 1 - \frac{Ne^2}{2\pi\epsilon_o mf} \qquad (7.1)$$

N may be found most conveniently by plotting μ^2 versus N, for

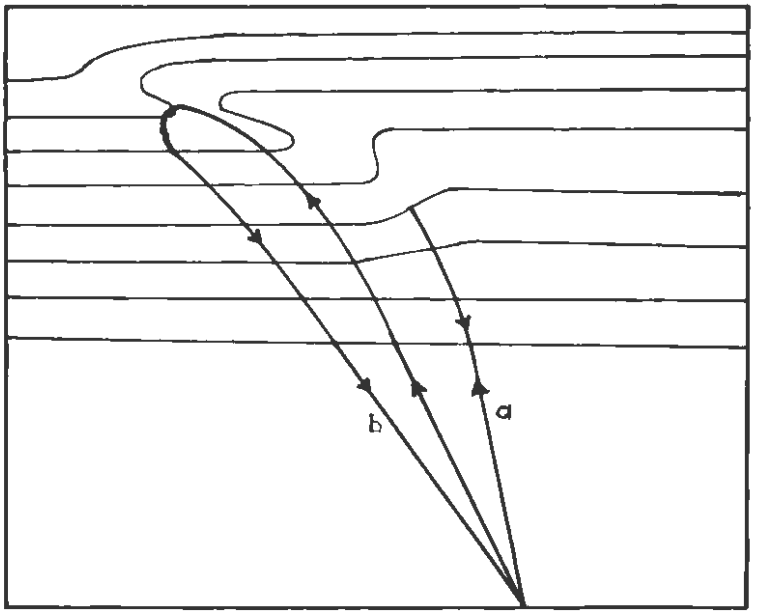

FIGURE 19: Types of path which may occur in an ionosphere where the stratifications are not horizontal.

various values of f. These curves are a family of straight lines, shown in Figure 20.

The chief error in tracing rays of type (b) would occur when the ray was reflected. Since μ varies rapidly in this region application of Snell's law is difficult unless inconveniently small segments are taken. The errors arising from assuming that this portion of the path was the arc of a circle were investigated by examining the paths of rays in ionospheric layers which gave analytic solutions for the path of the ray.

2. Differential Equation for the Path of a Ray in a Horizontally Stratified Ionosphere.

Consider a horizontally stratified ionosphere. Let a ray travel in a vertical plane, the (x-z) plane say. Suppose the line $x = 0$ represents the bottom of the ionosphere and the ray enters the ionosphere at the point (0,0) at an angle α_o. Suppose that the tangent to the ray makes an angle α with the z-axis at a point (x,y) in the ionosphere.

Obviously $dx/dz = \tan\alpha$ (7.2)

From Snell's law we have that

$$\mu \sin\alpha = \sin\alpha_o \tag{7.3}$$

$$\cos\alpha = \sqrt{1 - \sin^2\alpha_o/\mu} \tag{7.4}$$

If we combine (7.2), (7.3) and (7.4) we get

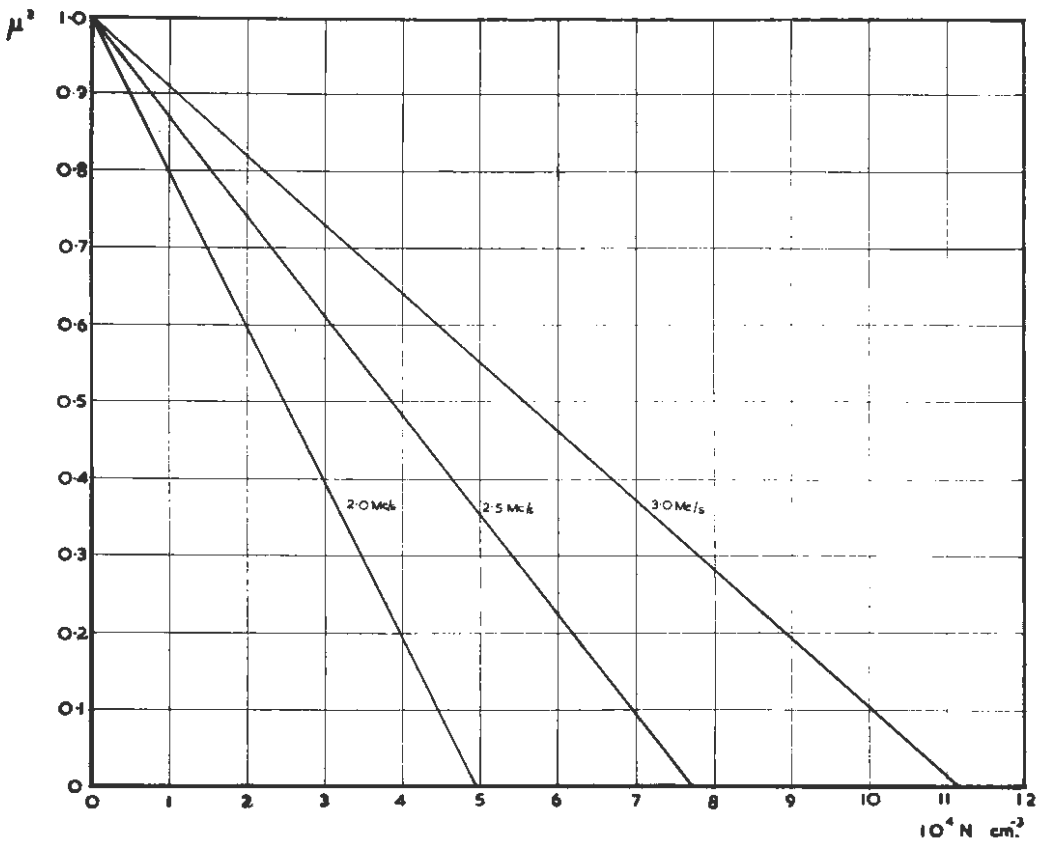

FIGURE 20: μ^2 vs N for various values of the probing frequency, f, when the earth's field is ignored.

$$dx/dz = \frac{\sin\alpha_o/\mu}{\sqrt{1 - \sin^2\alpha_o/\mu^2}}$$

$$= \frac{\sin\alpha_o}{\sqrt{\mu^2 - \sin^2\alpha_o}} \qquad (7.5)$$

which is the differential equation which must be solved to find the path of a ray in an ionosphere where μ is a function of z.

3. The Linear Layer.

APPLETON (57) first computed the paths of rays in ionospheres where the electron density was a simple function of height. The linear layer was one of the cases considered by him.

If the variation of the plasma frequency (and hence the electron density) is given by

$$f_o^2 = Az \qquad (7.6)$$

so that the refractive index is given by

$$\mu^2 = 1 - Az/f \qquad (7.7)$$

then, by substituting in equation (7.5) and integrating, Appleton showed that the equation of the path was

$$x^2 = \frac{4\sin^2\alpha_o f^4}{A^2}\left\{\cos^2\alpha_o - Az/f^2\right\} \qquad (7.8)$$

(The equation is derived in a different form by Appleton).

Figure 21 shows the path of a ray of frequency 3 Mc/s,

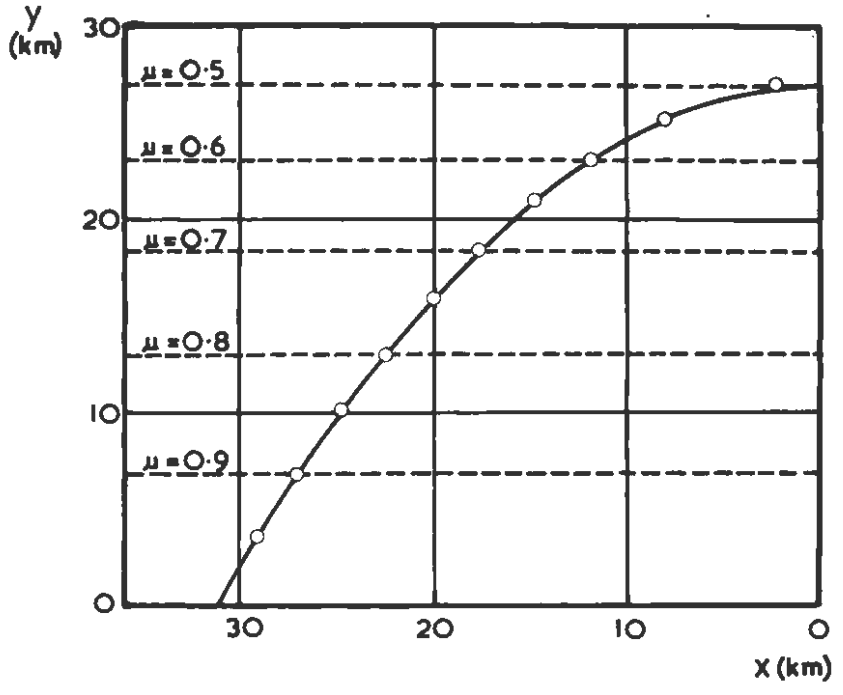

FIGURE 21: The path of a ray in a linear layer. The curve is the true path. The points plotted are obtained by the graphical construction $f = 3$Mc/s. $A = \frac{1}{4}$km^{-1} sec^{-1}. Angle of incidence $= 30^{\circ}$.

incident at an angle of 30° on a linear layer, where $A = 0.25 km.^{-1}$ Mc/s. Also shown is the path plotted by considering the ionosphere to be made up of a number of slabs, each of constant μ, and applying Snell's law at the boundaries of each slab. The maximum of the ray is approximated by the arc of a circle tangent to the ray and to the level where $\mu = \sin\alpha_o$. As can be seen from the diagram an error of 1.2 km. is introduced in the point of emergence of the ray. Since ionosonde records are rarely accurate to better than 2 km. this error is negligible.

4. The Parabolic Layer.

This is not the parabolic layer considered by Appleton (57). The vertex of the parabola in the case considered by him was at the base of the ionosphere and the electron density increased upwards without limit. The parabola considered here has its vertex at a height a in the layer, this being a maximum in the electron density. This layer approximates to a real ionospheric layer.

Suppose the plasma frequency (and hence the electron density) varies according to

$$f_o^2 = Az(a-z) \qquad (7.9)$$

where a and A are constants. Then the refractive index is given by

$$\mu^2 = 1 - Az(a-z)/f^2$$

and from equation (7.5)

$$dx/dz = \frac{f \sin\alpha_o}{A^{\frac{1}{2}}\left\{ f^2 \cos^2\alpha/A - h(a-h) \right\}^{\frac{1}{2}}}$$

$$= \frac{f \sin\alpha_o}{A^{\frac{1}{2}}\left\{ (h - \tfrac{1}{2}a)^2 - (\tfrac{1}{4}a^2 - f^2 \cos^2\alpha_o/A) \right\}^{\frac{1}{2}}}$$

If the layer is not penetrated $f^2 < f^2{}_o$ (max), (the value of the plasma frequency when z = a) and therefore the quantity $\left\{ (a^2/4) - (f^2 \cos^2\alpha_o/A) \right\}$ is positive.

Thus $$\frac{(C + x)A^{\frac{1}{2}}}{f \sin\alpha_o} = \cosh^{-1} \frac{\tfrac{1}{2}a - h}{\left\{ \tfrac{1}{4}a^2 - f^2 \cos^2\alpha_o/A \right\}^{\frac{1}{2}}}$$

where C is a constant of integration. Now, if at h = 0

$$\cosh \frac{x A^{\frac{1}{2}}}{f \sin\alpha_o} = \frac{\tfrac{1}{2}a}{\left\{ \tfrac{1}{4}a^2 - f^2 \cos^2\alpha_o/A \right\}^{\frac{1}{2}}}$$

Then $$C = 0$$

and the equation of the ray is

$$\frac{\tfrac{1}{2}a - h}{\left\{ \tfrac{1}{4}a^2 - f^2 \cos^2\alpha_o/A \right\}^{\frac{1}{2}}} = \cosh \frac{A^{\frac{1}{2}}x}{f \sin\alpha_o} \qquad (7.10)$$

If the layer is penetrated, which occurs when $f^2 > f^2{}_o$ (max), then the quantity $\left\{ \tfrac{1}{4}a^2 - f^2 \cos^2\alpha_o/A \right\}$ is positive and in the same way the equation of the ray is

$$\frac{\tfrac{1}{2}a - h}{\left\{ (f^2 \cos^2\alpha_o/A) - \tfrac{1}{4}a^2 \right\}^{\frac{1}{2}}} = \sinh \frac{A^{\frac{1}{2}}x}{f \sin\alpha_o} \qquad (7.11)$$

In the limiting case where $\frac{1}{4}a^2 = f^2 \cos^2\alpha_o/A$ the equation is

$$\frac{a}{2} - h = \exp\left\{\frac{A^{\frac{1}{2}}x}{f \sin\alpha_o}\right\} \qquad (7.12)$$

and the ray neither penetrates the layer nor is reflected from it but approaches the level of maximum electron density asymptotically.

Figures 22 and 23 show rays in a parabolic layer, both the true path and the path obtained by approximating the top portion of the ray by the arc of a circle as previously described being shown. Of especial interest is Figure 23 which shows that even when the frequency is 0.995 of the critical frequency of the layer the last part of the curve (i.e. that part within 10% of the maximum height reached) may be approximated by a circle of appropriate radius with an error of only 1 km. in the position of the point where the ray emerges from the layer.

The sum $\Sigma \frac{\Delta s}{\mu}$, was evaluated along the true path and the approximate path in Figure 23. This gave a value of h' of 34.4 km. in the first case and 33.1 km. in the second case. This error is negligible.

5. Ray Tracing in an Ionosphere where the Variation of N with the Height is Arbitrary.

A number of attempts were made to trace rays such as that shown in Figure 21b. The errors in each case were fairly large. The ray which returned to the starting point had to be found by

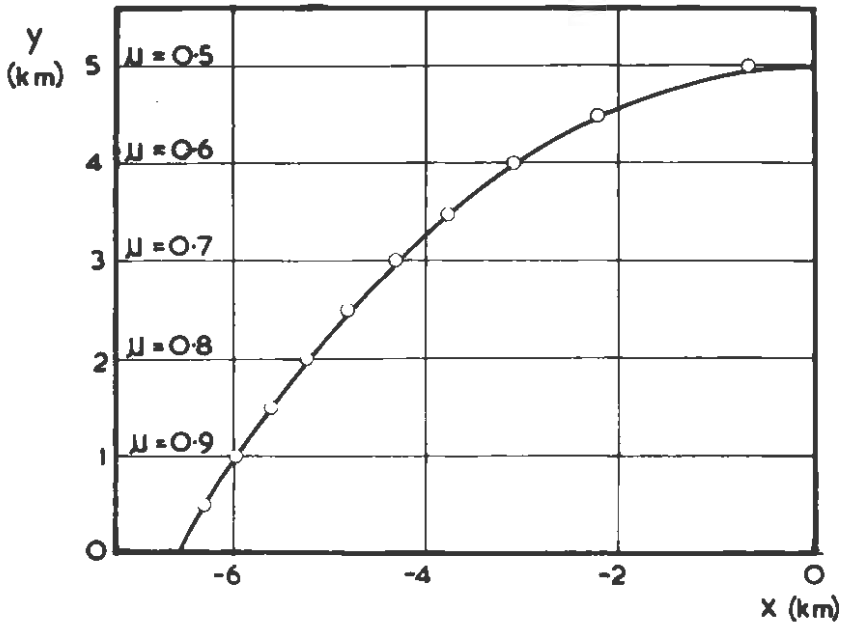

FIGURE 22: The path of a ray in a parabolic layer. The curve is the true path. The points plotted are obtained by graphical construction. f = 5Mc/s. a = 20km. A = $\frac{1}{4}$km^{-1}Mc/s. Angle of incidence = 30°.

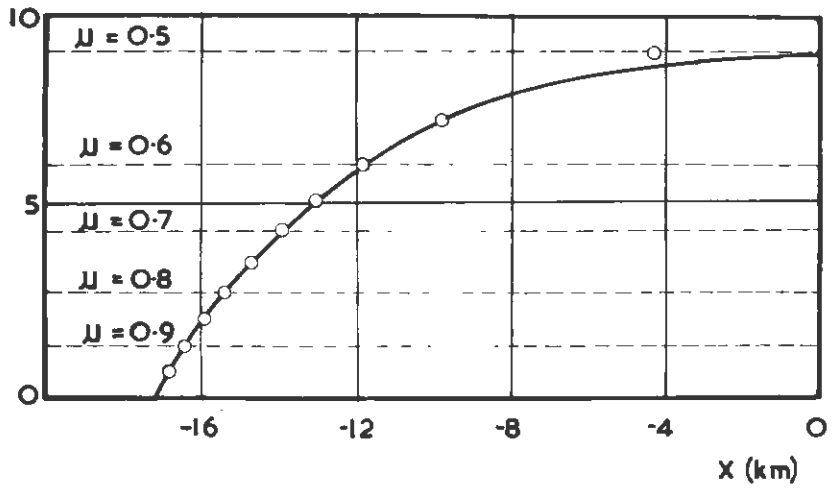

FIGURE 23: The path of a ray in a parabolic layer. The curve is the true path. The points plotted are obtained by graphical construction. f = 5.7Mc/s. a = 20km. A = ¼km-1Mc/s. Angle of incidence = 30°.

trial and error. Further, in every case there was a ray path such as that shown in Figure 19a possiblo, along which the virtual path length was less than that for a path of the type shown in Figure 19b. Ray paths of type (a) were therefore exclusively considered since they would give rise to the main trace on an h'-f record although those of type (b) could possibly cause extra traces and cusps on the record. The method of ray tracing which was adopted was as follows:-

It is assumed that the ray is normal to the reflecting layer at the point of reflection. Starting at the reflection point by making an intelligent guess about its position we trace a ray downwards and observe where it reaches the ground. By a process of trial and error we trace further rays until we find one which passes through the desired point on the ground. In practice it is usual to find the correct reflection point on the second attempt. To trace the ray a table such as that shown in Table 11 was set up. We measure the true path length, which is of course slightly greater than the height of the layer at that point, and calculate the virtual path length by evaluating the sum $\Sigma \frac{\Delta s}{\mu}$ along the ray, assuming a linear variation of electron density with height in each lamination. In the topmost lamination where $\mu = 0$ at one boundary the value of $\frac{1}{\mu}$ which corresponds to the mean value of N is not the mean value of $\frac{1}{\mu}$ in the slab because $\frac{1}{\mu}$ goes to infinity at the one boundary. If we assume that N is linear with z, which is true

TABLE 11: Method of ray tracing.

$N.10^4$ cm^{-3}	(1) Angle of incidence with vertical.	(2) Angle of refracting layer with horizontal.	(3) Angle of incidence on layer = (1) - (2).	(4) μ_1 (from graph)
5.95	18.1°	16.9°	1.2°	0.006
5.90	17.4°	3.2°	14.2°	0.015
5.80	10.8°	2.0°	8.8°	0.028
5.60	6.8°	1.0°	5.8°	0.052
5.00	3.5°	0.8°	2.7°	0.120
4.00	2.1°	0.6°	1.5°	0.250
3.00	1.5°	0.3°	1.2°	0.415
2.00	1.2°	0.2°	1.0°	0.580
1.00	1.0°	0.1°	0.9°	0.745

$N.10^4$ cm^{-3}	(5) μ_2 (from graph)	(6) $\sin(7)=\frac{\mu_1 \sin(7)}{\mu_2}$	(7) Angle of refraction from layer.	(8) Angle of refracted ray with vertical=(7)+(2)
5.95	0.015	0.00836	0.5°	17.4°
5.90	0.028	0.1320	7.6°	10.8°
5.80	0.052	0.0830	4.8°	6.8°
5.60	0.120	0.0439	2.5°	3.5°
5.00	0.250	0.0226	1.3°	2.1°
4.00	0.415	0.0158	0.9°	1.5°
3.00	0.580	0.0150	0.9°	1.2°
2.00	0.745	0.0143	0.8°	1.0°
1.00	0.910	0.0129	0.7°	0.8°

enough except near the critical frequency we can proceed to find the mean value of $\Delta z/\mu$ for the topmost slab as follows:-

We must evaluate the integral

$$I = \int_0^{z_0} dz/\mu \qquad (7.13)$$

where $z = 0$ at the bottom of the last section of the path and $z = z_0$ at the reflection point.

If μ_1 is the value of μ at the point $z = 0$ we may write

$$I = \int_0^{z_0} \frac{dz}{\sqrt{1 - (f_o/f)^2}}$$

Since N is linear with z, $(f_o/f)^2 = az-b$ where a and b are constant

$$dz = \frac{2}{a}\frac{f_o}{f}\, d\left(\frac{f_o}{f}\right)$$

When $z = z_0$ $\quad f_o/f = 1$, and when $z = 0$ $\quad \mu_1^2 = 1 - (f_o/f)^2$

so that the integral becomes

$$I = \frac{2}{a} \int_{\sqrt{1-\mu_1^2}}^{1} \frac{(f_o/f)\, d(f_o/f)}{\sqrt{1 - (f_o/f)^2}}$$

Let $\quad f_o/f = \sin\theta$

thus $\quad d(f_o/f) = \cos\theta\, d\theta$

and so

$$I = \frac{2}{a} \int_{\sin^{-1}\sqrt{1-\mu_1^2}}^{\pi/2} \sin\theta\, d\theta$$

$$= \frac{2}{a} \cos \sin^{-1} \sqrt{1 - \mu_1^2}$$

$$= \frac{2\mu_1}{a}$$

At $z = 0$ $\qquad 1 - \mu_1^2 = -b$

$\therefore$ at $z = z_o$ $\qquad az_o + 1 - \mu_1^2 = 1$

$$a = \frac{\mu_1^2}{z_o}$$

and thus $\qquad I = 2z_o/\mu_1 \qquad (7.14)$

Thus the value of $\Delta z/\mu$ in the last lamination is $2z_o/\mu_1$ where z_o is the thickness of the lamination and μ_1 is the value of μ at the bottom of the lamination.

Near the critical frequency where the layer may not be linear within the lamination we can calculate a similar result for a parabolic layer. We can represent the layer which is parabolic in N by one which is linear in f_o,

$$f_o/f_c = az - b \qquad (7.15)$$

where f_c is the critical frequency of the layer and a and b are constants. We therefore get

$$\frac{f_o}{f} \cdot \frac{f}{f_c} = az - b$$

so that $\qquad d(f_o/f) = \frac{af_c}{f}\, dz$

Whereupon I is given by

$$I = \frac{f}{af_c} \int_{\sqrt{1-\mu_1^2}}^{1} \frac{d(f_o/f)}{\sqrt{1 - (f_o/f)^2}}$$

$$I = \frac{f}{af_c} \sin^{-1}\left(\frac{f_o}{f}\right) \Bigg|_{\sqrt{1-\mu_1^2}}^{1}$$

$$= \frac{f}{af_c}\left\{\frac{\pi}{2} - \sin^{-1}\sqrt{1-\mu_1^2}\right\}$$

$$= \frac{f}{af_c} \sin^{-1}\mu_1$$

$$\simeq \frac{f}{af_c}\,\mu_1\left(1+\frac{\mu_1^2}{6}\right)$$

At $z = 0$ $\qquad \frac{f}{f_c}\sqrt{1-\mu_1^2} = -b$

At $z = z_o$ $\qquad f/f_c = az_o + (f/f_c)\sqrt{1-\mu_1^2}$

$$\therefore \quad a = \frac{f}{f_c}\,\frac{1-\sqrt{1-\mu_1^2}}{z_o}$$

$$\simeq \frac{f\mu_1^2}{2z_o f_c} \quad \text{if } \mu_1 \text{ is sufficiently small}$$

$$\therefore \quad I \simeq \frac{2z_o}{\mu_1}\left(1+\frac{\mu_1^2}{6}\right) \qquad (7.16)$$

which reduces to equation (7.14) if μ_1 is sufficiently small

We can justify this formula by means of a numerical example. First we know an analytic expression for the virtual height in a parabolic layer of the form given in equation (7.9). APPLETON (57) first calculated this. In the symbols we have adopted the expression is

$$h' = \frac{f}{A^{\frac{1}{2}}} \cosh^{-1}\frac{a/z}{\sqrt{a^2/4 - f^2/A}} \qquad (7.17)$$

Suppose that the constants in the formula have the values,

$a = 200$ km, $f_c = 4.0$ Mc/s, $A = 1.6 \times 10^{-3}$ $(\text{Mc/s})^2 \text{km}^{-2}$.

For a value of f of 3.0 Mc/s we have from equation (7.17)

$$h' = 72.7 \text{ km.}$$

The author has evaluated h' by computing the sum $\Sigma \Delta s/\mu$. If it is assumed that in the last slab μ is that value which corresponds to the mean value of N in the slab we get

$$h' = 64.3 \text{ km.}$$

If we use equation (7.14) to get the value of μ in the last slab we get

$$h' = 71.2 \text{ km.}$$

which is very much closer to the true value.

In another example where f is much closer to the critical frequency, say f = 3.8 Mc/s we get

$$h' = 174.0 \text{ km.}$$

in the exact case,

$$h' = 151.9 \text{ km.}$$

in the case where we assume that the value of μ in the last slab is that which corresponds to the mean value of N in the slab, and

$$h' = 165.7 \text{ km.}$$

where equation (7.16) is applied in the last slab.

6. Results.

Typical rays traces according to the method of this chapter

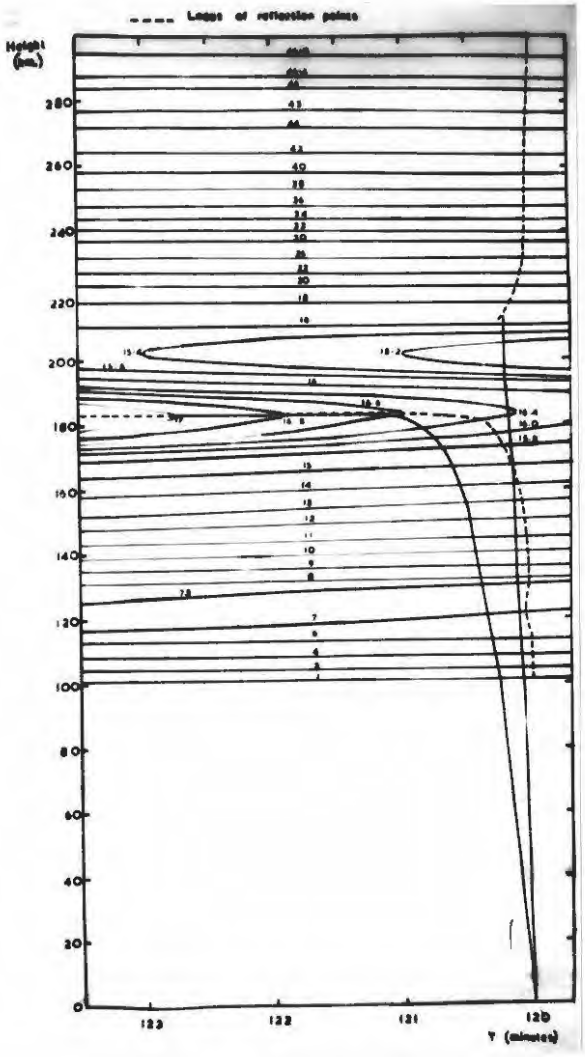

FIGURE 24: Typical rays constructed on the ionosphere map.

are shown in Figure 24. As can be seen, the rays which are deviated most from the vertical are those which have a frequency which is near to the critical frequency of the F1 layer. All other rays are reflected at very nearly vertical incidence. The errors caused by assuming vertical incidence are negligible in all cases except where the ray is deviated considerably from the vertical. However, the retardation for these rays is very large so that the incorrect virtual heights fall very near the cusp in the h'-f record. In the Kelso method of scaling it is wise to select the scaling points so that none of the frequencies at which the virtual heights are read falls on a cusp as this can lead to serious errors. Thus the effects due to deviation from vertical incidence do not make themselves felt in a Kelso scaling. For this reason it was decided that it would be adequate to assume vertical incidence for the remainder of the work. The h'-f records calculated by the method of this chapter are considered together with those calculated by assuming vertical incidence.

CHAPTER VIII.

THE EFFECT OF THE VALLEY ON VERTICAL INCIDENCE SOUNDINGS WHEN THE EARTH'S MAGNETIC FIELD IS IGNORED.

1. Method.

We have seen in the previous chapter that the effect of ignoring deviation of rays from the zenith is negligible. The form of the ionograms which would be obtained at any time during the eclipse could be found simply by evaluating the time delay of the echo, using the curves in Figures 16 and 17. This was done by evaluating $\Delta s/\mu$ for successive thin slabs of the ionosphere, Δs in thickness. Over each of these except the topmost the refractive index was assumed constant and equal to that corresponding to the average electron density in the slab. The average value of μ in the topmost slab was found from equation (7.14) or (7.16). The values of $\Delta s/\mu$ were summed from the ground to the level in the ionosphere at which the ray was reflected, thus giving the time delay of the reflected pulse. The calculation was repeated for a number of frequencies and hence the form of the ionogram at the given time was plotted.

The resulting ionograms were scaled by Kelso's method (37), ignoring the earth's field. This was done at a fairly large number of frequencies to eliminate scatter in the points scaled. This scatter occurs because of the number of scaling points which have sampling frequencies near cusps, so giving spuriously

high values. The N-h curves so obtained were those which would have been obtained by workers scaling, by Kelso's method, h'-f records obtained during the eclipse. They differed from the correct N-h curves shown in Figures 16 and 17 because of the presence of the valley which the Kelso method of scaling ignores.

By reading off the electron density at fixed heights from the N-h curves, obtained from the Kelso scaling, graphs were plotted showing the apparent variation of the electron density during the eclipse.

2. Results.

Figure 25 shows one of the N-h curves obtained by a Kelso scaling at a time during the latter part of the eclipse when a valley was present. It is compared with the true distribution at the same time. The curves for the true height obtained by Kelso scaling have been smoothed to eliminate the irregularities due to sampling frequencies falling near a cusp. This has been done as suggested by PIGGOTT (58). The effect of the valley is greatest just above the critical frequency where the retardation is greatest.

Figure 26 shows the variation of electron density with time at various fixed heights. It is taken from the paper by GLEDHILL & WALKER (59) which describes the work of this chapter. It shows that there is a large apparent maximum in electron

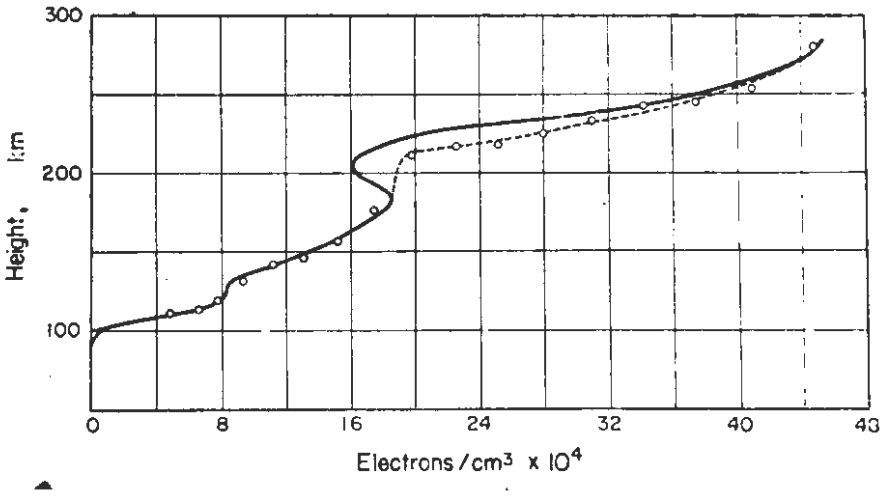

FIGURE 25: A typical Kelso scaling. Full curve: true distribution. Dashed curve: scaled distribution ignoring valley.

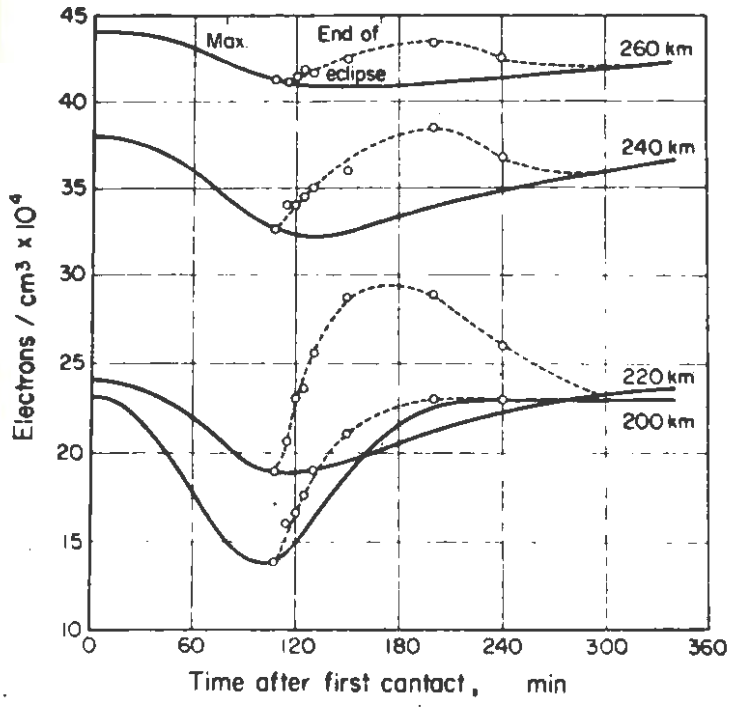

FIGURE 26: Variation of electron density with time at various fixed heights in the model ionosphere. Full line: true values. Dashed line: apparent values from Kelso scaling.

density in the lower F2 layer during the second half of the eclipse. The electron density returns to normal some time after the optical eclipse is over. At greater heights the effect is smaller but still noticeable. At the height 200 km., which falls in the valley, the apparent curve is deceptive, looking rather like the true one but with much too rapid a recovery after the minimum. Below the valley the apparent curves coincide with the true ones.

3. Discussion.

Figure 26 should be compared with Figure 14 which shows the experimental curves of Szendrei and McElhinny. There is great similarity between the two. The maximum after the middle of the optical eclipse appears in both figures leaving little doubt that a valley formed between the F1 and F2 layers during the eclipse of 25 December 1954.

MINNIS's curves shown in Figure 12 do not show a definite maximum. The maximum which does appear also appears on the control record and is due merely to the fact that the eclipse took place near noon so that the rate of production at that time was maximum.

SAVITT's curves, shown in Figure 11 do, however, show some signs of a maximum after the centre of the optical eclipse. He has not analysed a large enough number of records to show whether this is indeed a maximum or merely a rather higher value

of electron density than usual. However, the high value could easily be spurious and due to a valley rather than to the descent of the F layer as suggested by Savitt.

Since from the above it seems highly likely that a valley formed between the F1 and F2 layers during the eclipse of 25 December 1954, it was thought desirable to investigate this line further, including the effects of the earth's magnetic field and using TITHERIDGE's (45) method to eliminate the effect of the valley.

CHAPTER IX.

THE EFFECT OF THE VALLEY ON VERTICAL INCIDENCE SOUNDINGS WHEN THE EARTH'S FIELD IS CONSIDERED.

1. Method.

A similar treatment to that described in the previous chapter was used except that the effect of the earth's magnetic field was included and the valley effect considered.

Because of the considerable lateral deviation of rays incident vertically on the ionosphere when we include the effect of the earth's magnetic field one would expect that the effects of tilts in the layers would be quite considerable because of the comparatively large angles of incidence which the ray makes with the layers. As mentioned in Section 9 of Chapter I, the lateral deviation may be as large as 50 km. for the extraordinary ray. The question therefore arises as to whether one is justified in assuming vertical incidence. We should note that the deviation is in the magnetic meridian which is approximately at right angles to the path of the eclipse. This means that the horizontal component of the ray is unaffected by the tilts. The vertical component will be affected to much the same extent as is the vertical ray when the effects of the earth's field are ignored. We have seen in Chapter VII that this effect is small. The assumption of vertical incidence is thus not very far from the truth.

The method used to consider a given N-h curve was as follows:-

The curve was divided into a number of laminations whose boundaries were determined by the Titheridge scaling frequencies. At each frequency the virtual height was calculated by evaluating the sum, $\Sigma\mu'\Delta h$, for both the ordinary and extraordinary ray. This gave an h'-f curve corresponding to the given N-h curve. The ordinary h'-f curve was scaled by Titheridge's method, giving an N-h curve which did not include the effect of the valley. This was then used to find an apparent h'-f curve for the extraordinary ray and the effect of the valley was assessed as described in Chapter IV. Since all measurements were taken at the same set of frequencies the calculations could easily be made without the necessity of making numerous graphical measurements.

2. Results.

Tables 12 to 15 show values of the virtual height and of the true height obtained by a Titheridge scaling, corresponding to true heights at various times throughout the eclipse. Figure 27 shows a typical curve. Figure 28 shows the variation of electron density with time at various fixed heights. If the valley is ignored we once more find a large apparent maximum in the electron density in the F2 layer during the second half of the eclipse. If the valley is taken into account this maxi-

TABLE 12: Titheridge scaling in model ionosphere 130 mins. after onset of eclipse.

f	True height h.	h' O-wave	h by Titheridge scaling.	h' X-wave.	h' X-wave ignoring valley.	h corrected for valley.
Mc/s	km.	km.	km.	km.	km.	km.
0.948	90.9	105.6	90.9	107.0		
1.621	96.1	107.6	96.1	116.5		
2.143	101.3	117.8	101.3	120.8		
2.570	129.5	239.7	129.5	223.1		
2.930	138.3	192.4	138.3	217.8		
3.243	148.5	218.4	148.6	223.2		
3.518	159.7	246.9	159.6	250.5		
3.765	176.2	299.9	174.0	295.1		
3.988	221.3	438.6	199.9	465.3	407.4	219.3
4.191	223.8	309.0	205.8	366.7	353.0	222.9
4.378	226.2	304.9	211.0	335.6	330.8	226.1
4.552	229.0	304.9	215.1	331.0	324.6	228.9
4.713	231.7	308.0	218.7	328.2	321.9	231.6
4.864	234.6	314.4	222.1	330.6	322.9	234.7
5.006	237.8	323.0	225.5	336.6	326.9	327.8
5.139	241.0	329.5	228.7	342.7	330.6	241.0
5.266	244.4	337.9	231.9	349.7	334.8	244.2
5.386	247.6	343.8	235.0			247.7
5.500	251.1	356.7	238.3			251.4
5.609	255.0	372.8	241.9			255.5
5.713	259.1	386.6	245.8			259.9
5.813	263.5	403.5	250.0			265.3
5.908	269.0	437.7	255.4			270.0
6.000	274.1	666.0	260.0			

TABLE 13: Titheridge scaling in model ionosphere 150 mins. after onset of eclipse.

f	True height h.	h' O-wave.	h by Titheridge scaling.	h' X-wave.	h' X-wave ignoring valley.	h corrected for valley.
Mc/s	km.	km.	km.	km.	km.	km.
0.948	90.8	105.3	90.8	106.8		
1.621	95.1	104.7	95.1	113.6		
2.143	98.1	107.9	98.1	111.0		
2.570	104.0	123.0	104.0	127.1		
2.930	132.7	270.0	132.7	245.0		
2.243	140.1	198.7	140.1	227.3		
3.513	147.8	214.4	147.8	221.6		
3.765	158.4	254.5	158.2	253.0		
3.988	173.5	320.2	173.1	309.7		
4.191	223.0	477.7	200.7	501.5	438.7	221.6
4.378	225.7	327.3	206.6	392.4	373.9	225.1
4.552	228.5	321.2	211.8	356.6	345.8	228.8
4.713	231.4	321.3	216.0	350.0	339.7	231.8
4.864	224.4	325.6	219.8	348.0	337.3	234.6
5.006	237.5	329.9	223.2	349.9	336.6	237.5
5.139	240.7	336.5	226.5	354.0	338.9	240.6
		345.9	229.8	359.6	342.3	243.9
5.365	247.6	354.5	233.1			247.4
5.500	251.3	366.4	236.6			251.2
5.609	255.2	379.1	240.3			255.1
5.713	259.4	394.3	244.3			259.4
5.813	263.9	411.2	248.0			263.9
5.908	268.8	431.7	253.4			268.7
6.000	274.1	454.3	258.6			274.2

TABLE 14: Titheridge scaling in model ionosphere 180 mins. after onset of eclipse.

f	True height h.	h' O-wave	h by Titheridge scaling.	h' X-wave.	h' X-wave ignoring valley.	h corrected for valley
Mc/s	km.	km.	km.	km.	km.	km.
0.948	90.4	104.4	90.4	105.8		
1.621	94.4	103.3	94.4	112.0		
2.143	98.3	110.7	98.3	113.1		
2.570	102.0	117.7	102.0	119.7		
2.930	131.1	269.6	131.1	241.6		
2.243	137.1	187.8	137.1	218.4		
3.518	144.0	204.3	144.0	210.8		
3.765	152.0	228.0	151.8	230.3		
3.988	161.5	259.3	161.1	258.7		
4.191	179.5	365.9	178.9	341.8		
4.378	227.2	528.0	207.4	538.8	478.2	224.0
4.552	229.0	334.3	212.2	407.6	391.3	227.5
4.713	230.7	320.3	216.2	362.4	354.0	230.4
4.864	232.9	322.2	219.6	353.1	345.1	232.9
5.006	235.6	328.2	222.8	352.9	342.0	235.7
5.139	238.4	322.9	225.8	354.4	341.3	238.4
5.266	241.7	344.9	229.1	360.6	345.5	241.7
5.386	245.4	354.5	232.4			245.3
5.500	249.3	373.4	236.3			249.4
5.609	253.7	389.5	240.4			253.7
5.713	258.3	404.0	244.8			258.3
5.813	263.1	420.4	249.4			263.1
5.908	268.9	453.9	255.1			268.8
6.000	274.1	458.5	260.2			274.2

TABLE 15: Titheridge scaling in model ionosphere 210 mins. after onset of eclipse.

f	True height h.	h' O-wave.	h by Titheridge scaling.	h' X-wave.	h' X-wave ignoring valley.	h corrected for valley.
Mc/s	km.	km.	km.	km.	km.	km.
0.948	90.1	103.7	90.1	105.0		
1.621	94.6	104.6	94.6	112.9		
2.143	98.2	109.8	98.2	112.8		
2.570	102.1	118.6	102.1	120.1		
2.930	131.1	269.1	131.1	241.5		
2.243	138.1	194.2	138.1	223.3		
3.518	144.0	198.7	144.0	208.4		
3.765	151.4	222.8	151.5	225.3		
3.988	160.5	254.9	160.5	253.7		
4.191	172.0	300.2	171.9	294.0		
4.378	222.2	635.6	212.1	568.7	537.5	221.8
4.552	225.0	343.3	216.4	427.6	419.0	225.3
4.713	227.3	325.7	220.4	367.2	367.1	228.7
4.864	230.0	326.9	223.6	357.5	354.7	231.3
5.006	233.1	322.7	226.7	357.3	350.2	234.2
5.139	236.2	336.3	229.5	358.4	347.5	237.0
5.266	239.9	350.7	232.8	366.0	352.3	241.2
5.386	243.7	359.8	236.1			243.6
5.500	247.9	375.9	239.8			247.4
5.609	252.4	391.9	243.8			251.5
5.713	257.5	414.9	248.4			252.3
5.813	262.9	434.3	253.4			261.4
5.908	268.8	459.7	259.0			267.0
6.000	274.3	467.9	264.2			272.3

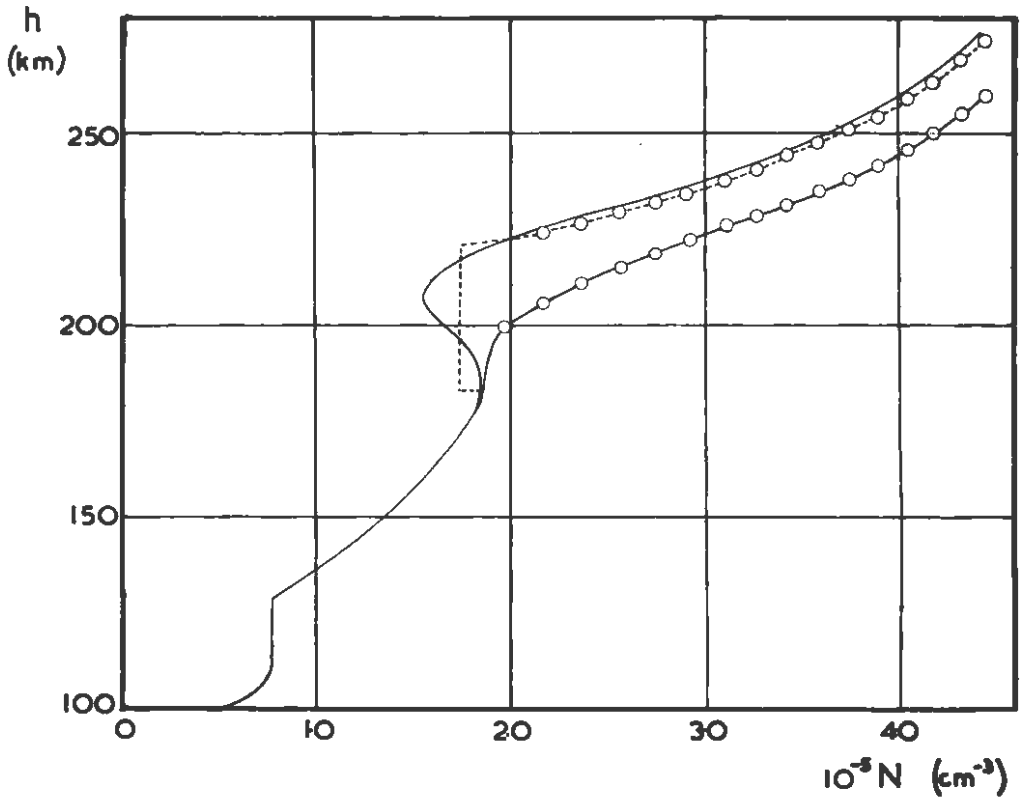

FIGURE 27: A typical N-h curve obtained from a Titheridge scaling. Upper full curve: true profile. Lower full curve: apparent profile when valley is ignored. Dashed curve: profile obtained when valley correction is included.

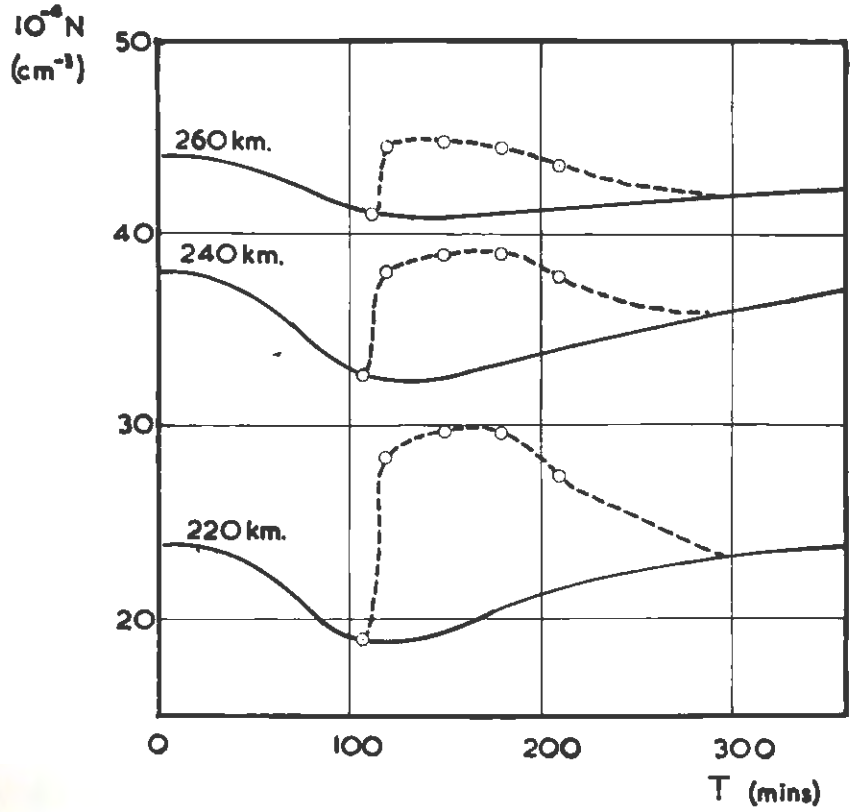

FIGURE 28: Variation of electron density with time at various fixed heights in the model ionosphere obtained by Titheridge scaling. Full curve: true variation. Dashed curve: Apparent variation ignoring valley. The variation obtained when the valley correction is made does not differ significantly from the true variation.

mum no longer appears and the derived variation of the electron density at any height agrees very well with the true variation.

3. Discussion.

We see that Titheridge's method is very successful in removing effects which occur because of the presence of a valley between two layers. If we do not take the valley into account the same errors occur as in the case when the earth's field was ignored and the arguments of Chapter VIII, Section 3, apply. When Titheridge's method is used we get a true picture of the variation of the electron density.

In Chapter X we apply this method to some of the ionograms obtained by SZENDREI & McELHINNY during the eclipse of 25 December 1954 at Grahamstown.

CHAPTER X.

SOME EXPERIMENTAL RESULTS.

1. The Scaling of some Ionosphere Eclipse Records.

Some of the records which were taken during the solar eclipse of 25 December 1954 have been scaled by the author, using Titheridge's method and correcting for any valley which might have been present.

The records chosen were all taken in the latter half of the eclipse because it seemed likely from the theoretical work described in the previous chapters that this would be where the presence of valleys would be most likely. Six of the best records taken between 0845 and 1015 hours, South African Standard Time, were used. Sporadic E reflections masked portions of the F1 layer in many of the records and in most cases the F1 extraordinary trace was almost entirely missing. Even when portions did appear these were invariably at the high frequency end of the F1 trace. This made it difficult to distinguish between the effects of a valley between the F1 and F2 layers, one between the E and F1 layers, and low level ionization whose density was lower than could be detected by the ionosonde. Because of this the correction applied for the valley was, of necessity, fairly crude.

Low level ionization was partially corrected for when possible by examining those portions of the F1 extraordinary

trace which were present. When the theoretical extraordinary trace had been constructed on the assumption that no valley existed, the F1 portion was compared with that of the experimental trace. If they did not agree because of low level ionization the whole of the F2 trace in the theoretical curve was raised or lowered by an appropriate amount. This correction takes no account of the distribution of the low-level ionization nor indeed of the different amount by which it would retard different frequencies, thus it only served to remove gross inaccuracies introduced by low-level ionization. More accuracy could only be obtained by taking a very much greater number of scaling points so that more fell on the small portions of the F1 extraordinary trace which had been recorded. This would necessitate the calculation of a new set of Titheridge coefficients. A full analysis of low-level ionization and of valleys between the E and F1 layers might then be possible.

The N-h curves so obtained are shown in Figure 29. In each case the lower curve is that which would be obtained if the valley were ignored and the upper is that obtained when the effect of the valley is included. A valley was present in all but one of the records scaled. In this one, taken at 0905 hours, a valley may have been present but, if so, it was smaller than the error produced by the crude method of

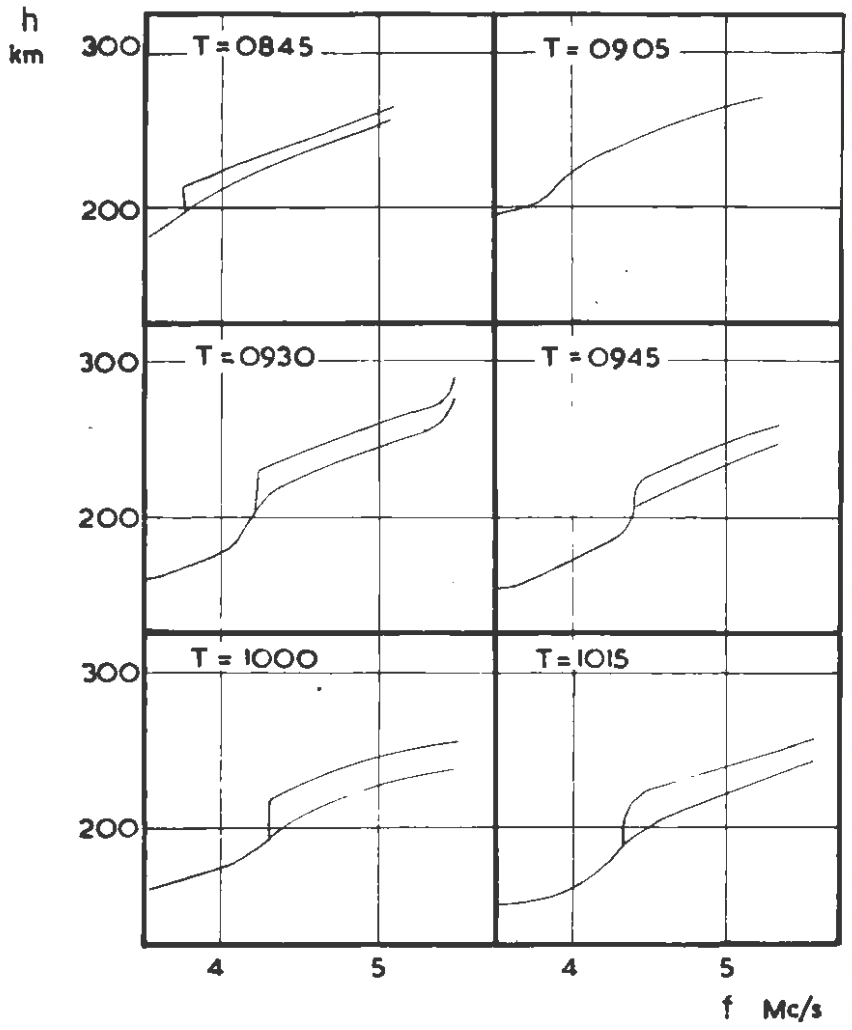

FIGURE 29: N-h curves obtained by Titheridge scaling from ionograms taken at various times during the eclipse of 25 December 1954. The upper curve in each case has been corrected for a valley. Times are South African Standard Time.

correcting for low-level ionization. From these curves the true and apparent variations of electron density with time at various fixed heights in the F2 layer were plotted. These are shown in Figure 30. The curves are compared with those obtained by Szendrei and McElhinny using Kelso's method.

2. Results.

In Figure 30 it will be noticed that the electron density at a given height, obtained by the Titheridge method of scaling is somewhat lower than that obtained by the Kelso scaling even when the valley is not taken into account. This is probably due to the fact that the Kelso method does not take the earth's magnetic field into account. However, the general features of the curve obtained by the Kelso scaling and that obtained by the Titheridge scaling ignoring the valley are the same. Both show the same spurious maximum during the later stages of the eclipse. When the valley correction is introduced this maximum disappears.

Curves showing the variation of electron density when recombination is the dominating mechanism of electron loss and when attachment is the dominating mechanism have also been plotted in Figure 30. These were calculated from equations (1.3) and (1.6). q was obtained from the control day data given by Szendrei and McElhinny; it was calculated at various times during the eclipse on the assumption that dN/dt

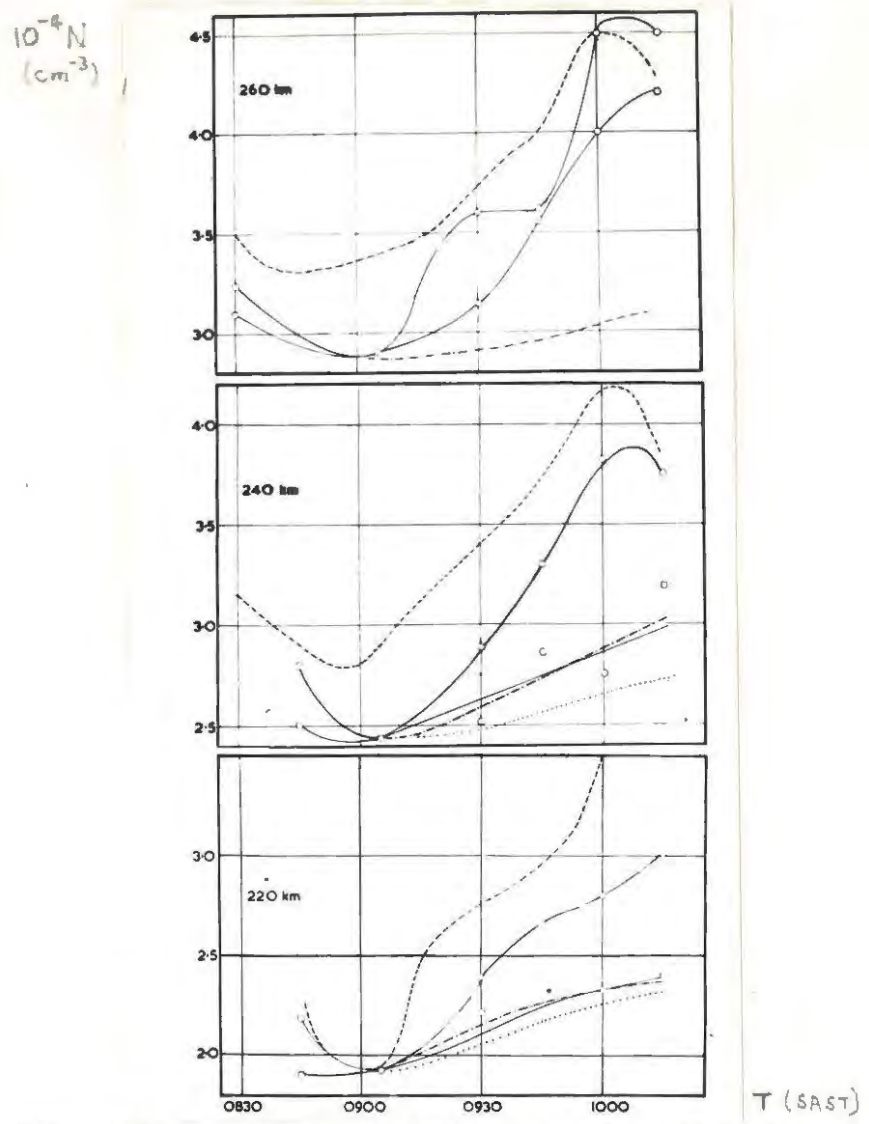

FIGURE 30: The variation of electron density with time at various fixed heights during the eclipse of 25 December 1954.

——— Upper curve: Titheridge scaling, no correction for valley.

Lower curve: Titheridge scaling with valley correction.

- - - Kelso scaling.

-·-·- Recombination.

····· Attachment.

220 km: $\alpha = 4 \times 10^{-10} cm^3 sec^{-1}$ $\beta = 7 \times 10^{-5} sec^{-1}$

240 km: $\alpha = 2 \times 10^{-10} cm^3 sec^{-1}$ $\beta = 4.5 \times 10^{-5} sec^{-1}$

260 km: $\alpha = 8 \times 10^{-11} cm^3 sec^{-1}$

was zero at those times on the control days. This assumes that equilibrium had been reached at these times on the control days. It will be seen that at 220 km. and 240 km. the experimental curves follow the recombination curve fairly closely. The agreement is much better than that found by Szendrei and McElhinny. However, in view of the errors in estimating the thickness of the valley, attachment could nonetheless be the dominating mechanism of electron loss. At 260 km. the agreement is not good. Only the curve assuming recombination is shown. That assuming attachment is not very different from it and neither agrees with the experimental curve. This might be due to the fact that the greatest errors introduced by the correction made for the low-level ionization would be at the high frequency end of the record. The values of the recombination coefficient and attachment coefficient used are not very different from those used by Szendrei and McElhinny.

It is interesting at this point to note that VILA (60) has analysed records taken during the eclipse of 2 October 1959. His curves of the variation of electron density with time at given heights show maxima very similar to those on the curves of Szendrei & McElhinny. These maxima he interprets as being caused by valleys as suggested by Gledhill and Walker. He proposes to analyse them by the methods described in this thesis.

It may thus be concluded that the results obtained by scaling ionosonde records during an eclipse may well be erroneous unless allowance is made for the valleys which occur between the layers and for low-level ionization. It may well be that a more detailed analysis will show that the behaviour of the F2 layer is much more regular than has been thought until now to be the case.

CHAPTER XI.

SOME SUGGESTIONS FOR FURTHER RESEARCH.

The most urgent task arising from the work described in this thesis seems to be a full analysis of the records obtained during a solar eclipse, including an analysis of control day data. The records obtained by Szendrei and McElhinny might yield very valuable results if so treated. It would be best if Titheridge coefficients which had more scaling points falling in the F1 region were used. Twenty-five equal frequency intervals would probably be the best choice. This would mean that the points would not be so crowded at the high frequency end. It would be preferable if the correction for low-level ionization were improved and also if the shape of the valley were taken into account. It is conceivable, however, that the accuracy of the ionograms themselves might not justify the extra precision so obtained.

The effects of tilts in the layers should also be investigated further. It seems doubtful whether tilts such as those described have any great effect on the virtual heights obtained but they may well cause the extra cusps observed on some eclipse records. Further, only tilts in the line of the eclipse have been considered. Tilts may also develop in a line perpendicular to the line of the eclipse. These would probably not be so pronounced because the changes in the amount

of incident ionizing radiation along this line would not be as great as along the line of the eclipse. However, because of the lateral deviation of the rays in the magnetic meridian the angle of incidence of the ray on the tilts may be fairly large and the effect on the line of propagation, and hence on the path length, may be considerable. An investigation on these lines might therefore be profitable.

When irregularities caused by the valley and by the tilts have been removed it might be interesting to see whether any remaining irregularities are caused by non-uniform radiation from the sun's discs.

Investigations along these lines, perhaps with the help of an electronic computer to do some complicated ray tracing, could do a great deal to explain the capricious behaviour of the F2 layer.

APPENDIX A.

μ' and μ^2 were computed for both ordinary and extraordinary waves on the ZEBRA electronic computer of the South African Council for Scientific and Industrial Research. Simple code was used. The program is given below for reference. The symbolism is that given in the Stantec Zebra Programming Manual.

Values of X from 0.01 to 0.98 at intervals of 0.01 for each value of Y from 0.100 to 0.500 at intervals of 0.025 were used. The value of the angle of dip used was 64° 36'. Results were printed out to ten figures in floating point form as this was the only form convenient in the simple code.

The values of μ' for the ordinary and extraordinary waves, rounded off to three decimal places, are given in Tables 23 and 24.

PROGRAM.

Instruction Tape:

Y	T304	H306	T309	NOR100
Q1ZL01	V0304	DR800	H310	A3
Q2L0100	A302I	A3	D309	V2
Q3L0250	Z1	UR1000	TR300I	KR800
+017	TR500	Z1	H307	VR1000
HR250	SR500	TR200I	V303	T310
T5	TR600	H3	V303	HR800
U0250	HR400	NOR100	T308	VR200
+098	V2	U307	H3	T309
H1	S301	V303	SR1000	H310
Z4	U305	V303	V308I	D309I
V5	AR500I	T308	T308	TR400
T301	TR700	H3	H3	Q5Z9
V0301	H305	SR900	S5	POR100
T301	AR600I	V308	T349	POR900
V0301	TR800	DR500	HR100	POR900
T302	HR400	SR900	D349	Z9
H1	VR100	NOR100	S3I	POR100
Z5	N2	A3	E04	POR1000
V5	U306	V2	H4	POR400
T303	DR700	KR700	TR400	+1
H3	A3I	VR900	X5	H0250
SR100	UR900	T310	Q4H308	+1
VR400	Z1	HR700	DR600	X1
V303	TR100	VR100	SR1000	Y1T00
V2				

Number Tape:

```
+.4292    (cos θ)
+2
+1
0
I
+.01      (values of X follow)
etc.
+.98
Y
+.1       (values of Y follow)
etc.
+.5
T
```

TABLE 16.

Ordinary ray group refractive indices, μ'_o.

X \ Y	0.100	0.125	0.150	0.175	0.200	0.225
0.01	1.004	1.004	1.004	1.004	1.004	1.004
0.02	1.009	1.008	1.008	1.008	1.007	1.007
0.03	1.013	1.012	1.012	1.011	1.011	1.011
0.04	1.017	1.017	1.016	1.015	1.015	1.014
0.05	1.022	1.021	1.020	1.019	1.019	1.018
0.06	1.026	1.025	1.024	1.023	1.023	1.022
0.07	1.031	1.029	1.029	1.028	1.027	1.026
0.08	1.036	1.034	1.033	1.032	1.031	1.030
0.09	1.041	1.039	1.037	1.036	1.035	1.033
0.10	1.045	1.044	1.042	1.040	1.039	1.037
0.11	1.050	1.048	1.046	1.045	1.043	1.041
0.12	1.055	1.053	1.051	1.049	1.047	1.046
0.13	1.060	1.058	1.056	1.054	1.052	1.050
0.14	1.066	1.063	1.060	1.058	1.056	1.054
0.15	1.071	1.068	1.065	1.063	1.061	1.058
0.16	1.076	1.073	1.070	1.068	1.065	1.063
0.17	1.082	1.078	1.075	1.072	1.070	1.067
0.18	1.087	1.084	1.080	1.077	1.074	1.072
0.19	1.093	1.089	1.085	1.082	1.079	1.076
0.20	1.098	1.094	1.091	1.087	1.084	1.081
0.21	1.104	1.100	1.096	1.092	1.089	1.086
0.22	1.110	1.106	1.101	1.098	1.094	1.091
0.23	1.116	1.111	1.107	1.103	1.099	1.095
0.24	1.122	1.117	1.113	1.108	1.104	1.100
0.25	1.129	1.123	1.118	1.114	1.110	1.106
0.26	1.135	1.129	1.124	1.119	1.115	1.111
0.27	1.141	1.136	1.130	1.125	1.120	1.116
0.28	1.148	1.142	1.136	1.131	1.126	1.121
0.29	1.155	1.148	1.142	1.137	1.132	1.127
0.30	1.162	1.155	1.149	1.143	1.137	1.132
0.31	1.169	1.162	1.155	1.149	1.143	1.138
0.32	1.176	1.168	1.162	1.155	1.149	1.144
0.33	1.183	1.175	1.168	1.162	1.155	1.150
0.34	1.191	1.183	1.175	1.168	1.162	1.156
0.35	1.198	1.190	1.182	1.175	1.168	1.162
0.36	1.206	1.197	1.189	1.182	1.175	1.168
0.37	1.214	1.205	1.196	1.188	1.181	1.175

X \ Y	0.100	0.125	0.150	0.175	0.200	0.225
0.38	1.222	1.212	1.204	1.195	1.188	1.181
0.39	1.230	1.220	1.211	1.203	1.195	1.188
0.40	1.239	1.228	1.219	1.210	1.202	1.194
0.41	1.247	1.237	1.227	1.218	1.209	1.201
0.42	1.256	1.245	1.235	1.225	1.217	1.209
0.43	1.265	1.254	1.243	1.233	1.224	1.216
0.44	1.275	1.263	1.251	1.241	1.232	1.223
0.45	1.284	1.272	1.260	1.249	1.240	1.231
0.46	1.294	1.281	1.269	1.258	1.248	1.239
0.47	1.304	1.290	1.278	1.267	1.256	1.247
0.48	1.314	1.300	1.287	1.275	1.265	1.255
0.49	1.325	1.310	1.297	1.285	1.273	1.263
0.50	1.335	1.320	1.306	1.294	1.282	1.271
0.51	1.347	1.331	1.316	1.303	1.291	1.281
0.52	1.358	1.342	1.327	1.313	1.301	1.290
0.53	1.370	1.353	1.337	1.323	1.311	1.299
0.54	1.382	1.364	1.348	1.334	1.321	1.309
0.55	1.394	1.376	1.359	1.344	1.331	1.318
0.56	1.407	1.388	1.371	1.355	1.341	1.328
0.57	1.420	1.400	1.383	1.367	1.352	1.339
0.58	1.434	1.413	1.395	1.378	1.363	1.350
0.59	1.448	1.426	1.407	1.390	1.375	1.361
0.60	1.462	1.440	1.420	1.403	1.387	1.372
0.61	1.477	1.454	1.434	1.416	1.399	1.384
0.62	1.493	1.469	1.448	1.429	1.412	1.397
0.63	1.508	1.484	1.462	1.442	1.425	1.409
0.64	1.525	1.500	1.477	1.457	1.439	1.422
0.65	1.542	1.516	1.492	1.471	1.453	1.436
0.66	1.560	1.533	1.508	1.487	1.468	1.451
0.67	1.579	1.550	1.525	1.503	1.483	1.465
0.68	1.598	1.568	1.542	1.519	1.499	1.481
0.69	1.618	1.587	1.560	1.536	1.516	1.497
0.70	1.639	1.607	1.579	1.554	1.533	1.514
0.71	1.660	1.627	1.598	1.573	1.551	1.532
0.72	1.683	1.649	1.619	1.593	1.570	1.551
0.73	1.707	1.671	1.640	1.614	1.591	1.571
0.74	1.732	1.695	1.663	1.636	1.612	1.592
0.75	1.758	1.720	1.687	1.659	1.635	1.614
0.76	1.786	1.746	1.712	1.683	1.659	1.638
0.77	1.815	1.774	1.739	1.709	1.684	1.663
0.78	1.846	1.803	1.767	1.737	1.712	1.691
0.79	1.879	1.834	1.797	1.767	1.741	1.720
0.80	1.914	1.868	1.830	1.799	1.773	1.752

X \ Y	0.100	0.125	0.150	0.175	0.200	0.225
0.81	1.952	1.906	1.865	1.833	1.808	1.786
0.82	1.992	1.942	1.903	1.871	1.846	1.826
0.83	2.035	1.984	1.944	1.912	1.888	1.869
0.84	2.082	2.030	1.989	1.958	1.935	1.918
0.85	2.133	2.080	2.040	2.010	1.988	1.973
0.86	2.189	2.136	2.096	2.068	2.049	2.036
0.87	2.252	2.198	2.160	2.135	2.119	2.110
0.88	2.323	2.269	2.234	2.212	2.201	2.198
0.89	2.403	2.352	2.321	2.305	2.301	2.305
0.90	2.496	2.450	2.426	2.418	2.423	2.438
0.91	2.608	2.569	2.555	2.560	2.579	2.607
0.92	2.744	2.719	2.721	2.744	2.782	2.830
0.93	2.919	2.916	2.944	2.994	3.060	3.137
0.94	3.156	3.189	3.258	3.351	3.459	3.577
0.95	3.500	3.598	3.734	3.894	4.068	4.248
0.96	4.057	4.272	4.524	4.795	5.071	5.343
0.97	5.103	5.545	6.007	6.462	6.895	7.299
0.98	7.560	8.465	9.293	10.023	10.653	11.190

X \ Y	0.250	0.275	0.300	0.325	0.350	0.375
0.01	1.003	1.003	1.003	1.003	1.003	1.003
0.02	1.007	1.007	1.006	1.006	1.006	1.006
0.03	1.010	1.010	1.010	1.009	1.009	1.009
0.04	1.014	1.013	1.013	1.013	1.012	1.012
0.05	1.017	1.017	1.016	1.016	1.015	1.015
0.06	1.021	1.020	1.020	1.019	1.018	1.018
0.07	1.025	1.024	1.023	1.022	1.022	1.021
0.08	1.028	1.028	1.027	1.026	1.025	1.024
0.09	1.032	1.031	1.030	1.029	1.028	1.027
0.10	1.036	1.035	1.034	1.033	1.032	1.031
0.11	1.040	1.039	1.037	1.036	1.035	1.034
0.12	1.044	1.043	1.041	1.040	1.039	1.037
0.13	1.048	1.046	1.045	1.043	1.042	1.041
0.14	1.052	1.050	1.049	1.047	1.046	1.044
0.15	1.056	1.054	1.053	1.051	1.049	1.048
0.16	1.061	1.058	1.057	1.055	1.053	1.051
0.17	1.064	1.063	1.061	1.059	1.057	1.055
0.18	1.069	1.067	1.065	1.063	1.061	1.059
0.19	1.074	1.071	1.069	1.067	1.065	1.063
0.20	1.078	1.075	1.073	1.071	1.068	1.066

X \ Y	0.250	0.275	0.300	0.325	0.350	0.375
0.21	1.083	1.080	1.077	1.075	1.072	1.070
0.22	1.087	1.084	1.082	1.079	1.077	1.074
0.23	1.092	1.089	1.086	1.083	1.081	1.078
0.24	1.097	1.094	1.091	1.088	1.085	1.082
0.25	1.102	1.098	1.095	1.092	1.089	1.087
0.26	1.107	1.103	1.100	1.097	1.094	1.091
0.27	1.112	1.108	1.105	1.101	1.098	1.095
0.28	1.117	1.113	1.109	1.106	1.103	1.099
0.29	1.122	1.118	1.114	1.111	1.107	1.104
0.30	1.128	1.123	1.119	1.115	1.112	1.109
0.31	1.133	1.129	1.124	1.120	1.117	1.113
0.32	1.139	1.134	1.130	1.125	1.122	1.118
0.33	1.144	1.139	1.135	1.131	1.127	1.123
0.34	1.150	1.145	1.140	1.136	1.132	1.128
0.35	1.156	1.151	1.146	1.141	1.137	1.133
0.36	1.162	1.157	1.151	1.147	1.142	1.138
0.37	1.168	1.163	1.157	1.152	1.147	1.143
0.38	1.175	1.169	1.163	1.158	1.153	1.149
0.39	1.181	1.175	1.169	1.164	1.159	1.154
0.40	1.188	1.181	1.175	1.170	1.164	1.160
0.41	1.194	1.188	1.181	1.176	1.170	1.165
0.42	1.201	1.194	1.188	1.182	1.176	1.171
0.43	1.208	1.200	1.194	1.188	1.183	1.177
0.44	1.215	1.208	1.201	1.195	1.189	1.183
0.45	1.223	1.215	1.208	1.201	1.195	1.190
0.46	1.230	1.222	1.215	1.208	1.202	1.196
0.47	1.238	1.230	1.222	1.215	1.209	1.203
0.48	1.246	1.237	1.230	1.222	1.216	1.210
0.49	1.254	1.245	1.237	1.230	1.223	1.217
0.50	1.262	1.253	1.245	1.237	1.230	1.224
0.51	1.271	1.261	1.253	1.245	1.238	1.231
0.52	1.279	1.270	1.261	1.253	1.246	1.239
0.53	1.288	1.279	1.270	1.261	1.254	1.247
0.54	1.298	1.288	1.278	1.270	1.262	1.255
0.55	1.307	1.297	1.287	1.279	1.271	1.263
0.56	1.317	1.306	1.297	1.288	1.279	1.272
0.57	1.327	1.316	1.306	1.297	1.289	1.281
0.58	1.337	1.326	1.316	1.307	1.298	1.290
0.59	1.348	1.337	1.326	1.317	1.308	1.300
0.60	1.359	1.347	1.337	1.327	1.318	1.310

X \ Y	0.250	0.275	0.300	0.325	0.350	0.375
0.61	1.371	1.359	1.348	1.338	1.329	1.320
0.62	1.383	1.370	1.359	1.349	1.340	1.331
0.63	1.395	1.382	1.371	1.361	1.351	1.343
0.64	1.408	1.395	1.383	1.373	1.363	1.354
0.65	1.421	1.408	1.396	1.385	1.376	1.367
1.66	1.435	1.422	1.410	1.399	1.389	1.380
1.67	1.450	1.436	1.424	1.412	1.403	1.394
1.68	1.465	1.451	1.438	1.427	1.417	1.408
1.69	1.481	1.467	1.454	1.442	1.432	1.424
1.70	1.498	1.483	1.470	1.459	1.449	1.440
1.71	1.515	1.500	1.487	1.476	1.466	1.457
1.72	1.534	1.519	1.506	1.494	1.484	1.476
1.73	1.553	1.538	1.525	1.514	1.504	1.495
1.74	1.574	1.559	1.546	1.535	1.525	1.517
1.75	1.596	1.581	1.568	1.557	1.548	1.540
1.76	1.620	1.605	1.592	1.581	1.572	1.565
1.77	1.646	1.630	1.618	1.608	1.599	1.592
1.78	1.673	1.658	1.646	1.637	1.629	1.622
1.79	1.703	1.689	1.677	1.668	1.661	1.656
1.80	1.736	1.722	1.711	1.703	1.697	1.693
1.81	1.771	1.759	1.749	1.742	1.737	1.734
1.82	1.811	1.800	1.791	1.786	1.783	1.781
1.83	1.856	1.846	1.839	1.836	1.834	1.835
1.84	1.906	1.898	1.894	1.893	1.894	1.897
1.85	1.963	1.958	1.957	1.959	1.963	1.969
1.86	2.030	2.028	2.031	2.036	2.044	2.055
0.87	2.108	2.111	2.119	2.129	2.142	2.157
0.88	2.202	2.211	2.224	2.241	2.261	2.282
0.89	2.317	2.334	2.355	2.380	2.407	2.437
0.90	2.460	2.487	2.519	2.555	2.593	2.632
0.91	2.643	2.685	2.731	2.781	2.832	2.885
0.92	2.886	2.948	3.013	3.081	3.150	3.220
0.93	3.221	3.309	3.400	3.493	3.586	3.677
0.94	3.701	3.827	3.954	4.080	4.203	4.322
0.95	4.429	4.608	4.783	4.952	5.113	5.267
0.96	5.607	5.858	6.094	6.316	6.522	6.713
0.97	7.668	8.004	8.307	8.580	8.824	9.042
0.98	11.647	12.033	12.362	12.641	12.879	13.084

X \ Y	0.400	0.425	0.450	0.475	0.500
0.01	1.003	1.003	1.003	1.003	1.003
0.02	1.006	1.005	1.005	1.005	1.005
0.03	1.009	1.008	1.008	1.008	1.008
0.04	1.011	1.011	1.011	1.010	1.010
0.05	1.014	1.014	1.014	1.013	1.013
0.06	1.017	1.017	1.016	1.016	1.016
0.07	1.020	1.020	1.019	1.019	1.018
0.08	1.024	1.023	1.022	1.022	1.021
0.09	1.027	1.026	1.025	1.024	1.024
0.10	1.030	1.029	1.028	1.027	1.027
0.11	1.033	1.032	1.031	1.030	1.030
0.12	1.036	1.035	1.034	1.033	1.032
0.13	1.040	1.039	1.037	1.036	1.035
0.14	1.043	1.042	1.041	1.040	1.038
0.15	1.046	1.045	1.044	1.043	1.042
0.16	1.050	1.049	1.047	1.046	1.045
0.17	1.053	1.052	1.051	1.049	1.048
0.18	1.057	1.055	1.054	1.052	1.051
0.19	1.061	1.059	1.057	1.056	1.054
0.20	1.064	1.063	1.061	1.059	1.058
0.21	1.068	1.066	1.064	1.063	1.061
0.22	1.072	1.070	1.068	1.066	1.065
0.23	1.076	1.074	1.072	1.070	1.068
0.24	1.080	1.078	1.076	1.074	1.072
0.25	1.084	1.082	1.079	1.077	1.075
0.26	1.088	1.086	1.083	1.081	1.079
0.27	1.092	1.090	1.087	1.085	1.083
0.28	1.097	1.094	1.091	1.089	1.087
0.29	1.101	1.098	1.095	1.093	1.091
0.30	1.105	1.102	1.100	1.097	1.095
0.31	1.110	1.107	1.104	1.101	1.099
0.32	1.115	1.111	1.108	1.106	1.103
0.33	1.119	1.116	1.113	1.110	1.107
0.34	1.124	1.121	1.117	1.114	1.112
0.35	1.129	1.125	1.122	1.119	1.116
0.36	1.134	1.130	1.127	1.124	1.121
0.37	1.139	1.135	1.132	1.128	1.125
0.38	1.144	1.140	1.137	1.133	1.130
0.39	1.150	1.146	1.142	1.138	1.135
0.40	1.155	1.151	1.147	1.143	1.140

X \ Y	0.400	0.425	0.450	0.475	0.500
0.41	1.161	1.156	1.152	1.148	1.145
0.42	1.166	1.162	1.158	1.154	1.150
0.43	1.172	1.168	1.163	1.159	1.156
0.44	1.178	1.174	1.169	1.165	1.161
0.45	1.184	1.180	1.175	1.171	1.167
0.46	1.191	1.186	1.181	1.177	1.173
0.47	1.197	1.192	1.187	1.183	1.179
0.48	1.204	1.199	1.194	1.189	1.185
0.49	1.211	1.205	1.200	1.196	1.191
0.50	1.218	1.212	1.207	1.202	1.198
0.51	1.225	1.219	1.214	1.209	1.205
0.52	1.233	1.227	1.221	1.216	1.212
0.53	1.240	1.234	1.229	1.224	1.219
0.54	1.248	1.242	1.237	1.231	1.227
0.55	1.257	1.250	1.245	1.239	1.234
0.56	1.265	1.259	1.253	1.248	1.243
0.57	1.274	1.267	1.262	1.256	1.251
0.58	1.283	1.277	1.271	1.265	1.260
0.59	1.293	1.286	1.280	1.274	1.269
0.60	1.303	1.296	1.290	1.284	1.279
0.61	1.313	1.306	1.300	1.294	1.289
0.62	1.324	1.317	1.310	1.305	1.299
0.63	1.335	1.328	1.322	1.316	1.311
0.64	1.347	1.340	1.333	1.327	1.322
0.65	1.359	1.352	1.346	1.340	1.335
0.66	1.372	1.365	1.359	1.353	1.348
0.67	1.386	1.379	1.372	1.367	1.362
0.68	1.400	1.393	1.387	1.381	1.376
0.69	1.416	1.409	1.402	1.397	1.392
0.70	1.432	1.425	1.419	1.414	1.409
0.71	1.449	1.443	1.437	1.432	1.427
0.72	1.468	1.462	1.456	1.451	1.447
0.73	1.488	1.482	1.476	1.472	1.468
0.74	1.510	1.504	1.499	1.495	1.491
0.75	1.533	1.528	1.523	1.519	1.517
0.76	1.559	1.554	1.550	1.547	1.544
0.77	1.587	1.582	1.579	1.577	1.575
0.78	1.616	1.614	1.611	1.610	1.609
0.79	1.652	1.649	1.648	1.647	1.648
0.80	1.690	1.688	1.688	1.689	1.690

X \ Y	0.400	0.425	0.450	0.475	0.500
0.81	1.733	1.733	1.734	1.736	1.739
0.82	1.782	1.783	1.786	1.790	1.795
0.83	1.837	1.841	1.846	1.853	1.860
0.84	1.902	1.908	1.916	1.925	1.935
0.85	1.977	1.987	1.998	2.010	2.023
0.86	2.067	2.081	2.095	2.111	2.128
0.87	2.174	2.193	2.213	2.233	2.255
0.88	2.305	2.330	2.356	2.382	2.409
0.89	2.468	2.500	2.533	2.567	2.601
0.90	2.673	2.715	2.758	2.800	2.843
0.91	2.939	2.993	3.047	3.100	3.153
0.92	3.290	3.359	3.428	3.495	3.560
0.93	3.768	3.856	3.942	4.025	4.106
0.94	4.438	4.550	4.657	4.759	4.856
0.95	5.413	5.551	5.681	5.803	5.917
0.96	6.980	7.053	7.203	7.341	7.468
0.97	9.238	9.413	9.570	9.711	9.837
0.98	13.260	13.412	13.545	13.661	13.763

TABLE 17.

Extraordinary ray group refractive indices, μ'_x.

X \ Y	0.100	0.125	0.150	0.175	0.200	0.225
0.01	1.006	1.006	1.007	1.007	1.008	1.008
0.02	1.012	1.013	1.014	1.015	1.015	1.016
0.03	1.019	1.020	1.021	1.022	1.023	1.025
0.04	1.025	1.026	1.028	1.030	1.031	1.033
0.05	1.032	1.033	1.035	1.037	1.040	1.042
0.06	1.038	1.040	1.043	1.045	1.048	1.051
0.07	1.045	1.048	1.050	1.053	1.056	1.060
0.08	1.052	1.055	1.058	1.061	1.065	1.069
0.09	1.059	1.062	1.066	1.070	1.074	1.078
0.10	1.066	1.070	1.074	1.078	1.083	1.088
0.11	1.073	1.077	1.082	1.086	1.092	1.098
0.12	1.081	1.085	1.090	1.096	1.102	1.108
0.13	1.088	1.093	1.099	1.105	1.111	1.119
0.14	1.096	1.101	1.107	1.114	1.121	1.129
0.15	1.104	1.110	1.116	1.123	1.131	1.140
0.16	1.112	1.118	1.125	1.133	1.141	1.151
0.17	1.120	1.127	1.134	1.143	1.152	1.162
0.18	1.128	1.136	1.144	1.153	1.163	1.174
0.19	1.137	1.145	1.153	1.163	1.174	1.186
0.20	1.145	1.154	1.163	1.174	1.185	1.198
0.21	1.154	1.163	1.173	1.184	1.197	1.210
0.22	1.163	1.173	1.184	1.195	1.208	1.223
0.23	1.172	1.183	1.194	1.207	1.220	1.236
0.24	1.182	1.193	1.205	1.218	1.233	1.249
0.25	1.191	1.203	1.216	1.231	1.246	1.263
0.26	1.201	1.214	1.227	1.242	1.259	1.277
0.27	1.211	1.224	1.239	1.255	1.272	1.292
0.28	1.222	1.235	1.251	1.267	1.286	1.307
0.29	1.232	1.247	1.263	1.280	1.300	1.322
0.30	1.243	1.258	1.275	1.294	1.315	1.338
0.31	1.254	1.270	1.288	1.308	1.330	1.355
0.32	1.266	1.282	1.301	1.322	1.345	1.372
0.33	1.277	1.295	1.315	1.337	1.361	1.389
0.34	1.289	1.308	1.329	1.352	1.378	1.407
0.35	1.302	1.321	1.343	1.367	1.395	1.426
0.36	1.314	1.335	1.358	1.384	1.413	1.446
0.37	1.327	1.349	1.373	1.400	1.431	1.466

X \ Y	0.100	0.125	0.150	0.175	0.200	0.225
0.38	1.340	1.363	1.389	1.417	1.450	1.486
0.39	1.354	1.378	1.405	1.435	1.469	1.508
0.40	1.368	1.393	1.422	1.453	1.489	1.531
0.41	1.383	1.409	1.439	1.472	1.510	1.554
0.42	1.398	1.425	1.457	1.492	1.532	1.578
0.43	1.413	1.442	1.475	1.512	1.555	1.604
0.44	1.429	1.460	1.494	1.534	1.578	1.630
0.45	1.446	1.478	1.514	1.556	1.603	1.658
0.46	1.463	1.496	1.535	1.579	1.629	1.687
0.47	1.480	1.516	1.556	1.602	1.656	1.717
0.48	1.493	1.536	1.578	1.627	1.634	1.750
0.49	1.517	1.557	1.602	1.653	1.713	1.783
0.50	1.537	1.578	1.626	1.680	1.744	1.818
0.51	1.557	1.601	1.651	1.709	1.776	1.856
0.52	1.578	1.624	1.677	1.739	1.810	1.895
0.53	1.600	1.649	1.705	1.770	1.847	1.937
0.54	1.623	1.674	1.734	1.803	1.885	1.982
0.55	1.647	1.701	1.764	1.838	1.925	2.030
0.56	1.672	1.729	1.796	1.874	1.968	2.081
0.57	1.698	1.758	1.829	1.913	2.014	2.136
0.58	1.725	1.789	1.865	1.955	2.062	2.194
0.59	1.753	1.821	1.902	1.998	2.115	2.258
0.60	1.783	1.856	1.942	2.045	2.171	2.327
0.61	1.814	1.892	1.984	2.095	2.232	2.403
0.62	1.847	1.930	2.029	2.149	2.297	2.485
0.63	1.882	1.970	2.077	2.207	2.369	2.577
0.64	1.919	2.014	2.128	2.269	2.447	2.678
0.65	1.958	2.060	2.183	2.337	2.533	2.792
0.66	2.000	2.109	2.243	2.411	2.628	2.920
0.67	2.044	2.161	2.307	2.492	2.735	3.066
0.68	2.091	2.218	2.378	2.582	2.854	3.235
0.69	2.141	2.280	2.454	2.682	2.990	3.433
0.70	2.196	2.346	2.539	2.793	3.146	3.670

X \ Y	0.100	0.125	0.150	0.175	0.200	0.225
0.71	2.254	2.419	2.632	2.919	3.327	3.961
0.72	2.317	2.499	2.737	3.063	3.542	4.327
0.73	2.386	2.587	2.854	3.230	3.802	4.810
0.74	2.462	2.685	2.989	3.426	4.125	5.487
0.75	2.545	2.794	3.141	3.660	4.541	6.536
0.76	2.637	2.918	3.320	3.947	5.106	8.501
0.77	2.739	3.060	3.552	4.310	5.932	14.849
0.78	2.854	3.224	3.789	4.789	7.317	∞
0.79	2.985	3.416	4.108	5.462	10.431	
0.80	3.136	3.647	4.521	6.505	∞	
0.81	3.312	3.931	5.081	8.463		
0.82	3.520	4.289	5.903	14.790		
0.83	3.773	4.764	7.282	∞		
0.84	4.087	5.431	10.388			
0.85	4.494	6.469	∞			
0.86	5.048	8.421				
0.87	5.864	14.738				
0.88	7.237	∞				
0.89	10.337					
0.90	∞					

X \ Y	0.250	0.275	0.300	0.325	0.350	0.375
0.01	1.009	1.009	1.010	1.011	1.011	1.012
0.02	1.017	1.019	1.020	1.021	1.023	1.025
0.03	1.026	1.028	1.030	1.032	1.035	1.038
0.04	1.035	1.038	1.041	1.044	1.047	1.051
0.05	1.045	1.048	1.051	1.055	1.059	1.064
0.06	1.054	1.058	1.062	1.067	1.072	1.078
0.07	1.064	1.068	1.073	1.079	1.085	1.092
0.08	1.074	1.079	1.085	1.091	1.098	1.106
0.09	1.084	0.090	1.096	1.104	1.112	1.121
0.10	1.094	1.101	1.108	1.117	1.126	1.136
0.11	1.105	1.112	1.121	1.130	1.140	1.152
0.12	1.116	1.124	1.133	1.143	1.155	1.168
0.13	1.127	1.136	1.146	1.157	1.170	1.185
0.14	1.138	1.148	1.159	1.172	1.186	1.202
0.15	1.150	1.160	1.173	1.186	1.202	1.219
0.16	1.161	1.173	1.186	1.201	1.218	1.237
0.17	1.174	1.186	1.201	1.217	1.235	1.256
0.18	1.186	1.200	1.215	1.233	1.252	1.275
0.19	1.200	1.214	1.230	1.249	1.270	1.295
0.20	1.212	1.228	1.246	1.266	1.289	1.315

X \ Y	0.250	0.275	0.300	0.325	0.350	0.375
0.21	1.225	1.242	1.262	1.283	1.308	1.336
0.22	1.239	1.257	1.278	1.301	1.328	1.358
0.23	1.253	1.273	1.295	1.320	1.348	1.381
0.24	1.268	1.289	1.312	1.339	1.369	1.405
0.25	1.283	1.305	1.330	1.359	1.391	1.429
0.26	1.298	1.322	1.349	1.379	1.414	1.455
0.27	1.314	1.339	1.368	1.400	1.438	1.481
0.28	1.331	1.357	1.388	1.422	1.462	1.506
0.29	1.348	1.376	1.408	1.445	1.488	1.537
0.30	1.365	1.395	1.429	1.469	1.514	1.567
0.31	1.383	1.415	1.451	1.493	1.542	1.599
0.32	1.402	1.436	1.474	1.519	1.571	1.632
0.33	1.421	1.457	1.498	1.546	1.601	1.666
0.34	1.441	1.479	1.523	1.574	1.633	1.703
0.35	1.462	1.502	1.549	1.603	1.666	1.741
0.36	1.483	1.526	1.576	1.633	1.701	1.781
0.37	1.505	1.551	1.604	1.665	1.738	1.824
0.38	1.529	1.577	1.633	1.699	1.776	1.869
0.39	1.553	1.604	1.664	1.734	1.817	1.917
0.40	1.578	1.632	1.696	1.771	1.861	1.968
0.41	1.604	1.662	1.730	1.810	1.906	2.023
0.42	1.631	1.693	1.765	1.852	1.955	2.082
0.43	1.660	1.726	1.803	1.896	2.008	2.145
0.44	1.698	1.760	1.843	1.943	2.063	2.213
0.45	1.722	1.797	1.885	1.993	2.123	2.286
0.46	1.755	1.835	1.930	2.046	2.188	2.367
0.47	1.790	1.875	1.978	2.103	2.258	2.455
0.48	1.826	1.918	2.029	2.164	2.334	2.551
0.49	1.865	1.964	2.083	2.231	2.417	2.659
0.50	1.907	2.013	2.142	2.303	2.508	2.779
0.51	1.950	2.065	2.205	2.381	2.609	2.914
0.52	1.997	2.121	2.273	2.467	2.721	3.067
0.53	2.047	2.181	2.348	2.562	2.846	3.245
0.54	2.100	2.246	2.429	2.667	2.989	3.452
0.55	2.158	2.316	2.512	2.784	3.152	3.699
0.56	2.219	2.393	2.617	2.917	3.342	4.001
0.57	2.286	2.477	2.727	3.068	3.566	4.380
0.58	2.359	2.570	2.850	3.242	3.836	4.879
0.59	2.439	2.673	2.990	3.446	4.170	5.575
0.60	2.526	2.789	3.151	3.689	4.599	6.651

X \ Y	0.250	0.275	0.300	0.325	0.350	0.375
0.61	2.623	2.919	3.337	3.986	5.179	8.660
0.62	2.731	3.067	3.558	4.361	6.026	15.136
0.63	2.853	3.239	3.824	4.853	7.446	∞
0.64	2.991	3.440	4.154	5.542	10.611	
0.65	3.149	3.680	4.579	6.606	∞	
0.66	3.333	3.973	5.152	8.596		
0.67	3.550	4.344	5.991	15.016		
0.68	3.813	4.831	7.392	∞		
0.69	4.140	5.513	10.538			
0.70	4.560	6.569	∞			
0.71	5.128	8.545				
0.72	5.960	14.923				
0.73	7.352	∞				
0.74	10.479					
0.75	∞					

X \ Y	0.400	0.425	0.450	0.475	0.500
0.01	1.013	1.014	1.016	1.017	1.019
0.02	1.027	1.029	1.032	1.035	1.038
0.03	1.041	1.044	1.048	1.053	1.058
0.04	1.055	1.060	1.065	1.072	1.079
0.05	1.070	1.076	1.083	1.091	1.100
0.06	1.084	1.092	1.101	1.111	1.122
0.07	1.100	1.109	1.119	1.131	1.145
0.08	1.116	1.126	1.138	1.152	1.168
0.09	1.132	1.144	1.158	1.174	1.192
0.10	1.148	1.162	1.178	1.196	1.217
0.11	1.166	1.181	1.199	1.219	1.243
0.12	1.183	1.200	1.220	1.243	1.270
0.13	1.201	1.220	1.242	1.268	1.298
0.14	1.220	1.241	1.265	1.293	1.372
0.15	1.239	1.262	1.289	1.320	1.357
0.16	1.259	1.284	1.313	1.348	1.388
0.17	1.280	1.307	1.339	1.376	1.420
0.18	1.301	1.331	1.365	1.406	1.454
0.19	1.323	1.355	1.393	1.437	1.490
0.20	1.346	1.381	1.422	1.470	1.527

X \ Y	0.400	0.425	0.450	0.475	0.500
0.21	1.369	1.407	1.451	1.504	1.566
0.22	1.394	1.434	1.482	1.539	1.607
0.23	1.419	1.463	1.515	1.577	1.651
0.24	1.445	1.493	1.549	1.616	1.696
0.25	1.473	1.524	1.585	1.657	1.744
0.26	1.501	1.557	1.622	1.700	1.795
0.27	1.531	1.591	1.661	1.746	1.849
0.28	1.562	1.626	1.703	1.795	1.907
0.29	1.595	1.664	1.746	1.846	1.969
0.30	1.630	1.704	1.792	1.901	2.035
0.31	1.666	1.745	1.841	1.959	2.106
0.32	1.704	1.789	1.894	2.022	2.183
0.33	1.743	1.836	1.949	2.089	2.266
0.34	1.785	1.886	2.008	2.161	2.356
0.35	1.830	1.939	2.072	2.240	2.456
0.36	1.878	1.995	2.140	2.325	2.565
0.37	1.928	2.055	2.214	2.418	2.686
0.38	1.982	2.120	2.295	2.520	2.822
0.39	2.039	2.190	2.382	2.633	2.976
0.40	2.101	2.266	2.478	2.760	3.151
0.41	2.167	2.348	2.584	2.902	3.354
0.42	2.239	2.439	2.702	3.063	3.593
0.43	2.317	2.538	2.833	3.248	3.880
0.44	2.402	2.648	2.982	3.465	4.235
0.45	2.495	2.771	3.152	3.723	4.688
0.46	2.598	2.909	3.350	4.037	5.299
0.47	2.713	3.066	3.583	4.431	6.186
0.48	2.841	3.247	3.863	4.947	7.663
0.49	2.987	3.458	4.210	5.666	10.965
0.50	3.153	3.710	4.653	6.775	∞
0.51	3.346	4.017	5.251	8.841	
0.52	3.574	4.403	6.121	15.483	
0.53	3.849	4.910	7.527	∞	
0.54	4.188	5.616	10.818		
0.55	4.624	6.706	∞		
0.56	5.212	8.740			
0.57	6.069	15.289			
0.58	7.498	∞			
0.59	10.702				
0.60	∞				

APPENDIX B.

The quantity μ't can easily be calculated for both the extra-ordinary and the ordinary ray except in the limiting case when $\mu' = \infty$ and $t = 0$. In this section we derive expressions for these quantities.

Ordinary Ray:

We shall first adopt a simple approach based on the QT approximation which will be valid provided that $\theta < 40^{\circ}$ at $X = 1$.

For the ordinary ray we have that the QT approximation is

$$\mu^2 = 1 - \frac{X}{1 + (1-X)\cot^2\theta} \qquad (1.22)$$

$$= 1 - \frac{X}{\operatorname{cosec}^2\theta - X\cot^2\theta}$$

$$= 1 - \frac{f_o^2}{f^2\operatorname{cosec}^2\theta - f_o^2\cot^2\theta}$$

$$\therefore \quad 2\mu\frac{d\mu}{df} = \frac{2ff_o\operatorname{cosec}^2\theta}{[f^2\operatorname{cosec}^2\theta - f_o^2\cot^2\theta]^2}$$

$$= \frac{2X\operatorname{cosec}^2\theta}{f\operatorname{cosec}^4\theta - 2fX\operatorname{cosec}^2\theta\cot^2\theta + fX\cot^4\theta}$$

Now $$\mu' = \mu + f\,d\mu/df \qquad (1.32)$$

$$= \mu + X\operatorname{cosec}^2\theta/(\operatorname{cosec}^2\theta - X\cot^2\theta)^2 \times \mu$$

Let $t2 = 1 - X$

so that $\mu' t = \mu t + tX \operatorname{cosec}^2\theta \,/\, \mu[\operatorname{cosec}^2\theta - X \cot^2\theta]^2$

Now $\mu^2/t^2 = \operatorname{cosec}^2\theta \,/\, [\operatorname{cosec}^2\theta - X \cot^2\theta]$

$\therefore\ t/\mu = (\operatorname{cosec}^2\theta - X \cot^2\theta)^{\frac{1}{2}}/\operatorname{cosec}\theta$

$\therefore\ \mu' t = \mu t + X \operatorname{cosec}\theta /(\operatorname{cosec}^2\theta - X \cot^2\theta)^{3/2}$

As $t \to 0$, $\mu t \to 0$, and thus

$$\mu' t \to \operatorname{cosec}\theta /(\operatorname{cosec}^2\theta - \cot^2\theta)^{3/2}$$

i.e. $\underline{\mu' t = \operatorname{cosec}\theta}$

A more rigorous approach yields the following:-

Equation (1.34), written in a slightly different form is

$$\mu' t = \frac{2t}{\mu}\left(\frac{1-X^2}{D} - \frac{\mu^2}{D} + \frac{(1-X^2)(1-\mu^2)Y^2\cos^2\theta}{SD}\right) + \mu t \qquad \ldots\ (1)$$

where $D = 2(1-X) - Y^2 \sin^2\theta + S$

and $S = + \sqrt{Y^4 \sin^4\theta + 4Y^2(1-X)^2 \cos^2\theta}$ for the ordinary ray.

We now must find $\lim_{t \to 0} \mu' t$.

We first find the limits as $t \to 0$ of t/μ, $(1-X^2)/D$, and μ^2/D.

t/μ :
$$\mu^2 = 1 - \frac{X}{1 - Y^2 \sin^2\theta/2(1-X) + \sqrt{Y^4\sin^4\theta/4(1-X)^2 + Y^2\cos^2\theta}} \qquad (1.10)$$

Now $t^2 = 1-X$ and t is small.

$$\mu^2 = 1 - \frac{1 - t^2}{1 - Y^2 \sin^2\theta/2t^2 + \sqrt{Y^4 \sin^4\theta/4t^4 + Y^2\cos^2\theta}}$$

$$\simeq 1 - \frac{t^2(1 - t^2)}{t^2 - \frac{1}{2}Y^2 \sin^2\theta + \frac{1}{2}Y^2 \sin^2\theta + t^2 \cot^2\theta}$$

(Note that this is mathematically exactly the same as making a QT approximation).

Thus $\mu^2 = 1 - (1-t^2)/(1+t^2\cot^2\theta)$

$$\simeq 1 - (1-t^2)(1-t^2\cot^2\theta)$$

$$= t^2 \operatorname{cosec}^2\theta$$

$$t/\mu = \sin\theta \qquad \ldots. \quad (2)$$

$(1-X^2)/D$:

$$(1-X^2)/D = \frac{1 - (1-t^2)^2}{2t^2(1+t^2\cot^2\theta)}$$

$$= \frac{1}{1 + t^2\cot^2\theta}$$

$$\to 1 \text{ as } t \to 0. \qquad \ldots. \quad (3)$$

$\underline{\mu^2/D:}$

$$\mu^2/D = t^2 \operatorname{cosec}^2\theta / 2t^2(1+t^2\cot^2\theta)$$

$$\to \tfrac{1}{2}\operatorname{cosec}^2\theta \quad \text{as } t \to 0. \qquad \ldots\ (4)$$

Now from (1), (2), (3), and (4)

$$\mu' t = 2\sin\theta\left(1 - \tfrac{1}{2}\operatorname{cosec}^2\theta + \frac{Y^2\cos^2\theta}{Y^2\sin^2\theta}\right)$$

$$= 2\sin\theta\left(1 - \tfrac{1}{2}\operatorname{cosec}^2\theta + \cot^2\theta\right)$$

$$= 2\sin\theta\left(1 - \tfrac{1}{2}\operatorname{cosec}^2\theta - 1 + \operatorname{cosec}^2\theta\right)$$

or $\underline{\mu' t = \operatorname{cosec}\theta}$ as before.

<u>Extraordinary Ray</u>:

In this case

$$t^2 = 1 - \frac{X}{1-Y} = \frac{1-X-Y}{1-Y} = \frac{\epsilon}{1-Y} \quad \text{say, where } \epsilon$$

is small near the reflection point. Equation (1.10) for the extraordinary ray can then be written

$$\mu^2 = 1 - \frac{1 - Y - \epsilon}{1 - \frac{Y^2\sin^2\theta}{2(Y+\epsilon)} - \left(\frac{Y^4\sin^4\theta}{4(Y+\epsilon)^2} + Y^2\cos^2\theta\right)^{\frac{1}{2}}}$$

$$\simeq 1 - \frac{1 - Y - \epsilon}{1 - \tfrac{1}{2}Y\sin^2\theta\,(1 - \frac{\epsilon}{Y}) - \left(\tfrac{1}{4}Y^2\sin^4\theta\,(1 - \frac{2\epsilon}{Y}) + Y^2\cos^2\theta\right)^{\frac{1}{2}}}$$

$$= 1 - \frac{1 - Y - \epsilon}{1 - \frac{1}{2}Y \sin^2\theta \left(1 - \frac{\epsilon}{Y}\right) - Y\left(\frac{1}{4}\sin^4\theta + \cos^2\theta - \frac{1}{2}\sin^4\theta \frac{\epsilon}{Y}\right)}$$

$$= 1 - \frac{1 - Y - \epsilon}{1 - \frac{1}{2}Y \sin^2\theta \left(1 - \frac{\epsilon}{Y}\right) - Y\left((1 - \frac{1}{2}\sin^2\theta)^2 - \frac{1}{2}\frac{\sin^4\theta}{Y}\epsilon\right)}$$

$$\simeq 1 - \frac{1 - Y - \epsilon}{1 - \frac{1}{2}Y \sin^2\theta\left(1 - \frac{\epsilon}{Y}\right) - Y\left(1 - \frac{1}{2}\sin^2\theta\right)\left(1 - \frac{\epsilon}{4Y}\frac{\sin^4\theta}{(1 - \frac{1}{2}\sin^2\theta)^2}\right)}$$

$$= 1 - \frac{1 - Y - \epsilon}{1 - \frac{1}{2}Y \sin^2\theta - Y + \frac{1}{2}Y \sin^2\theta + \left(\frac{1}{2}\sin^2\theta + \frac{1}{4}\frac{\sin^4\theta}{(1 - \frac{1}{2}\sin^2\theta)}\right)\epsilon}$$

$$\simeq 1 - \frac{1 - Y - \epsilon}{1 - Y} \left\{1 - \left(\frac{1}{2}\sin^2\theta + \frac{1}{4}\frac{\sin^4\theta}{(1 - \frac{1}{2}\sin^2\theta)}\right)\frac{\epsilon}{1 - Y}\right\}$$

$$= 1 - (1 - t^2)\left\{1 - \left(\frac{1}{2}\sin^2\theta + \frac{1}{4}\frac{\sin^4\theta}{1 - \frac{1}{2}\sin^2\theta}\right)t^2\right\}$$

$$\simeq 1 - 1 + t^2\left(1 + \frac{1}{2}\sin^2\theta + \frac{\frac{1}{4}\sin^4\theta}{1 - \frac{1}{2}\sin^2\theta}\right)$$

$$\text{or} \qquad \frac{\mu^2}{t} = \frac{1 - \frac{1}{4}\sin^4\theta + \frac{1}{4}\sin^4\theta}{1 - \frac{1}{2}\sin^2\theta}$$

$$= \frac{1}{1 - \frac{1}{2}\sin^2\theta}$$

$$\text{and thus} \qquad \frac{t}{\mu} = \sqrt{1 - \tfrac{1}{2}\sin^2\theta}$$

Now for the extraordinary ray S as defined above is negative so that

$$D = 2(1-X) - Y^2\sin^2\theta - \sqrt{Y^4\sin^4\theta + 4Y^2(1-X)^2\cos^2\theta}$$

$$= 2 - Y^2\sin^2\theta - Y^2(1 + \cos^2\theta) \qquad \text{when } t = 0$$

$$= 2Y(1-Y)$$

and since $\mu = 0$ for the extraordinary ray when $t = 0$, we have that $\mu^2/D = 0$ when $t = 0$. Now for the extraordinary ray equation (1) above takes the form

$$\mu' t = \frac{2t}{\mu D}\left(1 - X^2 - \mu^2 - \frac{(1-X^2)(1-\mu^2)Y^2\cos^2\theta}{Y^4\sin^4\theta + 4Y^2(1-X)^2\cos^2\theta}\right) + \mu^2 t.$$

and at $t = 0$ this is

$$\mu' t = \frac{2\sqrt{1 - \frac{1}{2}\sin^2\theta}}{2Y(1-Y)}\left(Y(2-Y) - \frac{(2-Y)Y^3\cos^2\theta}{\sqrt{Y^4\sin^4\theta + 4Y^4\cos^2\theta}}\right)$$

$$= \frac{\sqrt{\frac{1}{2} + \frac{1}{2}\cos^2\theta}}{Y(1-Y)}\left(Y(2-Y) - \frac{(2-Y)Y\cos^2\theta}{\sqrt{1 + 2\cos^2\theta + \cos^4\theta}}\right)$$

$$\mu' t = \frac{(2-Y)}{1-Y} \sqrt{\tfrac{1}{2} + \tfrac{1}{2}\cos^2\theta} \left(\frac{1 + \cos^2\theta - \cos^2\theta}{1 + \cos^2\theta} \right)$$

$$= \frac{2-Y}{1-Y} \sqrt{\frac{1}{2 + 2\cos^2\theta}}$$

The expression is given in this form without proof by TITHERIDGE (38).

APPENDIX C.

To calculate the coefficients in Table 8 it was assumed that the ionosphere was stratified in two layers, each linear with respect to frequency. Between them existed a valley of constant electron density.

The lower layer was supposed to vary as

$$h = 22.5\, f_o + 100$$

for $f_o < 4.0$ Mc/s.

The valley was supposed to have $f_o = 3.7$ Mc/s and to exist between the limits $190 < h < 200$ km.

The upper layer was supposed to vary as

$$h = 30 f_o + 80$$

for $f_o > 4.0$ Mc/s.

The ordinary and extraordinary ionograms corresponding to this distribution were constructed by evaluating $\Sigma \mu' \Delta s$ at the Titheridge frequencies. The ordinary record was scaled by Titheridge's method giving a distribution which differed from the true distribution by an amount δ_o at each frequency. This distribution was used to construct another extraordinary h'-f curve which differed from the true one by an amount Δ_o. The calculation is shown in Table 18.

TABLE 18: Calculation of Δ_o and δ_o.

f	h	h_o'	h computed from h_o'	h_x'	h_x' computed from curve with no valley	Δ	δ
3.988	189.6	246.8	189.6	251.1	251.1	0	0
4.191	205.7	283.4	197.1	290.1	277.3	12.8	8.6
4.378	211.3	293.8	203.7	300.6	293.2	7.4	7.6
4.552	216.6	301.9	209.6	308.5	302.7	5.8	7.0
4.713	221.4	309.1	214.9	315.7	310.8	5.1	6.5
4.864	225.9	316.3	219.8	322.6	318.5	4.1	6.1
5.006	230.2	322.5	224.3	329.5	324.3	5.2	5.9
5.139	234.2	328.2	228.4	336.0	330.5	5.5	5.8
5.266	238.0	334.6	232.2	341.5	335.1	6.4	5.8
5.386	241.6	339.6	235.7	-	-	-	5.9
5.500	245.0	345.4	239.0	-	-	-	6.0
5.609	248.3	351.3	242.2	-	-	-	6.1
5.713	251.4	355.5	245.2	-	-	-	6.2
5.813	254.4	360.4	248.1	-	-	-	6.3
5.908	257.2	364.1	250.9	-	-	-	6.3
6.000	260.0	369.1	253.6	-	-	-	6.4

REFERENCES.

(1)	Kennelly, A.E.	Elec. World. Eng. 39. 473. (1902).
(2)	Heaviside, O.	Encyclopaedia Brittanica 10th ed. 33. 213. (1902).
(3)	Balfour-Stewart	Encyclopaedia Brittanica 9th ed. 16. 181. (1878).
(4)	Appleton, E.V. & Barnett, M.A.F.	Proc. Roy. Soc. A. 109. 621. (1925).
(5)	Breit, G. & Tuve, M.	Phys. Rev. 28. 554. (1926).
(6)	Ratcliffe, J.A.	Jour. Geophys. Res. 56. 487. (1951)
(7)	Ratcliffe, J.A.	Yearbook of the Phys. Soc. (1959).
(8)	Chapman, S.	Proc. Phys. Soc. 43. 26. (1931).
(9)	Chapman, S.	Proc. Phys. Soc. 43. 484. (1931).
(10)	Bates, D.R. & Massey, H.S.W.	Proc. Roy. Soc. A. 187. 261. (1946).
(11)	Bates, D.R. & Massey, H.S.W.	Proc. Roy. Soc. A. 192. 1. (1947).
(12)	Bradbury, N.E.	Terr. Mag. 43. 55. (1938).
(13)	Appleton, E.V.	U.R.S.I. Proc. Washington Assembly (1927).
(14)	Appleton, E.V.	Jour. Inst. Elec. Engrs. 71. 642. (1932).
(15)	Hartree, D.R.	Proc. Camb. Phil. Soc. 25. 143. (1931).
(16)	Ratcliffe, J.A.	The Magneto-Ionic Theory and Its Applications to the Ionosphere (Cambridge) (1959) Chapters 2 and 3.

(17)	Budden, K.G.	Radio Waves in the Ionosphere (Cambridge) (1961) Chapters 2 - 5.
(18)	Budden, K.G.	Radio Waves in the Ionosphere (Cambridge) (1961) Chapter 9.
(19)	Booker, H.G.	Proc. Roy. Soc. A. 150. 267. (1935).
(20)	Walker, A.D.M.	Nature. 189. 742. (1961).
(21)	Ratcliffe, J.A.	The Magneto-Ionic Theory and its Applications to the Ionosphere (Cambridge) (1959) Chapter 8.
(22)	Budden, K.G.	Radio Waves in the Ionosphere (Cambridge) (1961) Chapter 6. p. 76.
(23)	Whitehead, J.D.	J.A.T.P. 2. 241. (1952).
(24)	Ratcliffe, J.A.	The Magneto-Ionic Theory and its Applications to the Ionosphere (Cambridge) (1959) Fig.8.1.
(25)	Ratcliffe, J.A.	Ibid. Chapter 6.
(26)	Eckersley, T.L.	Proc. Phys. Soc. 63. 49. (1950).
(27)	Rydbeck, O.E.H.	J. Appl. Phys. 21. 1205. (1950).
(28)	Rydbeck, O.E.H.	Trans. Chalmers Univ. Gothenburg. No. [illegible].
(29)	Booker, H.G.	Proc. Roy. Soc. A. 155. 235. (1936).
(30)	Shinn, D.H. & Whale, H.A.	J.A.T.P. 2. 85. (1952).
(31)	Millington, G.	Proc. Phys. Soc. 50. 561. (1938).
(32)	Booker, H.G.	Proc. Roy. Soc. A. 155. 253. (1936).
(33)	Booker, H.G.	Phil. Trans. Roy. Soc. A. 237. 411. (1938).
(34)	McElhinny, M.W.	Ph.D. Thesis. Rhodes University. Pub. (in). (1958).
(35)	Wadley, T.L.	J.I.E.E. Pt.III. 96. 483. (1949).

(36)	Thomas, J.O.	Proc. Inst. Rad. Engrs. 47. 162. (1959).
(37)	Kelso, J.M.	J. Geophys. Res. 57. 357. (1952).
(38)	Titheridge, J.E.	J.A.T.P. 17. 96. (1959).
(39)	Murray, F.H. & Hoag, J.B.	Phys. Rev. 51. 333. (1937).
(40)	Murray, F.J.	Phys. Rev. 51. 779. (1937).
(41)	Budden, K.G.	Rep. Camb. Conf. Ionosph. Phys. (Phys. Soc. London). p.332. (1954).
(42)	Jackson, J.H.	J. Geophys. Res. 61. 107. (1956).
(43)	Kelso, J.M.	J.A.T.P. 5. 11. (1954).
(44)	Jackson, J.H.	Loc. cit.
(45)	Titheridge, J.E.	J.A.T.P. 17. 110. (1959).
(46)	Szendrei, M.E. & McElhinny, M.W.	J.A.T.P. 8. 108. (1956).
(47)	Szendrei, M.E. & McElhinny, M.W.	Solar Eclipses and the Ionosphere. (Pergamon Press London). p.74. (1956).
(48)	Szendrei, M.E. & McElhinny, M.W.	J.A.T.P. 9. 118. (1956).
(49)	McElhinny, M.W.	J.A.T.P. 14. 273. (1959).
(50)	McElhinny, M.W.	Ph.D. Thesis Rhodes University. (1958).
(51)	Minnis, C.M.	Solar Eclipses and the Ionosphere. (Pergamon Press London). p.81. (1956).
(52)	Savitt, J.	J. Geophys. Res. 55. 385. (1950).

(53) Munro, G.H. and Heisler, L.H. J.A.T.P. 12. 57. (1958).

(54) Minnis, C.M. J.A.T.P. 12. 272. (1958).

(55) Gledhill, J.A. J.A.T.P. 16. 367. (1959).

(56) Gledhill, J.A. J.A.T.P. 16. 360. (1959).

(57) Appleton, E.V. Proc. Phys. Soc. 41. 43. (1928).

(58) Piggott, W.R. J.A.T.P. 5. 201. (1954).

(59) Gledhill, J.A. & Walker, A.D.M. J.A.T.P. 18. 61. (1960).

(60) Vila, P. Etude No.1221. Centre National D'Etudes des Telecommunications. Ministere des P.T.T.